

# Hydrocarbon Behavior at Nanoscale Interfaces

David R. Cole<sup>1,2</sup>, Salim Ok<sup>1</sup>

*<sup>1</sup>School of Earth Sciences and <sup>2</sup>Department of Chemistry  
The Ohio State University  
Columbus, Ohio 43210, U.S.A.  
cole.618@osu.edu ok.12@osu.edu*

Alberto Striolo, Anh Phan

*School of Chemical, Biological and Materials Engineering  
The University of Oklahoma  
Norman, Oklahoma 73019, U.S.A.  
astriolo@ou.edu aphan@ou.edu*

## INTRODUCTION

Throughout Earth's crust and upper mantle, fluids play the dominant role in transporting and concentrating Earth's energy and mineral resources (Liebscher and Heinrich 2007). Furthermore, the flux of fluids, which act as both reaction media and reactants, strongly influences the genesis and evolution of many different kinds of rocks. Among many different types of fluids, those containing volatile carbon, hydrogen and oxygen (C-H-O) species tend to dominate in the lithosphere along with various electrolytes and silica. These fluids commonly contain methane as both a major constituent and an important energy source. Conventional natural gas deposits reside in sedimentary basins where fluid overpressure often results in brittle failure of the confining rocks. Industry exploration and exploitation of shale gas (e.g., the Marcellus, Utica, and Barnett formations) has refocused attention on understanding the fundamental behavior of volatile hydrocarbon—rock interactions. Recent observations of hydrocarbons emanating from non-sedimentary systems (abiogenic), such as mid-ocean ridge hydrothermal systems or occurring within some crystalline rock-dominated Precambrian shield environments have challenged the view that organic rich sediments provide the only significant source of crustal hydrocarbons (Potter and Konnerup-Madsen 2003; Sleep et al. 2004; Sherwood Lollar et al. 2006; McColom 2013; Sephton and Hazen 2013). Geopressured-geothermal regimes contain C-H-O fluids with vast energy potential in the form of methane and hot water at high pressure. Even fluid inclusions from both metamorphic and igneous terrains record the presence of methane-bearing fluids reflecting reduced redox state conditions of formation.

The consequences of coupled reactive-transport processes common to most geological environments depend on the properties and reactivity of these crustal fluids over broad ranges of temperature, pressure and fluid composition. The relative strengths of complex molecular-scale interactions in geologic fluids, and the changes in those interactions with temperature, pressure, and fluid composition, are the fundamental basis for observed fluid properties. Complex intermolecular interactions of C-H-O-N-S fluids (H<sub>2</sub>O, CO<sub>2</sub>, CH<sub>4</sub>, H<sub>2</sub>, H<sub>2</sub>S, N<sub>2</sub>) result in their unique thermophysical properties, including large deviations in the volumetric properties from ideality, vapor-liquid equilibria, and critical phenomena. Indeed, a key goal in geochemistry is to develop a comprehensive understanding of the thermophysical properties, structures, dynamics, and reactivity of complex geologic fluids and molecules (water and other C-H-O-N-S fluids, electrolytes, and organic-biological molecules) at multiple length scales

(molecular to macroscopic) over wide ranges of temperature, pressure, and composition. This knowledge is foundational to advances in the understanding of other geochemical processes involving mineral-fluid interfaces and reactions. It is also becoming increasingly clear that organic molecules present as gas species, in aqueous and mixed-volatile fluids—ranging from simple hydrocarbons and carboxylic acids to branched and cyclic compounds, to proteins and humic substances—play major roles in controlling geochemical processes, not just at Earth's surface, but also deep within the crust. The origin of life may be partly attributable to the properties of such molecules in complex fluids under extreme conditions, as they appear to play an important role in mineral reactivity and templating of mineral precipitates.

Hydrocarbons (e.g.,  $\text{CH}_4$ ,  $\text{C}_2\text{H}_6$ , etc.),  $\text{CO}_2$ , and aqueous solutions can occupy the pores or fractures of numerous types of complex heterogeneous Earth materials present in the systems outlined above. This accessible porosity within the solids can span wide length scales ( $d$  as pore diameter or fracture aperture) including micro-, meso-, and macroporous regimes ( $d < 2.0$  nm,  $2.0 < d < 50$  nm, and  $d > 50$  nm, respectively, as defined by IUPAC). Porous solid matrices include rock or soil systems that contain clays and other phyllosilicates, zeolites, coal, graphite, or other carbonaceous-rich units; and weathered or altered silicates (e.g., feldspar to clay; olivine to serpentine), oxides, and carbonates. Examples of micro- and mesoporous features in natural solids and synthetic engineered proxies for natural materials are given in Figure 1. A number of factors dictate how fluids, and with them reactants and products of intrapore transformations, migrate into and through these nano-environments, wet, and ultimately adsorb and react with the solid surfaces. Factors include the size, shape, distribution, and interconnectedness of confined geometries, the chemistry of the solid and the fluids, and their physical properties (Cole et al. 2004). The dynamic behavior of fluids and gases contained within solids is controlled by processes occurring at the interface between the various phases (e.g., water-water, water-solute, water-volatile, water-solid, solute-solid, volatile-solid, etc.), as well as the rates of supply and removal of mobile constituents.

There is general agreement that the collective structure and properties of bulk fluids are altered by solid substrates, confinement between two mineral surfaces, or in narrow pores due to the interplay of the intrinsic length scales of the fluid and the length scale due to confinement (Gelb et al. 1999). However, compared with the effort expended to study bulk fluids, a fundamental understanding of the thermodynamic, structural and dynamic properties of volatile C-H-O fluids in nano-confined geometries, and their influence on the properties of the porous solid, is much less evolved, particularly for natural mineral substrates. Examples

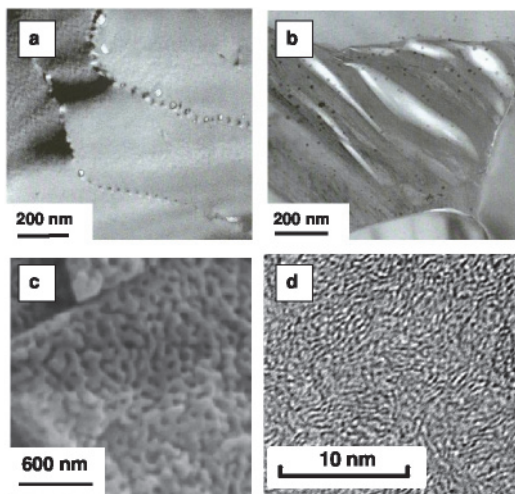


**Figure 1.** Electron microscopy images of micro- and mesoporous Earth and engineered materials: (a) pores along grain boundaries in weakly weathered basalt, (b) clay formation with large pores (white areas) at a grain boundary intersection in altered basalt, (c) controlled-pore glass, and (d) slit-like pores in carbon fiber monolith. [Used with kind permission of Springer Science+Business Media from Cole et al. (2009) *Neutron Applications in Earth, Energy and Environmental Sciences*, Fig. 1, p. 544.]

of experimental and computational efforts relevant to the behavior of Earth materials (defined as gases, solutions, and solids) include the study of CO<sub>2</sub> in thin pores (Belonoshko 1989), water structure and dynamics in clays (Skipper et al. 1995; Pitteloud et al. 2003; Wang et al. 2003; Skipper et al. 2006), ion adsorption into alumina mesoporous materials (Wang et al. 2002), and water within layered silicates at elevated pressure and temperature (Wang et al. 2004, 2005, 2006). These studies (and numerous others cited in Cole et al. 2006, 2009, 2010) demonstrate that a fluid can exhibit nano-confinement promoted phase transitions, including freezing, boiling, condensation, and immiscibility, which are intrinsic to the fluid-confining surface interactions (such as wetting and layering). Also crucial to the molecular behavior of fluids is the geometry of the pore, which can include simple planar walls (slits) such as encountered in clays and micas; cylinders, and spheres; and spheres linked with cylinders as observed in zeolites. Other factors that contribute to the modification of fluid properties include the randomness of the matrix and the connectivity of the pore network.

Given the complexity of natural C-O-H fluids and their roles in mediating surface interactions and reactivity with mineral phases, there can be no doubt that a quantitative understanding is needed of molecular-level fluid properties and fluid interactions with solids. A wide spectrum of analytical approaches can be brought to bear on Earth materials and engineered proxies, including, but certainly not limited to dynamic light scattering, IR, microscopy (e.g., electron; force), NMR, synchrotron-based X-rays, and neutron scattering and diffraction. When coupled with molecular simulation, this wide array of methods provides the means to which we can interrogate the structure and dynamics of fluids and their interactions with solids. Each of these methods provides a unique window into the properties and behavior of fluids and their reactivity. The inherent advantage of using engineered proxies for Earth materials is two-fold: (a) the mathematical rendering of details of the solid structure for simulation purposes is more straightforward when using synthetic materials and (b) interpretation of experimental results is less cumbersome.

The objective of this chapter is to provide fundamental, molecular- to microscopic-level descriptions of the sorptivity, structure, and dynamics of hydrocarbon (HC)-bearing fluids at mineral surfaces or within nanoporous matrices. The emphasis is on non-aqueous systems. Wherever possible we highlight results obtained from higher temperature-pressure sorption experiments, neutron scattering, NMR, and molecular-level modeling that have relevance to the deeper carbon cycle, although such studies are not common. We will not focus on the voluminous literature describing the behavior of hydrocarbons on activated carbon, carbon nanotubes, coal, synthetic gas storage materials such as metal-organic frameworks, and polymers. Rather we will emphasize key experimental and modeling results obtained on oxides and silicates, and synthetic engineered equivalents such as meso- and microporous silica and certain zeolites [the reader is referred to the book by Kärger et al. (2012) for more in-depth coverage of fluid behavior in zeolites]. We will assume as a first approximation that these engineered substrates act as reasonable proxies for the Earth materials. To best capture the behavior of hydrocarbons on mineral substrates or within nanoconfined volumes, we will address three key subtopics:

1. Adsorption-desorption behavior of methane and related HC fluids (and their mixtures) on a variety of substrates and in nanoporous matrices that yield microstructural insights,
2. Dynamical behavior of methane and related HC volatiles at mineral surfaces and within nanopores with and without surface H<sub>2</sub>O present,
3. Molecular-level modeling results that provide important insights into the interfacial properties of these mineral-volatile systems, assist in the interpretation of experimental data and predict fluid behavior beyond the limits of current experimental capability.

## Probing C-O-H behavior with neutron scattering and NMR

The properties of neutrons make them an ideal probe for comparing the properties of bulk hydrocarbons with those filling confined geometries (Pynn 2009). Neutrons can be scattered either coherently or incoherently, thus providing opportunity for various kinds of analysis of both structural and dynamic properties of confined liquids. Such analysis is possible due to the fact that the wavelengths of thermal and cold neutrons are comparable with intermolecular distances in condensed phases, while the neutron energy can be tailored to probe both high-(collective and single-particle vibrational) and low-frequency (single-particle diffusive) motions in the system. Importantly, the large incoherent scattering cross section of hydrogen compared to other elements allows obtaining scattering spectra dominated by the scattering from hydrogen-containing species (see recent review article by Neumann (2006)), whereas the X-ray scattering from such systems, which is virtually insensitive to hydrogen, would be dominated by the signal from the confining matrix. Last but not least, the large difference in the coherent and incoherent neutron scattering cross sections of hydrogen and deuterium allows selection of atoms to dominate the scattering signal by means of deuteration of the fragments of liquid molecules or the confining matrix.

Nuclear magnetic resonance (NMR) is a resonance concept between magnetization of nuclear spins and magnetic radio-frequency waves (Abragam 1961; Ernst 1987). NMR is employed in order to study local molecular properties of matter in detail regardless of the state of the system. One of the primary “fingerprints” of local structure probed by solid-state NMR is the chemical shielding, usually measured as the “chemical shift,” which is the difference in NMR resonance frequency of the species of interest from that of a known reference compound. Isotropic chemical shifts are indicative of local environment, and are often tabulated with typical ranges given for specific types of local bonding environments. For example,  $^{29}\text{Si}$  nuclei in silicon atoms bound through three bridging oxygen atoms to other silicon atoms and one oxygen that is part of a hydroxyl group are typically found in the range of  $-110$  to  $-120$  ppm of shift from the reference of a tetramethylsilane molecule in neat solution. However, when proposed chemical species are difficult to identify by shift alone, multiple-resonance NMR methods (Pantano et al. 2003) are used to probe and compare to quantum chemical calculations (Fry et al. 2006; Johnston et al. 2009) for determination of local ordering.

Many of the chemistries of interest in hydrocarbon systems will occur at surfaces of materials and “surface selective” NMR will aid in the understanding of adsorption and reactivity. Hydrocarbons whose under-confinement behaviors have been investigated by NMR include benzene, derivatives of benzene, diethyl ether, methane, and acetone (Stallmach et al. 2001; Krutyeva et al. 2007; Xu et al. 2007). These hydrocarbons and their derivatives were confined into various porous systems such as mesoporous and nanoporous MCM-41 (Stallmach et al. 2001; Xu et al. 2007), mesoporous Vycor glass (Dvoyaskin et al. 2007), trimethyl-silylized nanoporous silica gel (Fernandez et al. 2008), and silicate zeolite (Pampel et al. 2005). The first important issue regarding porous system surface characterization is the utilization of solid-state magic angle spinning (MAS) NMR. In MAS NMR, the effect of molecular dynamics on the NMR interactions is mimicked by fast sample spinning around an axis, including the “magic angle” of  $54.7^\circ$  with the external applied magnetic ( $B_0$ ) field. Fast sample spinning such as MAS NMR experiments removes most anisotropic nuclear interactions leading to line broadening in NMR spectra of solids. Nowadays, typical rotation speeds are in the range of 10-70 kHz with various outer diameter rotors of 7 mm to 1.5 mm (Xu et al. 2007; Vogel 2010). Solid-state MAS NMR on porous systems include, for instance, quantifying accessible hydroxyl sites of porous surfaces (Fry et al. 2003; Pantano et al. 2003). The detection of specific species on the surfaces of materials is often accomplished with heteronuclear correlation methods such as cross-polarization (Fry et al. 2003, 2006; Tsomaia et al. 2003) or J-coupled NMR spectroscopy. Surface selective spin correlation methods can be used on both raw samples and these same

samples during and after contact with fluids of interest to map out possible reactive structures as well as reaction products or sites depleted by interactions with the alkane species. NMR studies of the alkanes themselves, as well as any water or CO<sub>2</sub> incorporated with the alkanes, will focus on studies of chemical shift—primarily <sup>13</sup>C and <sup>1</sup>H—as well as spin relaxation and diffusion experiments using these same nuclides. Demonstrated efforts (Riehl and Koch 1972) have revealed the depth of information available from systematic measurements of longitudinal and transverse spin relaxation rates ( $1/T_1$  and  $1/T_2$ , respectively) as well as diffusion coefficients (Dawson et al. 1970; Helbaek et al. 1996). In NMR experiments, upon the application of radio-frequency pulses to disturb the magnetization of nuclear spins, the equilibrium distribution state is reestablished by relaxation processes. The longitudinal relaxation time  $T_1$  and transversal magnetization time  $T_2$  are the magnetization components parallel and perpendicular to external magnetic field  $B_0$ , respectively.  $T_1$  is an energy driven process, while  $T_2$  is governed by entropy. Both  $T_1$  and  $T_2$  are important parameters to be measured since they are traditional ways to study molecular reorientations (Abragam 1961; Vogel 2010).

## NON-AQUEOUS FLUID ADSORPTION BEHAVIOR: EXPERIMENTAL

### Background on adsorption concepts and approaches

The interaction of short-length linear alkanes including methane, ethane, propane, and *n*-butane and their mixtures with high surface area solids has received considerable attention over many decades, driven largely by the separations and catalysis communities. Substrates that have received the most attention include various types of carbon (e.g., activated carbon, carbon black, carbon fibers, and coal; Jiang et al. 2005), pillared clays (Li et al. 2007), clathrates (Roman-Perez et al. 2010), and zeolites, both natural and synthetic (Denayer et al. 2008). More recently synthetic materials such as micro- and mesoporous silica and metal-organic frameworks have been used to adsorb selectively light hydrocarbons from various gas mixtures.

Precise determination of adsorption/desorption isotherms at geological conditions is key to identifying surface-fluid interactions. Sorption measurements (volumetric, gravimetric, and calorimetric) are important because they provide valuable insights into the interfacial interactions between the solid substrate and the fluid phase. The magnitude of adsorption, the shape of the adsorption isotherm, and the presence or absence of hysteresis and its magnitude reveal a great deal about the properties of the surface, adsorbate molecule configurations, and the interactions between both adsorbate molecules themselves and with the substrate (Rouquerol et al. 1999; Myers and Monson 2002). Volumetric or gravimetric-based isotherms provide the most direct measure of such interactions to which other structural data, such as small angle neutron scattering (SANS) and neutron reflectivity (NR), can be compared. In most cases, however, these types of measurements are conducted at low temperature and modest pressures. Various kinds of carbon-based porous materials, zeolites, and modified organic frameworks are widely studied for methane adsorption (Zhang et al. 1991; Menon and Komarneni 1998; Cavenati et al. 2004; Wu et al. 2009). Carbon-based materials are more efficient adsorbents compared to zeolite on a weight basis. The reverse trend is observed on a volume basis because of the high solid density of zeolites (Zhang et al. 1991). Few studies explored the effect of moisture on adsorption capacity relative to methane (Clarkson and Bustin 1996; Rodriguez et al. 1997). Adsorption of methane and wet hydrocarbon gases on natural clays is rarely studied due to lower adsorption capacity of natural minerals (Stoessel and Byrne 1982). Pires et al. (2008) studied the selective adsorption of CO<sub>2</sub>, methane, and ethane on porous clay heterostructures at ambient temperature and demonstrated that alkanes adsorb proportionally to free volume of adsorbent but CO<sub>2</sub> shows an inverse trend. This anomalous behavior is attributed to clay composition as well as specific interactions of CO<sub>2</sub> with the surface. Cheng and Huang (2004) have reported a comparative study of adsorption of C<sub>1</sub>-C<sub>6</sub> hydrocarbons in gas mixtures on a variety of clays

and organic matter at lower pressures and temperatures up to 80 °C. This study confirms that despite the lower adsorption capacity for clay surfaces compared to coal substrates, the amounts adsorbed are significant (50–75% of the amount sorbed on coal). Similarly, few studies have been published on adsorption of methane and other hydrocarbon gases on natural silica (Wu et al. 1994). Although various studies discuss adsorption of CO<sub>2</sub> on coal substrates, zeolites, assorted metal oxides, and modified silica/clays, a limited number have tried to study CO<sub>2</sub> adsorption on natural minerals (e.g., Yong et al. 2002) particularly in the presence of water and aqueous carbonate species (e.g., Villalobos and Leckie 2000).

While adsorption-desorption phenomena have been the focus of many of these studies issues such as rates of sorption and transport behavior (diffusivity) have also been addressed (Schloemer and Krooss 2004; Kim and Dauskardt 2010). Techniques that have been used in these kinds of studies include but are not limited to volumetric and gravimetric sorption isotherm measurements, differential scanning and micro-calorimetry (DSC), NMR, FTIR, scattering (light, X-ray, and neutrons) and diffraction (X-ray, neutrons). For the most part these studies involve either high pressure at cryogenic to near-ambient temperature conditions or the converse, high temperature, but low pressures (few MPa). The use of extreme conditions of temperature and pressure is limited by the availability of novel high temperature-pressure sorption apparatus such as Rubotherm's magnetic suspension balance and appropriate high pressure-temperature scattering sample cells for *in situ* interrogation. Molecular dynamics, Monte Carlo, and *ab initio* methods are widely used to predict sorption and transport behavior (Combariza et al. 2011; Krishna and van Baten 2011) and/or help interpret experimental data (Lithoxoos et al. 2010). Collectively, results from these studies (and many more not formally cited) provide an important framework for gaining a fundamental understanding of the interfacial behavior of the light hydrocarbons interacting with synthetic "Earth" proxies, as well as natural mineral and rock matrices at conditions relevant to shallow crustal settings; ~200 °C and 100 MPa. However, to our knowledge, with the possible exception of coal, there has not been a systematic study of the effects of temperature, pressure, variable pore size, shape, roughness, and connectivity, and degree of surface hydrophobicity on light hydrocarbon-mineral interaction relevant to subsurface fine-grained sedimentary lithologies. Further, fundamental understanding of interfacial behavior involving interactions between hydrocarbons and aqueous films on minerals is very poor compared to studies that have explored H<sub>2</sub>O wetting phenomena (e.g., Fenter 2002), and the role of confinement, surface charge, and electrochemical reactions on surface forces at mineral surfaces (e.g., Alcantar et al. 2003; Anzalone et al. 2006; Greene et al. 2009).

Behavior of hydrocarbons and related C-O-H fluids in the presence of complex solution chemistry (e.g., elevated electrolyte concentrations; silica) at elevated temperatures and pressures is obviously of more relevance to our understanding of the deep carbon cycle. A number of sorption studies have been performed on supercritical and near-critical fluids, mainly using volumetric techniques. Experimental adsorption isotherms obtained over wider ranges of pressure extending to compressed liquid or dense supercritical fluid revealed effects that were not present or could be neglected in low-density gas adsorption. Pronounced high-pressure depletion effects over a large region of fluid densities have been reported for argon, neon, krypton, nitrogen, and methane physisorbed to activated carbon (Malbrunot et al. 1992). Thommes et al. (1995) studied the sorption of supercritical SF<sub>6</sub> to mesoporous CPG-10 silica and found adsorption at low fluid density, but a strong decrease of the adsorbed amount of fluid in the vicinity of the critical point, and named the effect *critical depletion*. Rayendran et al. (2002) report the occurrence of critical depletion for N<sub>2</sub>O sorption to silica gel. Several theoretical and simulation studies have been published on critical/high-density depletion phenomena (Maciolek et al. 1999; Brovchenko et al. 2004, 2005; Oleinikova et al. 2006; Brovchenko and Oleinikova 2008), with partly conflicting results. Part of the problem is that the common quantity measured in sorption experiments, excess adsorption, gives only the net sorption effect, but cannot provide a microscopic picture of the fluid-substrate interactions.

Observationally as one traverses from low to high density, the experimental adsorption isotherms for C-O-H fluids can exhibit a maximum at the density of bulk fluid approaching its critical value (Parcher and Strubinger 1989; Strubinger and Parcher 1989; Aranovich and Donohue 1998; Donohue and Aranovich 1999). At still higher densities, experimental excess adsorption isotherms may reach zero or even negative values. This behavior is independent of any additional volumetric effects, such as adsorbent swelling or deformation at elevated pressure. The decrease of the amount adsorbed with pressure may appear counterintuitive by implying a mechanical instability of the system. However, the quantity measured by all conventional methods does not represent the total amount of fluid present in the vicinity of solid surface but instead the excess adsorption (Gibbs surface excess; Fig. 2)—the difference between the actual amount of fluid contained inside a pore system and the hypothetical amount of fluid at bulk density filling the pore spaces, i.e. in absence of fluid-solid interactions.

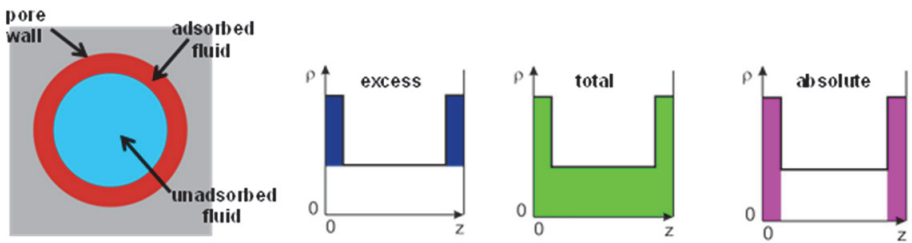


**Figure 2.** Schematic of a single pore (left panel) showing the adsorbed phase (red) and the unadsorbed fluid (blue). Also shown are the three types of sorption described in the text – excess, total and absolute.  $\rho$  refers to fluid density and  $z$  is the diameter of the pore. (G. Rother, pers. commun.)

### C-O-H pore fluid densities

As noted above, excess adsorption, which can be measured without the knowledge of any microscopic properties of the adsorbed phase, is an important quantity used for thermodynamic analysis of many aspects of adsorption and is routinely used in modeling and control of technological processes (Sircar 1999). However, the properties of the adsorbed phase, including the average density of the pore-filling fluid, are essential in quantifying fluid-rock interactions in systems dominated by nano- to microscale pore features (Rother et al. 2007). Gruszkiewicz et al. (2012) reported results on propane ( $C_3H_8$ ) and  $CO_2$  obtained from a novel high temperature-high pressure vibrating tube densimeter (VTD) capable of measuring pore fluid density and total adsorption capacity in mesoporous solids. The densities were determined for propane at subcritical and supercritical temperatures (between 35 °C and 97 °C) and carbon dioxide at supercritical temperatures (between 32 °C and 50 °C) saturating hydrophobic mesoporous silica aerogel (0.2 g/cm<sup>3</sup>, 90% porosity) synthesized inside Hastelloy U-tubes (Fig. 3). In this method the porous solid completely fills the tube, so that virtually no bulk fluid outside of the pore system is present in the measurement zone; i.e., the contact with the bulk fluid reservoir occurs outside of the vibrating cantilever. The mass of the pore fluid, proportional to its average density, is measured directly as the inertia of the cantilever containing the solid sample imbedded with fluid. Additionally, supercritical isotherms of excess adsorption for  $CO_2$  and the same porous material were measured gravimetrically using a precise Rubotherm magnetically-coupled microbalance.

The densities of pore-filling propane measured at four subcritical temperatures (35, 70, 92, and 95 °C) and at 97.0 °C, about 0.3 °C above the critical temperature ( $T_c = 96.7$  °C) are given in Figure 4 plotted against pressure. Also shown are the densities of bulk fluid calculated from the equation of state (Span and Wagner 1996; Lemmon et al. 2010). Pore fluid densities and

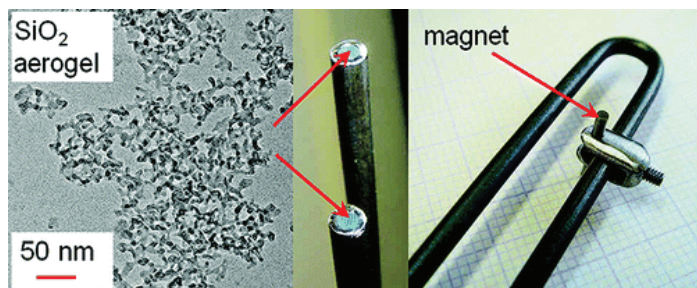


**Figure 3.** A transmission electron microscopy (TEM) image of the silica aerogel structure (silica strands are darker), the Hastelloy U-tube with the silica aerogel synthesized inside, and magnet clamp attached to the U-tube. [Used by permission of the American Chemical Society © 2012, from Gruskiewicz et al. (2012) *Langmuir*, Vol. 28, Fig. 1, p. 5073.]

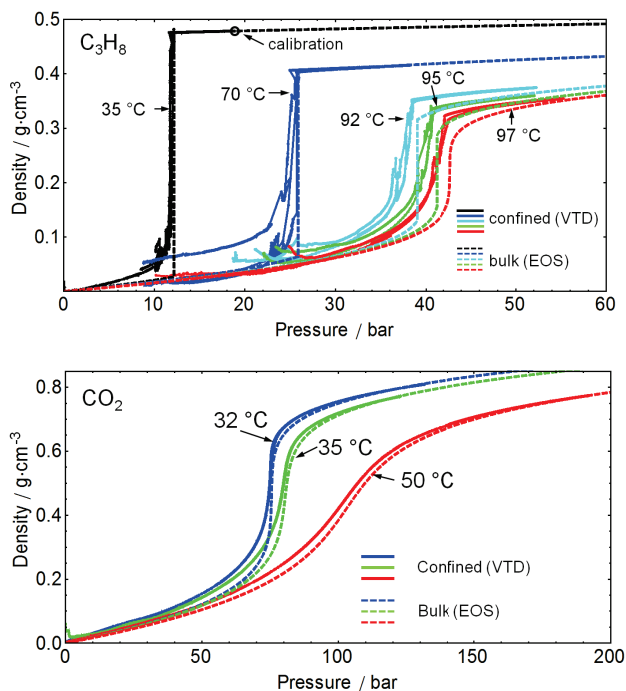


**Figure 4.** (top) Subcritical (35 °C, 70 °C, 92 °C, and 95 °C) and supercritical (97 °C) isotherms of confined fluid density for propane in silica aerogel. (bottom) Supercritical (32, 35 and 50 °C) isotherms of confined and bulk fluid density for carbon dioxide in silica aerogel. [Used by permission of the American Chemical Society © 2012, from Gruskiewicz et al. (2012) *Langmuir*, Vol. 28, Fig. 4, p. 505 (top panel), Fig. 6, p. 5076 (bottom panel).]

total adsorption isotherms increased monotonically with increasing density of the bulk fluid, in contrast to excess adsorption isotherms, which reached a maximum and then decreased towards zero or negative values above the critical density of the bulk fluid (Fig. 4). Compression of the confined fluid significantly beyond the density of the bulk fluid at the same temperature was observed even at subcritical temperatures. The isotherms of confined fluid density and excess adsorption (not shown) contain complementary information. For instance, the maxima

of excess adsorption occur below the critical density of the bulk fluid at the beginning of the plateau region in the total adsorption, marking the end of the transition of pore fluid to a denser, liquid-like pore phase. No measurable effect of pore confinement on the liquid-vapor critical point was found. The results for propane and carbon dioxide showed similarity in the sense of the principle of corresponding states. Good quantitative agreement was obtained between excess adsorption isotherms determined from VTD total adsorption results and those measured gravimetrically at the same temperature, confirming the validity of the vibrating tube measurements. The flatter initial slopes exhibited in the propane isotherms are indicative of relatively weak fluid-pore wall interactions. The step increase in density at higher pressures can be indicative of pore condensation and/or stronger fluid-fluid interactions. The somewhat steeper initial slopes associated with lower pressures observed for the  $\text{CO}_2$  are typical for a fluid that experiences a somewhat stronger fluid-pore wall interaction compared to propane.

To better compare these results and to emphasize the corresponding states' similarity between the fluids, the results are also shown in Figure 5 in terms of reduced densities,  $\rho_r = \rho/\rho_c$ , where  $\rho_c = 0.220 \text{ g/cm}^3$  for  $\text{C}_3\text{H}_8$  and  $\rho_c = 0.4676 \text{ g/cm}^3$  for  $\text{CO}_2$ . The diagonal dashed straight line in Figure 5 represents the hypothetical condition where the confined fluid density is equal to the bulk fluid density; the deviations of the experimental isotherms from this line represent the excess density due to solid-fluid interactions. This figure demonstrates that the confined fluid densities, and consequently total adsorption isotherms, are non-decreasing functions of increasing bulk fluid density. Each of the subcritical isotherms features a plateau formed by a straight tie line extending between the densities of bulk vapor and liquid phases in equilibrium. The dotted curve in Figure 5 represents the vapor-liquid equilibrium envelope of bulk propane with the densities of the phases in equilibrium and the bulk fluid critical point marked with symbols.

### Hydrocarbon-interfacial microstructure

As noted previously, the sorption of gaseous subcritical fluids on solid substrates has been studied extensively (Schreiber et al. 2002; Sel et al. 2007), while only a few studies exist on the nanoscale structure and dynamics of interfacial fluids, and almost nothing is known about the interfacial properties of near-critical and supercritical fluids. In the context of hydrocarbons, this is an important  $P$ - $T$  regime because these fluids will be present at supercritical conditions. A poorly constrained yet fundamentally important fluid behavior has been identified wherein at  $P$ - $T$ -density conditions below the critical point, fluid volume and density increase as the critical point is approached, while above the critical density fluid volume remains essentially constant but density decreases—the so-called fluid depletion effect where negative values of excess adsorption are estimated (Malbrunot et al. 1992; Thommes et al. 1995; Rajendran et al. 2002). However, theoretical and simulation efforts to model these data give conflicting results

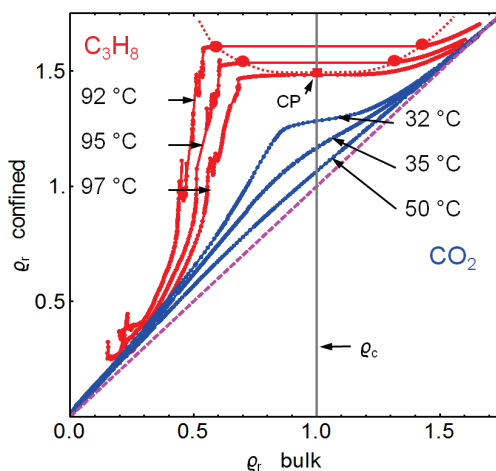


**Figure 5.** Total confined fluid reduced density ( $\text{g/cm}^3$ ) isotherms for  $\text{C}_3\text{H}_8$  and  $\text{CO}_2$  plotted as a function of bulk fluid reduced density. [Used by permission of the American Chemical Society © 2012, from Gruszkiewicz et al. (2012) *Langmuir*, Vol. 28, Fig. 7, p. 5077.]

(Maciolek et al. 1998, 1999; Brovchenko et al. 2004, 2005; Oleinikova et al. 2006), which is due to the lack of experimental micro-structural characterization.

Many studies deal with the properties of fluids and fluid mixtures imbibed in the pores of engineered nanoporous materials. Porous silica ( $\text{SiO}_2$ ) is frequently chosen because it can be synthesized with well-defined pore sizes in the range of less than 1 nm up to several tens of nm. The structural properties of confined liquids can be assessed using coherent scattering techniques, neutron diffraction (ND), and small-angle neutron scattering (SANS). The former allows one to measure the static structure factor,  $S(Q)$ , which can be then Fourier transformed to obtain the radial pair-distribution function,  $g(r)$ , that describes the distribution of the distances between the coherently scattering nuclei in the liquid. While ND measurements of liquids in confinement probe structural correlations not exceeding a few molecular diameters, SANS measurements provide coverage over much broader range in the real space (Radlinski 2006; Triolo and Agamalian 2009). This is because SANS involves measuring neutron intensities at very low values of the scattering vector,  $Q$  (i.e., at small angles).

SANS has been widely used in the study of fluid behavior in porous media and recently became the first technique capable to quantify the sorption properties of C-O-H fluids in porous media in terms of the mean density and volume of the adsorbed phase (Rother et al. 2007). In this study, the sorption properties of supercritical deuterated propane and  $\text{CO}_2$  in silica aerogel with 96% porosity and pores ranging from 20-50 nm were investigated. SANS and neutron transmission data have been measured for fluid-saturated silica at different fluid densities and temperatures. The mean density  $\rho_3$  and volume fraction  $\phi_3$  of the sorption phase were calculated from the SANS and neutron transmission data by application of a new model, which makes use of the three-phase model by Wu (1982) and a mass balance consideration of the pore fluid, which can be obtained from neutron transmission measurements or gravimetric sorption measurements. It was found that the fluid is adsorbed to the porous matrix at low fluid densities but depleted from the pore spaces at higher fluid densities (i.e., in the vicinity of the critical density and above). Figure 6 shows the evolution of the physical properties of the sorption phase, expressed in terms of  $\rho_3$  as a function of temperature and (bulk) fluid density  $\rho_2$ . The bulk critical density of deuterated propane is  $\rho_c \approx 0.27 \text{ g/cm}^3$ , and the critical temperature is  $T_c \approx 91.0 \text{ }^\circ\text{C}$ . The fluid density in the adsorbed phase is up to about three times higher than  $\rho_2$  in the low-pressure region, while it remains constant and below  $\rho_2$  at and above the critical pressure.

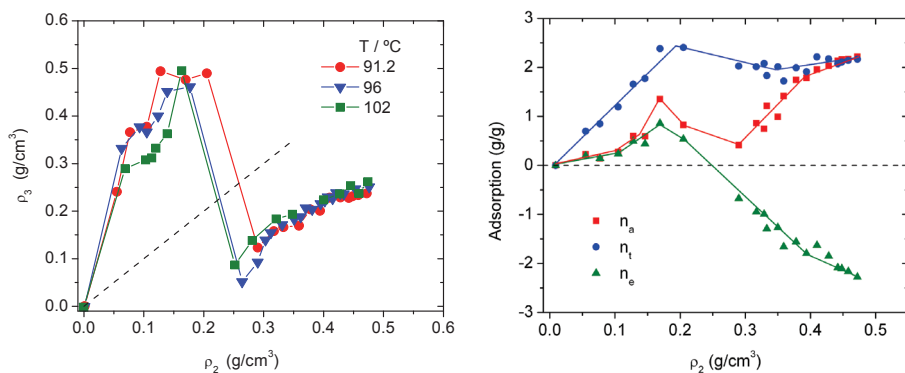


**Figure 6.** Results of SANS on deuterated propane inside silica mesoporous aerogel (0.1 g/cc) at three supercritical temperature from; (left) mean density  $\rho_3$  of the sorption phase as a function of the density of the unadsorbed fluid; dashed line represents behavior for a fluid-porous solid system with no adsorption; (right) adsorption quantities calculated from the density and volume of the sorption phase.  $n_a$  = absolute adsorption;  $n_t$  = total adsorption;  $n_e$  = excess adsorption. [Used by permission of the American Chemical Society © 2007, from Rother et al. (2007) *J Phys Chem-C*, Vol. 111, Fig. 6, p. 15740 and Fig. 8, p. 15740.]

With the information on  $\rho_3$  and  $\phi_3$  (not shown), calculation of the absolute adsorption, which is the relevant quantity for the application of the equation of adsorption and molecular modeling work, is possible without the introduction of further assumptions. The calculated values for the absolute adsorption ( $n_a$ ), total adsorption ( $n_t$ ) and excess adsorption ( $n_e$ ) are given in Figure 6. The absolute adsorption is similar to the commonly measured excess adsorption only at low fluid densities but differ significantly at higher fluid densities. Cole et al. (2010) has been able to theoretically emulate the shape of this trend by using an integral equation approximation. From the sorption phase density and volume the excess sorption, total sorption and absolute sorption can be calculated. These neutron results have been compared to excess sorption data measured with gravimetric techniques and total sorption data measured with the vibrating tube densimeter (Rother et al 2012; Gruszkiewicz et al 2012). General agreement of the data has been found, verifying the validity of the neutron method.

In a related study, Kainourgiakis et al. (2010) studied the behavior of water, hexane, and hexane-water mixtures at ambient temperature imbibed in macroporous  $\alpha$ - $\text{Al}_2\text{O}_3$  (34% porosity;  $\sim 180$  nm pores; total pore volume of  $\sim 0.14$   $\text{cm}^3/\text{g}$ ), using ultra-small angle neutron scattering (USANS). The intent was to quantify the multiphase pore-filling behavior of a wetting (water) and non-wetting fluid (hexane). They used a 7.3%  $\text{H}_2\text{O}/\text{D}_2\text{O}$  mixture that matched the scattering length of the alumina matrix, which allowed the study of the contributions to the scattering signal of the individual phases in water-water and water-hexane systems, and the hydrocarbon in hexane-air systems. In the case of the water-loaded samples (and to a certain extent also when water-hexane mixtures are used) the progressive hydration leads towards the formation of larger water-hydrocarbon clusters. These clusters can be considered as biphasic "aggregates," comprising continuous solid- and water-rich regions, which nevertheless can be characterized as homogeneous in terms of scattering behavior since the 7.3%  $\text{H}_2\text{O}/\text{D}_2\text{O}$  mixture used has the same scattering length density as alumina. This characterization is indeed confirmed by the practically zero intensity recorded when the pore space is fully occupied ( $V_{\text{water}} = 1$ ) by the aqueous phase. On the other hand, the spectra of the samples impregnated with hexane exhibit, in practice, the same trend, while the slight variation of intensity is attributed to the reduced contrast achieved as increased quantities of the hydrocarbon are introduced in the pore network. Most interestingly, the autocorrelation function curves obtained from scattering for the cases of the partial filling (e.g.,  $V_{\text{water}} = 1/3$  or  $2/3$  where  $V_s$  is defined as the fraction of total pore volume occupied by a certain fluid component) of the pore volume with only the aqueous phase and the complete saturation with an equivalent water-hexane mixture (i.e.,  $V_{\text{water}} = 1/3$  or  $2/3$  and  $V_{\text{hexane}} = 2/3$  or  $1/3$ ) practically coincide despite the differentiation of the fluids occupying the pore volume and the significant variation therefore of the interfacial energies coupled in the respective systems. In practical terms this important observation provides direct experimental evidence that the spatial distribution of the fluid phases is related to their wetting/non-wetting relative behavior and is not affected significantly by the actual values of their particular interfacial properties. Simulations of this wetting process for different loadings are shown in Figure 7.

Zeolites are microporous aluminosilicate minerals that play an important role in many natural and industrial processes, including water purification through ion exchange, catalytic hydrocarbon cracking, and separation of pollutants from natural gas. They possess pore widths of typically a few tenths of a nanometer, making X-ray and neutron diffraction suitable tools for the study of these materials and guest molecules inside their pore systems. Neutron diffractometers exist in a variety of configurations for thermal and cold neutrons optimized for resolution or flux and interrogate length scales of up to 2 nm. The ND technique has been recently used by Mentzen to study the adsorption of hydrogen and benzene in MFI-type zeolites (Mentzen 2007). The positions of the guest molecules in the microporous host structure were determined through Rietveld analysis to define the binding sites. The sorption of several hydrocarbons, including heptane, in silicalite-1 zeolite was studied by Floquet et al. (2003,

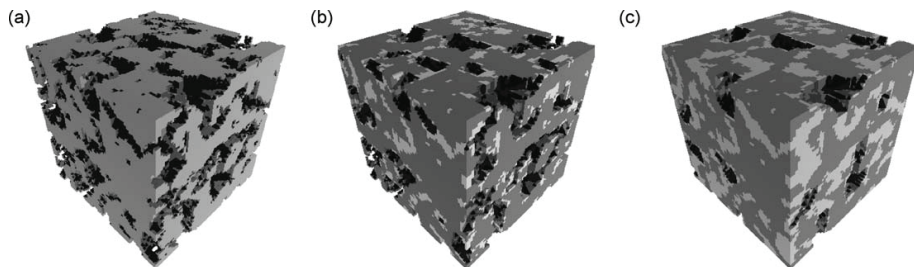


**Figure 7.** 3D simulation images of (a) dry alumina structure; (b) spatial distribution of a wetting fluid for  $V_s = 1/3$  and (c)  $V_s = 2/3$ . Each block is approximately 500 nm on a side. . [Used by permission of Elsevier © 2010, from Kainourgiakis et al. (2010) *Appl Surf Phys*, Vol. 256, Fig. 3, p. 5332.]

2007), who used ND. Their results indicate that heptane populates the straight channels of the silicalite pore network first, while the sinusoidal channels and intersections fill with heptane only above a heptane concentration of about 3.9 molecules per unit cell.

## NON-AQUEOUS FLUID DYNAMICS AT INTERFACES: EXPERIMENTAL

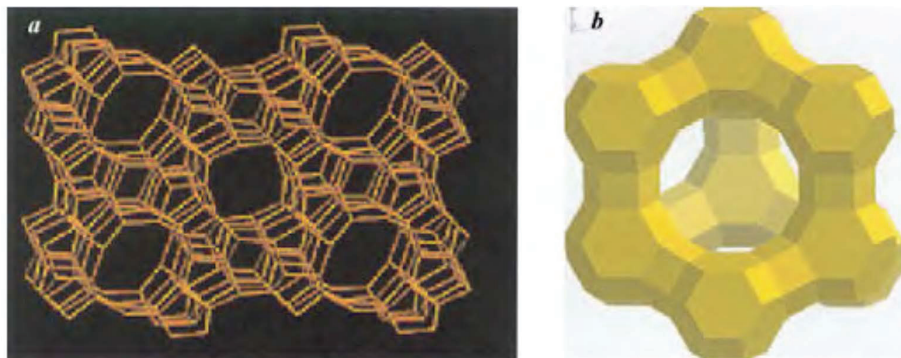
Dynamical fluid behavior is controlled by processes occurring at the fluid-pore wall or fluid-fluid interface, as well as by the rates of supply and removal of mobile constituents. Key issues pertaining to these types of interactions that remain largely unresolved, particularly for conditions of elevated temperature and pressure, include the extent of possible hydrogen bonding, molecular translation and rotation, average times between molecular jumps, and self-diffusion, which involve specific interactions between neighboring molecules leading to preferred molecular orientation that are affected by reduced dimensionality and fluid-pore wall interactions (Cole et al. 2006, 2009). Of the techniques that are available, neutron scattering and nuclear magnetic resonance are probably the most heavily used to obtain dynamical information on hydrogen-bearing fluids, such as self-diffusion, translational, and rotational motion from hydrocarbon-matrix interactions. More specifically, Pulsed Field Gradient NMR (PFG-NMR) was the first “microscopic” method advanced for the measurement of diffusion in zeolites in the late 1970s. It allowed accessing molecular displacements down to 0.1-1  $\mu\text{m}$  for times on the order of 1 ms and was thus instrumental in elucidating intracrystalline and intercrystalline transport phenomena for a wide variety of systems (Jobic and Theodorou 2007). Quasielastic neutron scattering (QENS) is a complementary method to NMR that tracks the diffusive motions that take place on the timescale of a pico- to nano-second, which corresponds to the energy scale from a fraction of  $\mu\text{eV}$  to several hundred  $\mu\text{eV}$  (Bee 2003). The more energetic (on the energy scale from several to several hundreds of meV) vibrational and librational modes are typically probed using dedicated neutron spectrometers with moderate energy resolution and reasonably high incident neutron energies. On the timescale of such spectrometers, rotational and translational motions are very slow and can be neglected. This type of measurement is known as inelastic neutron spectroscopy (INS). Compared to infrared spectroscopy, INS benefits from the absence of optical selection rules and the large incoherent scattering cross section of hydrogen.

### QENS probe of hydrocarbons in nanopores

As noted above QENS is an excellent tool to probe the mobility of confined hydrogen-bearing fluids, the property affected the most by a confinement; a change by one to two orders of magnitude in the mobility of a confined liquid is common. QENS targets the signal from incoherently scattering nuclei such as H, leading to a description of self-diffusion. The signal

measured by a spectrometer as a function on neutron energy transfer,  $E$ , is a Lorentzian with a half-width at half maximum (HWHM)  $\Gamma = \hbar D Q^2$ , where  $Q$  is the momentum transfer to the particle in the scattering process and  $D$  is the diffusion coefficient (Cole et al. 2006). In general, QENS probes rotational and translational diffusive motions of molecules that result in the broadening of the elastic peak. In QENS measurements, the effects of faster vibrational and librational motions manifest themselves in the overall reduction of scattering intensities (Debye-Waller factor). It should be noted that knowledge of the resolution function and an extremely good energy resolution are of paramount importance in QENS. For this reason, time-of-flight and backscattering spectrometers built at cold neutron sources are frequently employed in this type of experiment.

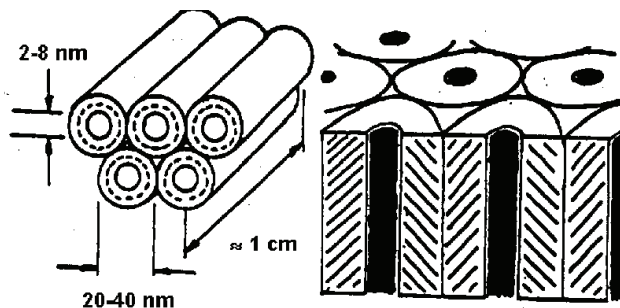
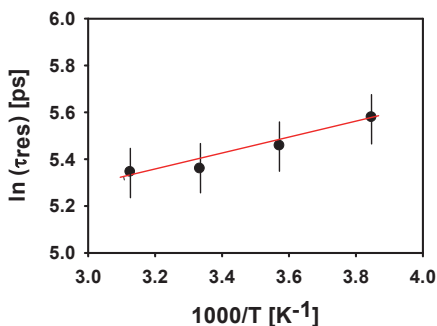
Even though water has been by far the most extensively investigated medium in nanoconfinement, other fluids in confined environments such as methane and other alkanes have attracted some attention. The majority of studies using QENS to interrogate hydrocarbon dynamics have focused on behavior in a variety of synthetic silicas and zeolites. For example, Benes et al. (2001) presented QENS results on the temperature dependence (200 to 250 K) of methane self-diffusion and molecular rotation in microporous silica with pores smaller than 1 nm. The self-diffusion coefficients of translational motion range from  $1.1 \times 10^{-8} \text{ m}^2 \text{ s}^{-1}$  at 200 K to  $1.9 \times 10^{-8} \text{ m}^2 \text{ s}^{-1}$  at 250 K with an estimated activation energy of  $4 \text{ kJ mol}^{-1}$ . The isotropic rotation diffusion constant is on the order of  $10^{11} \text{ s}^{-1}$ . Jobic (2000a, b) described the dynamics of complex hydrocarbon molecules in confinement (linear and branched alkanes, for hydrocarbon chains up to C-14, confined in ZSM-5 zeolite, Fig. 8a). In ZSM-5 zeolite there are two types of channels consisting of ten-membered oxygen rings. The straight elliptical channels (0.57-0.52 nm) are interconnected by near-circular channels (0.54 nm) in a zig-zag fashion, and there are four channel intersections per unit cell. Because of the relatively large size of the confined molecules, the diffusion could be observed within the time window of a backscattering spectrometer only at high temperatures. Branched alkanes were found to diffuse much more slowly than linear alkanes. Mitra and Mukhopadhyay (2004) reported on the residence times ( $\tau$ ), mean jump length ( $l$ ), and translational motion ( $D$ ) of propane in Na-Y zeolite (Na:Al = 1.7). The Na-Y zeolite structure is made up of a network of tetrahedrally connected pores ( $a$ -cages) of diameter  $\sim 1.18 \text{ nm}$ . The pores are interconnected through windows of diameter  $\sim 0.8 \text{ nm}$ . A schematic of Na-Y zeolite structure is shown in Figure 8b. They compared the experimental results with MD as shown in Table 1. Mamontov et al. (2005) explored the diffusion and relaxation dynamics of benzene ( $\text{C}_6\text{H}_6$ ) in oriented 5-nm nanochannels of chrysotile [ $\text{Mg}_3\text{Si}_2\text{O}_5(\text{OH})_4$ ] asbestos fibers from 260 to 320 K (Fig. 9). The



**Figure 8.** Schematic of cage pore structure in two commonly used zeolites (a) ZSM-5; channel diameter 0.52-0.57 nm and (b) Na-Y; channel diameter 0.8 nm. [Used by permission of Indian Academy of Sciences © 2003, from Mitra and Mukhopadhyay (2003) *Curr Sci*, Vol. 84, Fig. 3, p. 657.]

**Table 1.** Dynamical parameters for residence times ( $\tau$ ), jump length ( $l$ ) and translational motion of propane adsorbed in Na-Y zeolite (Mitra and Mukhopadhyay 2004).

$T$ (K)	$\tau$ (ps)	$(l^2)^{0.5}$ (nm)	$D$ ( $\times 10^{-5}$ cm <sup>2</sup> s <sup>-1</sup> ) QENS	$D$ ( $\times 10^{-5}$ cm <sup>2</sup> s <sup>-1</sup> ) MD
300	$4.6 \pm 0.5$	$0.25 \pm 0.02$	$2.3 \pm 0.3$	3.6
324	$4.3 \pm 0.4$	$0.29 \pm 0.02$	$3.2 \pm 0.3$	3.2
350	$3.8 \pm 0.3$	$0.30 \pm 0.03$	$4.0 \pm 0.4$	3.0

**Figure 9.** (top) Schematic picture of a bundle of chrysotile asbestos fibers. (left) temperature dependence of the average residence time ( $\tau$ ) between translational diffusion jumps of benzene and its fit with Arrhenius law. [Used by permission of American Physical Society © 2005, from Mamontov et al. (2005) *Phys Rev E*, Vol. 72, Fig. 1, p. 051502-1, and Fig. 6, p. 051502-5. <http://link.aps.org/doi/10.1103/PhysRevE.72.051502>]

macroscopic alignment of the nanochannels provided an opportunity to study the anisotropy of the dynamics of a confined fluid by means of collecting the data with the scattering vector either parallel or perpendicular to the fibers axes. The translational diffusive motion of benzene molecules was observed to be isotropic. Diffusivities were not strongly temperature dependent and ranged from  $0.88 \times 10^{-10}$  m<sup>2</sup> s<sup>-1</sup> to  $1.31 \times 10^{-10}$  m<sup>2</sup> s<sup>-1</sup>. Conversely, the residence times between translational jumps exhibited a weak temperature dependence (Fig. 9) and yielded a low activation energy of 2.8 kJ mol<sup>-1</sup>.

A recent survey by Jobic and Theodorou (2007) provides an excellent overview of QENS studies of confined media in a number of zeolites and their synergy with molecular dynamic simulations. They compared the behavior of various alkanes in Al-Si-O-based zeolites with or without counterions such as Na (e.g., Si-only silicalite-1; Na-ZSM-5 [ $\text{Na}_n\text{Al}_n\text{Si}_{96-n}\text{O}_{192}\cdot 16\text{H}_2\text{O}$  ( $0 < n < 27$ )]): their unit cells contain 96 tetrahedral units with Si or Al as central atoms and oxygen as corner atoms. These structures (MFI; mordenite framework inverted) contain straight channels and zigzag channels, both with free apertures of about 0.55 nm in diameter. In general, self-diffusion coefficients decrease with increasing carbon number, are faster by a factor of 4-5

for zeolites without a counterion such as Na, and tend to be faster than comparable systems interrogated by pulse-field gradient NMR. In all probability, this discrepancy can be attributed to defects in the silicalite-1 structure. PFG-NMR, which measures displacements on the order of micrometers, is much more sensitive to such defects than QENS, which has an effective length scale of nanometers. Molecular simulations, which postulate a perfect crystalline structure, are closer to QENS than to PFG-NMR. For linear pores less than 1 nm in diameter there is a general tendency for the diffusion coefficients to decrease with increasing alkane chain length (Jobic et al 2010). This unexpected result (Fig. 10) can be explained by the fact *n*-butane keeps the same orientation in the 1D channels of the V<sup>4+</sup>-metal organic framework (MIL-47) so that it loses less momentum than propane, which tumbles within the pore channel.

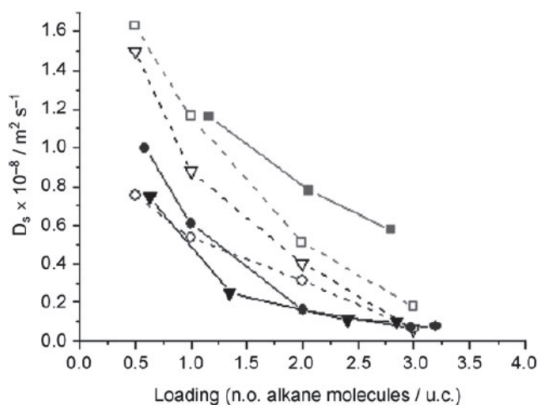


**Figure 10.** Self-diffusion coefficients ( $D_s$ ) for ethane (square), propane (inverted triangle) and *n*-butane (circle) in V<sup>4+</sup> MIL-47 metal organic framework as a function of the loading at 300 K. QENS (solid symbols), MD (open symbols). Note that the reported  $D_s$  values are orientationally averaged. [Used by permission of Wiley-VCH © 2010, from Jobic et al. (2010) *Chem Eur J*, Vol.16, Fig. 5, p. 10340.]

The properties of organic molecules in hydrated 2:1 clays have been studied by Skipper et al. (2006), who used QENS to show that methane interacts strongly with the clay, snugly fitting into the hexagonal ring sites on the clay surface, thus leading to a decrease of the diffusion coefficient by one order of magnitude as compared to bulk water-methane. Chathoth et al. (2010) presented results from a SNS-QENS study of the behavior of methane in a mesoporous carbon aerogel; a proxy for coal. The QENS portion of this study focused on the pressure and surface hydration effects on methane mobility. They observed a slowing of the motion for hydrated carbon pore walls compared to a “dry” carbon matrix. The pressure effect was non-linear with a subtle, yet measurable, maximum observed between ~3-4 MPa (maximum interrogated pressure was ~9 MPa). For the most part these various experiments were carried out at cryogenic to ambient temperatures and modest pressures, up to ~10 MPa.

### NMR probes of hydrocarbons in nanopores

Diffusion considered as random motion of the elementary components of matter is among the most fundamental concepts in nature (Heitjans and Kärger 2005). This conceptual model is correct in the case of nanoporous systems as well. For this reason, studies of molecular diffusion in nanoporous materials attracted large interest. Among different techniques, pulsed field gradient (PFG) NMR has been proven to be very useful method to investigate systems with small molecules confined into the “subsurfaces” of nanoporous hosts (e.g., Meresi et al. 2001; Seland et al. 2001; Stallmach et al. 2000, 2001; Kärger et al. 2003; Krutyeva et al. 2007). PFG NMR diffusion measurements are based on pulse sequences forming a primary or stimulated spin echo of the magnetization of nuclei in resonance (Stallmach et al. 2000, 2001). In other words, the potential of PFG NMR depend on the amplitude and the rise and fall times of the

field gradient pulses (Kärger et al. 2003). Applying appropriate pulsed magnetic field gradients of duration  $\delta$ , intensity  $g$ , and observation time  $t$  during the defocusing and refocusing cycles of the NMR pulse sequence leads to the spin echo being sensitive to the translational motion of the molecules (Stallmach et al. 2000, 2001). Depending on the measuring conditions, PFG NMR experiments on molecular diffusion in cavities of nanoporous host systems result in valuable information on different aspects of mass transfer. The valuable information covers 1) molecular diffusion in the interior particles; 2) hindered transportation by outer surface of particles; and 3) long-range diffusion. Thus, PFG NMR may yield the probability distribution  $P(x,t)$  function that, during time  $t$ , a randomly selected molecule of the sample is shifted over a distance  $x$  in the direction of applied field gradient (Kärger 2008). Such capabilities of PFG NMR provides an opportunity to investigate diffusion behavior of molecules confined to both mesoporous and nanoporous systems (Stallmach et al. 2000, 2001; Kärger et al. 2003, 2009), to explore surface permeability of nanoporous particles (Krutyeva et al. 2007), to study transport properties of supercritical fluids in confined geometry (Dvoyashkin et al. 2007), and to study diffusion of small molecules such as methane and carbon dioxide in carbon molecular sieve membranes (Mueller et al. 2012). However, there are some problems in performing NMR experiments of diffusion of mixtures within porous materials since they represent heterogeneous systems (Pampel et al. 2005; Fernandez et al. 2008). In such heterogeneous systems, the transverse proton magnetization is decayed due to a continuous dipolar interaction between the spins of interest, as well as differences in the internal magnetic fields. These effects, including the restricted mobility of adsorbed molecules, broaden the NMR signal and results in reduced resolution (Pampel et al. 2005; Fernandez et al. 2008). The combination of PFG and MAS techniques overcomes this problem (Nivarthi et al. 1994; Pampel et al. 2003; Gaede et al. 2004). MAS PFG NMR enabled, for example, studying complex formation in an acetone-alkane mixture confined to nanoporous host systems (Fernandez et al. 2008) and molecular diffusion in zeolites (Pampel et al. 2005). A more interesting MAS probe without FG was designed to investigate the evolution of adsorption on nanoporous solids (see Fig. 11 by Xu et al. 2007). The results obtained by this technique depicted clearly the viability of a new technique for performing *in situ* solid-state NMR investigations of adsorption processes into nanoporous host systems and possible subsequent reactions. In addition to such PFG NMR and MAS PFG NMR studies on hydrocarbon derivatives confined into various host systems, there are recent attempts for studying such heterogeneous systems at low temperatures and high pressures (Huo et al. 2009; Hoyt et al. 2011).

One more potential method in analyzing small molecules in confined geometry is low-field (LF) NMR. LF-NMR has been used not only for the fast determination of the water and oil components in several food samples (Aeberhardt et al. 2007; Straadt et al. 2008), but also was applied for studying protein aggregation (Indrawati et al. 2007), detecting heterogeneities in polymer networks (Saalwachter 2003), and water diffusivity in aggregated systems (Guichet et al. 2008). LF-NMR measures the response of  $^1\text{H}$  protons after immersing the collection of nuclei into an external magnetic field. Then the protons inside the sample

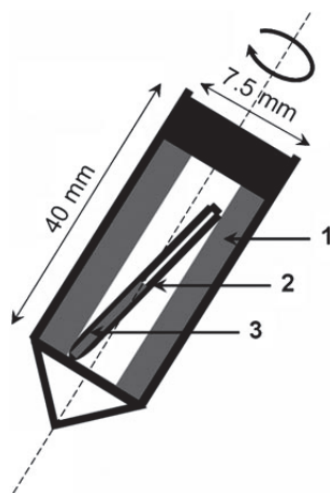


**Figure 11.** Schematic illustration of the setup for the *in situ* adsorption experiment inside the solid-state NMR rotor: 1) nanoporous material compacted on the walls of the rotor by prior spinning; 2) thin-walled glass capillary tube; 3) liquid to be adsorbed on the nanoporous material. [Used by permission of Wiley-VCH © 2007, from Xu et al. (2007) *Chem Phys Chem*, Vol. 8, Fig. 1, p. 1311.]

are polarized in the same direction with the external field. A radio-frequency field is applied to bring the protons to the perpendicular transverse plane. The magnetic signal processing in the transverse plane induces electric current, which is called the NMR signal or free induction decay (FID; Levitt 2001). The main advantage of LF-NMR experiments are based on time-domain relaxation measurements, such as transverse relaxation and longitudinal relaxation (no need to do Fourier transformed spectra analysis) and calibration of the instrument response or model-dependent analyses of the relaxation functions (Saalwachter 2003; Kantzas et al. 2005; Indrawati et al. 2007). The other benefits of LF-NMR technique are very short experimental time, very little if any sample preparation is necessary, and being non-destructive and non-invasive (Indrawati et al. 2007). In addition to relaxation measurements by LF-NMR, water diffusion coefficients in complex food products by low-field  $^1\text{H}$  PFG-NMR were determined with standard errors lower than 0.5 % (Metais and Mariette 2003). Similar to this low-field, bench-top PFG NMR study on water diffusion in food products, Blümich et al. (2009) mentioned 2D relaxation exchange NMR of water in contact with nanoporous silica particles measured by low-field NMR. It seems that various NMR techniques ranging from low-field PFG NMR to high-pressure MAS NMR will contribute positively to the understanding of small molecule behaviors in confined geometry of subsurfaces.

### Representative NMR studies

NMR studies of various hydrocarbons in nanoporous materials (mostly zeolites) are too voluminous to do justice to in this chapter, rather we will highlight some key results that illustrate the kinds of dynamical behavior hydrocarbons exhibit under nanoconfinement. Collectively these studies provide quantitative insights into hydrocarbon behavior as a function of particle size (i.e., transport length), pore diameter, pore geometry and pore intersection dimensions, cation size, ratio of Si:Al, hydrophobicity of the pore wall, load rate (i.e., amount of hydrocarbon), and hydrocarbon chain length.

Stallmach et al. (2001) demonstrated that PFG NMR can monitor anisotropic diffusion of slowly moving sorbate molecules arising from the inherent anisotropy of the MCM-41 nanopore system. As shown in Figure 12, there is significant deviation in non-exponentially decaying

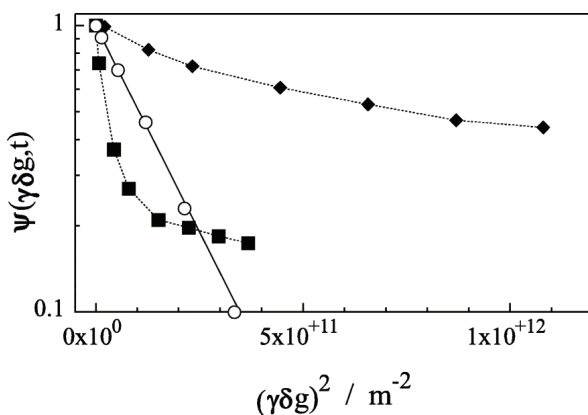


**Figure 12.** Examples for experimentally observed non-exponentially decaying PFG NMR spin echo intensities for benzene in two MCM-41 species (full symbols) compared with the exponential decay in the bulk liquid (open symbols) under the same conditions ( $T = 298\text{ K}$ ,  $t = 3\text{ ms}$ ). (◆) MCM-41 having particle size between 1 and 10  $\mu\text{m}$  and pore radius 1.5 nm (■) Si-MCM-41 having particle size smaller than 1  $\mu\text{m}$  and pore radius between 1.5 and 1.7 nm. [Used by permission of Elsevier © 2001, from Stallmach et al. (2001) *Microporous and Mesoporous Materials*, Vol. 44, Fig. 2, p. 750.]

PFG NMR spin echo intensities for benzene in two MCM-41 nanoporous hosts with respect to exponential decay in bulk benzene under the same experimental conditions. For instance, in sample MCM-41 the benzene exhibits slower decay than the bulk liquid, while in the case of Si-MCM-41 there is faster motion than the benzene in bulk.

Another host system of interest, zeolite NaX, has been studied by Kärger et al. (2003) with a mixture of *n*-butane and benzene. The zeolite hosts 0.8 molecules per supercage for *n*-butane and 2 molecules per supercage for benzene. The mobility of ethane in the nano-volume of zeolite NaX was also measured by PFG NMR. Figure 13 depicts temperature dependence of the coefficients of long-range diffusion of ethane upon confining into beds of zeolite NaX for two different loadings (Geier et al. 2002). The lower-temperature exponential dependence shifts to a much weaker dependence for higher temperatures. This change reflects the transition from Knudsen diffusion to bulk diffusion.

In a recent study by Dvoyashkin et al. (2007) using Vycor pore glass particles of about 500- $\mu\text{m}$  size with mesoporous structure inside and 6-nm pore diameter, it was shown that a sufficiently large size of porous particles prevented extensive exchange between the bulk and the mesopores within the observation time  $t = 3$  ms of the  $T_2$  Hahn-echo pulse sequence (Figs. 14a,b). Both diffusivities  $D_b$  and  $D_p$ , in the bulk liquid and in the mesopores, respectively, increase at high temperatures following an Arrhenius law (the difference in absolute values attributed to the tortuosity of the porous space). Around 438 K an important deviation from the Arrhenius pattern in  $D_p$  was observed. However, at that temperature the diffusivity of the bulk liquid for the sample with Vycor did not exhibit noteworthy deviation from normal behavior.

One of the other NMR techniques employed in analyzing confined molecules behaviors was MAS PFG NMR. Fernandez et al. (2008) studied complex formation in acetone—*n*-alkanes (including hexane, heptane, and octane) mixtures by MAS PFG NMR diffusion measurements in two different specimens of trimethyl-silylized nanoporous silica gel. The silica gel nanoporous systems were synthesized from tetraethyl orthosilicate and had average pore sizes of 4 and 10 nm. MAS  $^1\text{H}$  NMR was applied in order to resolve the signals of the acetone and the alkane constituent of interest. Upon resolving the signals of the two mixture components, comparing the  $\text{CH}_3$  signals of acetone and the *n*-alkanes molecule yielded the acetone to *n*-alkane ratio. Selective diffusion measurements of acetone—*n*-alkane mixtures in both narrow (4 nm) and large

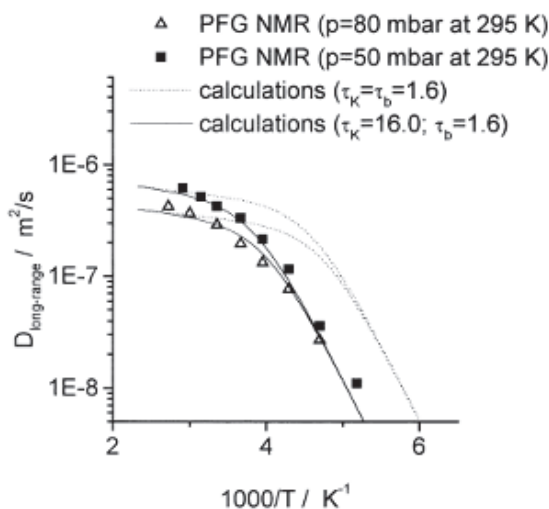


**Figure 13.** Temperature dependence of the coefficients of long-range diffusion of ethane measured by the PFG NMR method in beds of zeolite NaX for two different loadings (shown by the two different adsorbate pressures inside the sample tube at 295 K), comparison with the diffusivities calculated for identical and different tortuosity factors  $\tau_{k(b)}$  in the cases of Knudsen and bulk diffusion using a simple kinetic gas approach. [Used by permission of American Institute of Physics © 2002, from Geier et al. (2002) *J Chem Phys*, Vol. 117, Fig. 1, p. 1936.]

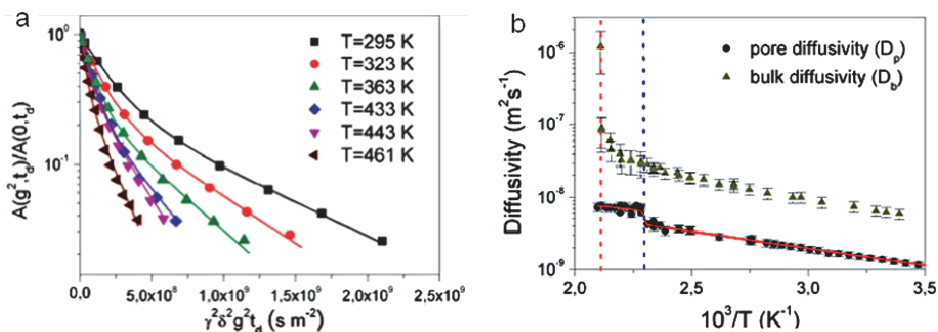


**Figure 14.** (a) Normalized spin-echo attenuation functions for *n*-pentane in Vycor porous glass obtained at different temperatures using PFG NMR. The solid lines show fits to the experimental data by two-exponential functions. (b) Arrhenius plot of the bulk and pore fluid diffusivities for *n*-pentane in Vycor porous glass. The solid line was calculated by assuming a transition to the supercritical state at  $T = T_{cp}$ . The vertical dashed lines show the positions of the bulk (left line) and pore (right line) critical points. [Used by permission of the American Chemical Society © 2007, from Dvoyashkin et al. (2007) *J Am Chem Soc*, Vol. 129, Fig. 1a, p. 10344-10345 (a), Fig. 1b, p. 10344-10345 (b).]

(10 nm) pore silica gels as a function of gradient amplitude at 298 K illustrated a notable deviation from a mono-exponential behavior observed in the free liquids. The deviation is stronger in the narrow-pore gel than in the large-pore one. This behavior was attributed to the deviation of the pore shapes (channel structure) from a cubic resulting in an orientation dependent anisotropic diffusion behavior. Additionally, examining the diffusion behavior of the two component mixtures in large and narrow pores indicated the following differences: 1) in large-pore gels the diffusivities increased by one or two orders of magnitude, 2) in large-pore gels the diffusion behavior difference of the *n*-alkanes and acetone disappeared, 3) in large-pore gels there is no longer any clear oscillation indication of the acetone diffusivities as a function of chain length of *n*-alkane molecules.

As mentioned in the introduction, Xu et al. (2007) developed a facile technique to handle MAS NMR for probing the adsorption of  $^{13}\text{C}$ -labeled acetone on nanoporous MCM-41 and ZSM-5. MAS  $^{13}\text{C}$  NMR spectra of acetone in MCM-41 pores acquired by spin rate of 3 kHz depicted that liquid acetone signals disappeared rapidly and were replaced by broader signals typical of acetone molecules in a less mobile environment (Fig. 15). Such a result indicates

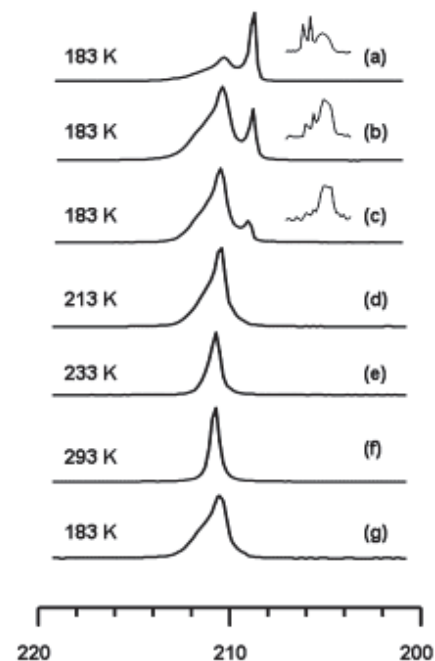


**Figure 15.**  $^{13}\text{C}$  NMR spectra acquired as a function of time and temperature following adsorption of acetone on MCM-41, indicating the region of the spectrum for the (labeled) carbonyl carbon. In the spectra obtained at 183 K, the region corresponding to the (unlabeled) methyl carbon (between 27 and 32 ppm) is depicted as an inset. Each spectrum was acquired within 2 h. [Used by permission of Wiley-VCH © 2007, from Xu et al. (2007) *Chem Phys Chem*, Vol. 8, Fig. 2, p. 1311.]



They amount to several  $\mu\text{m}$  in PFG-NMR and to a few nm in QENS. The agreement between the two methods, within experimental error, indicates that the two techniques are measuring the same process; i.e., long-range translational motion. This result means that there are no dramatic transport resistances with spacing above the nm scale. The presence of transport resistance would lead to a reduction of the NMR diffusivities, while the QENS results would remain essentially unaffected by them (Jobic et al. 1995). At low loading (0.02 and 0.04 g cyclohexane per g  $\text{SiO}_2$ ), the diffusion coefficients appear to be insensitive to the concentration, whereas at high loading, (0.08 g cyclohexane per g  $\text{SiO}_2$ ) lower diffusivities are measured. Jobic et al. (1995) attribute this decrease in mobility to mutual hindrance of the molecules, which evidently becomes effective only at high concentrations. Activation energies of 10.9 and 11.6  $\text{kJ mol}^{-1}$  were determined for lower loadings and the higher loading, respectively.

Another good example of the power of using combined  $^2\text{H}$ -NMR and QENS was described by Stepanov et al. (2003) in a study of the translational and rotational dynamics of *n*-hexane in ZSM-5 and 5A zeolites (the characteristics of these are described above). There are profound differences between the two systems. In ZSM-5, the molecule sits in the channel segments and the energy barrier between two sites is small. On the other hand, in 5A zeolite, the molecule spends a longer time in the  $\alpha$ -cages before jumping to the next cage. The  $^2\text{H}$ -NMR spectra point out the more confined adsorption geometry of the molecule in the ZSM-5 structure, in the form of anisotropic motions, whereas isotropically reorienting molecules are evidenced in the  $\alpha$ -cages of 5A zeolite. This result is in agreement with the larger entropy variations measured in silicalite (the Al-free analog of ZSM-5; Millot et al. 1998) compared with 0.5 nm zeolite (Paoli et al. 2002). Finally, the long-range diffusion coefficient of *n*-hexane, derived from neutron scattering techniques, is more than 4 orders of magnitude larger in ZSM-5, at 300 K, compared with 0.5 nm zeolite. This difference illustrates the drastic effect of the pore size and shape on the diffusivity of molecules in microporous materials. The reader should consult the excellent review articles on NMR studies of liquids in confined geometry by Packer (2003), Buntkowsky et al. (2007), and Webber (2010). For recent reviews of the application of neutron scattering and MD to both natural and engineered materials and their interaction with fluids see Cole et al. (2006, 2009, 2010).

## ATOMIC AND MOLECULAR-LEVEL SIMULATIONS

### Properties of confined fluids: do they differ compared to the bulk?

We briefly discuss herein effects on (1) the diffusivity of confined gas/liquids; (2) fluid adsorption and vapor-liquid equilibria for the confined fluids; and (3) liquid-solid transitions under confinement. These observations will be used in the section on “*Selected simulations of alkanes within alumina and silica-based pores,*” where we will discuss in a few more details the properties of confined alkanes. We provide a brief overview on simulation methods in the “*Simulation Details*” section.

**Diffusion under confinement.** The seminal works of Knudsen (1909), von Smoluchowski (1910), Pollard and Present (1948), and Mason et al. (1967) described confined fluid particles as hard spheres and took into consideration the momentum exchange between the fluid particles and the solid wall when the fluid-fluid interactions could be neglected, and later considered the effect of density on the mobility of the confined gases. More recently, theoretical developments have attempted to consider dispersive and longer-ranged fluid-fluid interactions (Guo et al. 2005, 2006). Building on the Chapman-Enskog kinetic theory approach (Davis 1992), Jepps et al. (2003) provided a significant improvement in our theoretical understanding of the diffusion of confined Lennard-Jones fluids by developing the “oscillator model” theory, which is exact at low confined fluid densities (i.e., low-pressure gases). The theory builds on the diffusive reflection model for fluid particles bouncing on the confining walls. To investigate the fluid

diffusion within pores of nano-scale dimensions (e.g., “nanopores”), theoretical investigations have benefited from advances in molecular simulation techniques. For example, recent simulation results suggest that, for fluids confined in carbon nanotubes, the specular reflection might be more accurate than the diffusive reflection model invoked in the groundbreaking theories discussed above (Skoulidas et al. 2002; Sokhan et al. 2002; Bhatia et al. 2005; Striolo 2006).

Bhatia and Nicholson (2007) recently extended the theories above to include the effect of loading (i.e., increased pressure). They compared the theoretical results to molecular simulation data, achieving satisfactory, though not quantitative agreement. In narrow cylindrical pores they showed that the diffusivity of confined methane is constant as the density increases (the simulations show slight increase), while in wider pores (albeit of diameter comparable to that of confined molecules) the diffusivity decreases as the density increases. In even larger pores it has been reported that the diffusivity increases as the density of the confined fluid increases because of viscoelastic effects (Bhatia and Nicholson 2006; Nguyen et al. 2006). In the case of alkanes adsorbed within silica mesopores at low loadings, it was observed by molecular dynamics simulations that the diffusivity of the alkane chains increases at the loading increases because of screened fluid-pore interactions (Raghavan and Macelroy 1995). Recent interest has been devoted to enhancing the permeability of natural gas through rock formations (e.g., shale deposits), as well as in sequestering carbon dioxide in geological formations. It has also been proposed to employ carbon dioxide as a fluid to enhance the permeability of natural gas, achieving simultaneously carbon dioxide sequestration and natural gas extraction. Clearly, for these applications to succeed it is necessary to understand how each of the gases diffuses in sub-micron, often nanometer scale pores. We summarize a few contributions to highlight extreme confinement effects.

Zeolites are among the most widely used porous materials in industrial applications. We refer here to the zeolite ZK5, which has a framework consisting of two different cages (the largest cavity, known as the  $\alpha$ -cage, has diameter  $\sim 1.16$  nm; the other cavity, the  $\gamma$ -cage, has cross section  $0.66 \times 1.08$  nm) interconnected via circular rings of diameter 0.39 nm composed by 8 oxygen atoms (Zorine et al. 2004; Baerlocher et al. 2007). The size of both cages as well as that of the connecting ring is comparable to the molecular dimensions of alkane molecules such as *n*-pentane. At most, the unit cell of ZK5 can contain 12 *n*-pentane molecules, 3 in each of the  $\alpha$ -cages, and 1 in each of the  $\gamma$ -cages. The question of interest here is how fast *n*-pentane molecules can diffuse across the zeolite. Experimental data have been obtained by  $^{13}\text{C}$  NMR techniques when the zeolite was filled with *n*-pentane (Magusin et al. 1999). The results are consistent with a “hopping” diffusion mechanism with molecules jumping between neighboring cages with a hopping rate of 1 to  $10^3$  jumps per second in the temperature range 247 to 317 K. The resultant self-diffusion coefficient was found to be of the order  $10^{-18}$  to  $10^{-15}$   $\text{m}^2/\text{s}$ .

Because of the extremely long time that separates distinct hopping events traditional “brute force” molecular dynamics simulation techniques cannot yield satisfactory information regarding this phenomenon. Alternative approaches have been designed. Saengsawang et al. (2010) applied the “high-temperature configuration-space exploration (HTCE)” method of Schuring et al. (2007) to overcome the limitations of standard molecular dynamics. In short, the rare-event hopping event of one *n*-pentane molecule from one  $\alpha$ -cage to another was investigated at extremely high temperature (i.e., 6000 K), which makes the event more likely to be observed, and the results were appropriately corrected to become applicable in the temperature range of experimental interest. The transition state theory was then applied to obtain self-diffusion coefficients from the relative probability of observing the *n*-pentane molecules either within the cages, or inside the connecting oxygen rings. The self-diffusion coefficients obtained show Arrhenius dependence as a function of temperature, in general agreement with experiments. In Figure 17 we report a schematic for the ZK5 zeolite, the two cages occupied by *n*-pentane to

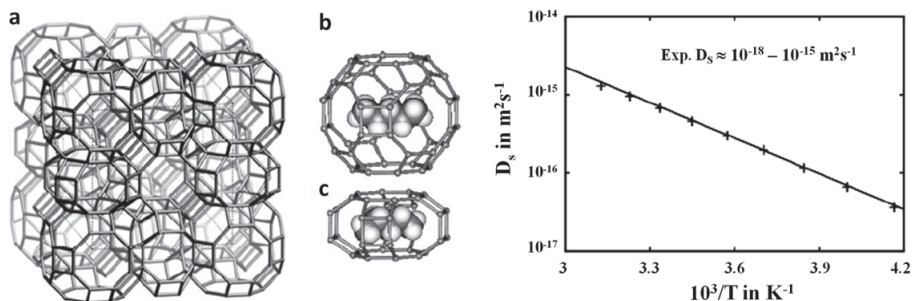


**Figure 17.** (left) Schematic representation of the ZK5 zeolite. Silicon or aluminum atoms constitute the vertexes of the structure in panel (a). The various cages and how they are interconnected are visible from the schematic. Panels (b) and (c) show one *n*-pentane molecule inside  $\alpha$ - and  $\gamma$ -cage, respectively. (right) predicted self-diffusion coefficients as a function of temperature. The predictions are in relatively good agreement with experiments. [Used by permission of Elsevier © 2010, from Saengsawang et al. (2010) *Chem Phys*, Vol. 368, Fig. 1, p. 122 and Fig. 5, p. 125.]

illustrate the level of confinement considered, and the self-diffusion coefficients predicted as a function of  $T$ . Although some differences do exist between experimental and simulated results (in part due to the different *n*-pentane loadings considered), this example shows how advanced simulations can elucidate the mechanism of diffusion for fluid molecules within extremely narrow porous networks.

To prevent, and when necessary remediate, environmental and energy challenges, it has been proposed to store  $\text{CO}_2$  in deep un-minable coal beds, with the possible additional advantage of extracting trapped natural gas in the process (Busch et al. 2004; White et al. 2005). For such an application to be practically realized it is important to understand, quantify, and predict several physical-chemical aspects, including the adsorption and diffusion of both  $\text{CH}_4$  and  $\text{CO}_2$  within typical coal bed porous networks. Molecular dynamics simulations are being used for such purposes (i.e., to identify the relative diffusion and adsorption propensity of the two gases in the carbon-based pores; Hu et al. 2010). Firouzi and Wilcox (2012) employed the dual control volume grand canonical molecular dynamics algorithm (Heffelfinger and Van Swol 1994; Cracknell et al. 1995; Ford and Glandt 1995) to investigate the flux of pure methane, pure  $\text{CO}_2$ , and their mixtures across representations of the carbon-based porous networks. The porous materials were obtained by implementing a geometric algorithm and the resultant models were characterized in terms of overall porosity and pore size distribution. Although some simplifications were necessary, the porous networks reproduced important experimental properties. Because of the large computational requirements, the fluid molecules were treated as spherical particles and all interactions were described by pair-wise Lennard-Jones potentials. One simulated system is reproduced in Figure 18, where an equimolar mixture of  $\text{CH}_4$  (squares) and  $\text{CO}_2$  (circles) are present in the two bulk reservoirs (left and right), and in the porous network (middle). The carbon atoms of the coal bed are not shown for clarity. The image represents pictorially the flux of both gases from the high-pressure region on the left (5 MPa) to the low pressure region on the right (2 MPa), and the presence of regions within the porous network that are not accessible to the fluid molecules, presumably because of the small pore size or because of lack of pore connectivity (the porosity of the material is 25% and the average pore size is 1.25 nm). Simulations were conducted as a function of the feed composition, the porosity of the substrate, and the difference in pressure between the two reservoirs. The results were quantified in terms of the permeability of the various gases. In the right panel of Figure 18 we reproduce simulation results for the permeability of the two gases in the mixture as a

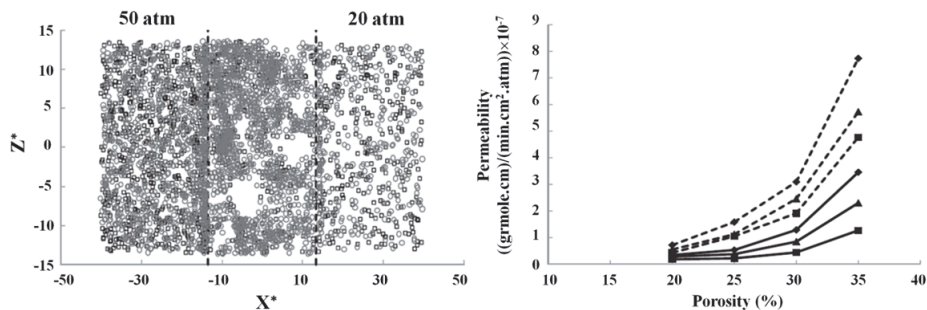


**Figure 18.** (left) Schematic representation of the system simulated by Firouzi and Wilcox to study the permeability of  $\text{CH}_4$ - $\text{CO}_2$  mixtures across model coal beds. Squares and circles are for  $\text{CH}_4$  and  $\text{CO}_2$  molecules, respectively. The carbon atoms in the porous network are not shown for clarity. (right) Permeability of  $\text{CH}_4$  (continuous lines) and  $\text{CO}_2$  (dashed lines) through carbon-based porous materials with average pore size 1.25 nm and varying porosity. Different symbols are for varying methane mole fraction in the feed: diamonds, triangles, and squares are for 0.75, 0.5, and 0.25  $\text{CH}_4$  mole fraction, respectively. [Used by permission of Elsevier © 2012, from Firouzi and Wilcox (2012) *Microporous and Mesoporous Materials*, Vol. 158, Fig. 7, p. 201 and Fig. 10, p. 201.]

function of total porosity. The average pore size in all cases was 1.25 nm. As expected, the permeability increases with porosity. Important is that no detectable permeability was reported at porosity lower than  $\sim 20\%$  because of the lack of connectivity between the pores. Simulations were conducted at varying methane mole fractions in the feed. The interesting observation is that both  $\text{CH}_4$  and  $\text{CO}_2$  permeability increase as the  $\text{CH}_4$  mole fraction in the feed increases. Fully understanding the molecular reasons for these observations will certainly enhance the possibility of sequestering  $\text{CO}_2$  in coal beds.

The simulations discussed above contrast a number of simulations available in the literature in which the adsorption and the diffusion of various gases were considered in simple pores, varying, for example, the pore width. Restricting our analysis to the case of carbon dioxide and methane, the recent reports by Lim and coworkers appear to be important. For example, Lim et al. (2010) simulated the adsorption of carbon dioxide (simulated using two different models, one spherical, the other, more realistic, linear) in carbon slit pores of various widths. The simulations were conducted at various bulk pressures and at various temperatures. The simulated diffusions were found to be much larger compared to experimental measurements, and were interpreted invoking a modified Knudsen diffusion mechanism. The authors suggest that the predicted values could be the upper limit available, when membranes could be prepared with perfect carbon pores as long as pore-entrance and pore-exit effects can be neglected. Lim and Bhatia (2011) extended the study to methane, and found that in the temperature range 298–318 K, and pressure range from 0.001 to 8 MPa, the permeability of methane in pores of width 0.65–0.75 nm is controlled more by the adsorption of the gas within the pores than by the self-diffusion coefficient.

When simulation results in individual pores, such as those just summarized, are available for individual gases and their mixtures, and when the resistance for the various gases to enter/exit the various pores are known, it will be possible to predict the permeability across realistic materials by implementing pore network models such as the one presented by Seaton and coworkers for the diffusion in nanoporous carbons (Cai et al. 2008). The validation of such models could be done by comparing the predicted permeability to simulated ones, such as those presented by Firouzi and Wilcox (2012), provided that the same porous network is used in both approaches.

Regarding the diffusion of trace elements (e.g., heavy metal ions) confined within narrow pores, we point out the work of Ho et al. (2012). These authors employed brute force equilibrium molecular dynamics simulations to quantify the mobility of aqueous NaCl or CsCl within slit-shaped silica-based pores of size  $\sim 1$  nm. These simulations face several challenges, including the long time required to achieve equilibrium, the uncertainty regarding the composition of the confined system, and the slow dynamics typical of aqueous solutions under confinement. Despite these problems, the enormous computational resources that have become available to researchers have allowed Ho et al. (2012) to estimate the mobility of the various ions as a function of the degree of protonation of the confining surfaces. In Figure 19 we report a schematic of the system simulated, together with predicted planar self-diffusion coefficients, and the density distributions across the pore width for the various confined molecules. The results have been interpreted based on the expectation that water molecules diffuse slowly near a silica-based substrate (Argyris et al. 2009). As the degree of protonation changes, the preferential distribution of the various electrolytes across the pore width changes. Those ions that are preferentially found near the pore center have higher mobility than those that are preferentially found near the solid substrate. Such observations, if verified experimentally, could be useful for predicting the environmental fate of heavy metal ions accidentally released during operations such as mining.

**Adsorption and vapor-liquid equilibria under confinement.** Gelb and Gubbins provided an extensive review on the extent to which confinement leads to significant deviations for fluid thermodynamics properties compared to bulk (Gelb et al. 1999). One such effect is on the vapor-liquid coexistence curve (Striolo et al. 2005). A Monte Carlo study by Singh et al. (2009) elucidated the phase behavior of methane, butane, and other short alkanes confined in narrow slit-shaped carbon and mica pores. The results showed that as the pore width decreases the critical temperature decreases. Representative results are shown in Figure 20 for butane in mica and in carbon-based pores. Confinement was found to have a strong effect on the densities of the coexisting phases, and it was also found that the vapor-liquid surface tension for the confined alkanes is significantly reduced compared to values obtained in the bulk, possibly a direct consequence of the lower critical temperature for confined fluids.

As in the case of diffusion, the simulation studies that are being conducted for adsorption and phase transitions of various fluids in porous materials will help the interpretation of experimental data, as well as better understanding the behavior of fluids in subsurface conditions. However, to be useful the simulations need to be conducted carefully. For example, it is often tempting to employ simplified representations for the confining material. Smooth surfaces and simple geometries (e.g., cylindrical and slit shaped) lead to enormous savings of computational resources. However, details on the porous wall structure can lead to significant changes in the simulated adsorption isotherms (used to obtain results such as those in Figure 20, but also to predict the permeability of various gases). The simulation community is striving to generate computer models for the solid adsorbent that are more and more realistic. The literature is vast and not summarized here for the sake of brevity. Instead, we highlight a contribution from Coasne et al. (2006), who simulated the adsorption of simple Lennard-Jones gases in two models of the silica-based porous material MCM-41. One model had atomically smooth pore walls, the other was rough at the atomic scale. The adsorption isotherms obtained showed large adsorption-desorption hysteresis loops in the case of the smooth pore, and more gradual adsorption curves in the case of the rough surface. Careful analysis suggested that the smooth model yields results in agreement with experiments at short length, but not at large scales, while the rough model reproduces the surface disorder at large length scales but does not at short length scales. When the structure of the confined fluid is considered at those relative pressures at which the pores are not completely filled, the simulation results are dramatically different, as shown in Figure 21. Within the smooth pore (left panel) a clear separation is observed between

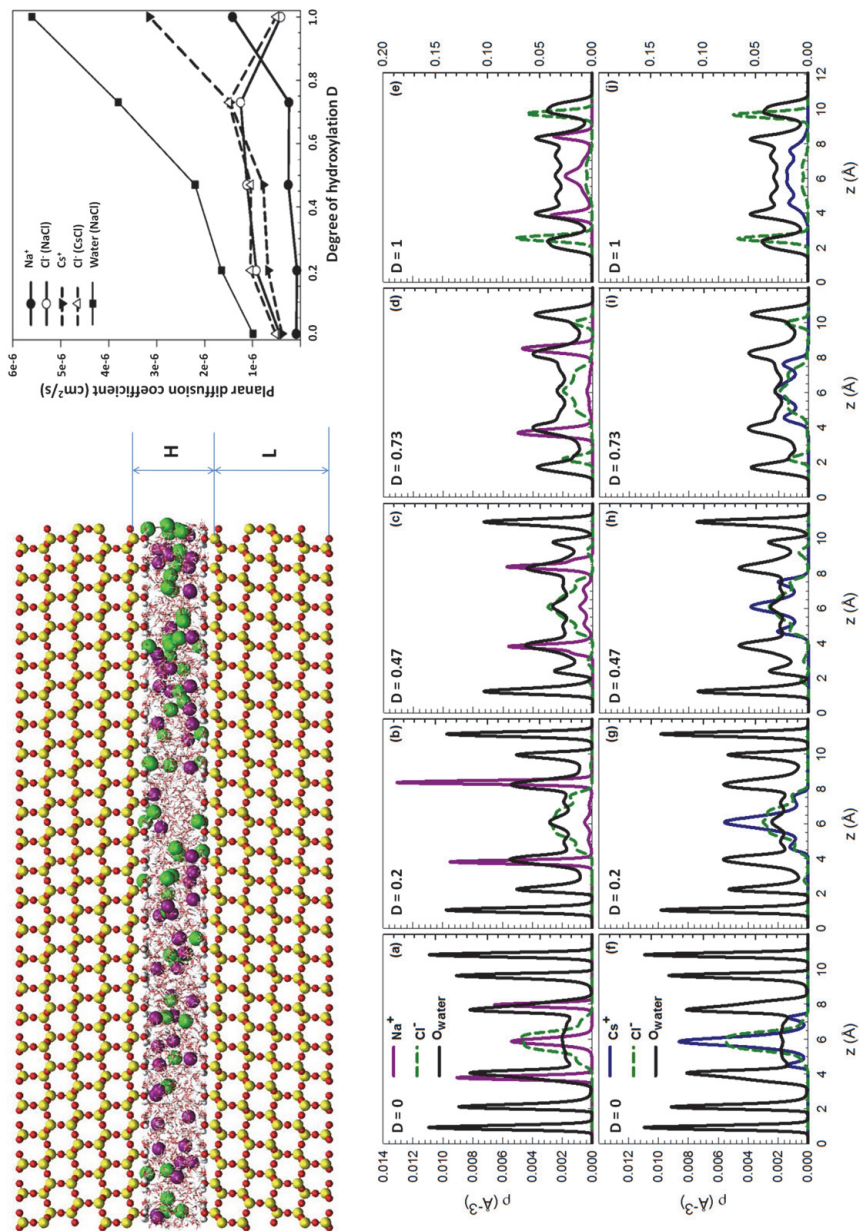


**Figure 19.** (top left) Schematic representation of the slit-shaped silica pores simulated by Ho et al. (2012). The pore width,  $H$ , is  $\sim 1$  nm. (top right) Predicted in-plane self-diffusion coefficients for water and electrolytes within the pores as a function of the degree of protonation  $D$ . (bottom) Density distribution across the pore volume for oxygen atoms of water (dashed lines), Na<sup>+</sup> (purple), Cs<sup>+</sup> (blue), and Cl<sup>-</sup> ions (dashed green lines) as a function of  $D$ . [Used by permission of the American Chemical Society © 2012, from Ho et al. (2012) *Langmuir*, Vol. 28, Fig. 1, p. 1257, Fig. 5, p. 1261, and Fig. 4, p. 1259.]

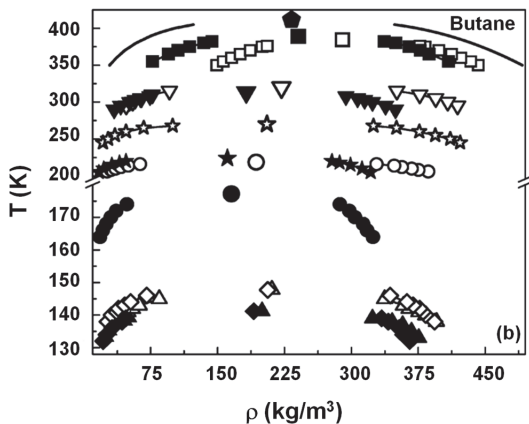


**Figure 20.** Vapor-liquid coexisting curves for butane confined in mica and graphite slit-shaped pores. The line represents the phase diagram in the bulk. Filled symbols are for graphite, open ones for mica pores. Different symbols are for pores of different widths. As the pore width decreases, the critical temperature decreases. [Used by permission of the American Chemical Society © 2009, from Singh et al. (2012) *J Phys Chem-C* Vol. 113, Fig. 2, p.7173.]

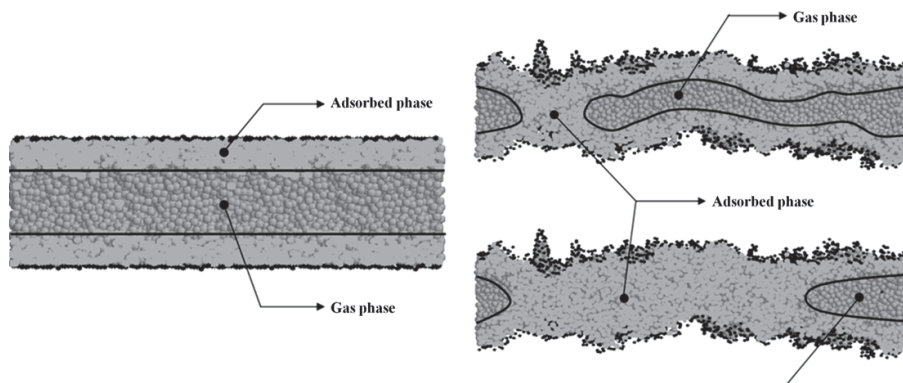


**Figure 21.** (left) Transverse section of a simulation snapshot illustrating Ar atoms adsorbed within a smooth model of the MCM-41 pore at 87K and relative pressure 0.69. The black lines divide the adsorbed fluid from the gaseous phase within the pore. (right) Transverse section of an atomically rough model pore partially filled with Ar at 87 K and relative pressures 0.44 (top) and 0.46 (bottom). Although the relative pressure is lower, the snapshots on the right suggest that the adsorbed phase fills more of the pore volume, and that the gaseous phase is trapped only within a few bubbles. [Used by permission of the American Chemical Society © 2006, from Coasne et al. (2006) *Langmuir*, Vol. 22, Fig. 7, p. 199 and Fig. 8, p. 200.]

the adsorbed fluid and the confined gas at the center of the pore, while in the rough pore model (right panel) a few bubbles of gas are found trapped within the adsorbed fluid. It is very likely that the transport properties in this dual-phase system strongly depend on the structure of the confined fluid, and therefore the predictions obtained with the two models are expected to be very different [no transport properties were reported by Coasne et al. (2006)]. Because subsurface pores are likely to be very heterogeneous in size, shape, surface morphology, and even chemical composition, in our opinion the observations from Coasne et al. (2006) should be kept in mind when simulation data are compared to experiments.

It is very likely that the phase equilibrium within the pores will determine the diffusion of confined substances. Ho et al. (2012), for example, found that aqueous  $\text{Na}^+$ ,  $\text{Cs}^+$ , and  $\text{Cl}^-$  ions partition at different distances from the solid surface within the pores depending on the protonation state of the surface, leading to significantly different mobility for the various ions (see Fig. 19). Analogous results obtained for organic systems could lead to strategies for enhancing the

dislocation of various fluids trapped in subsurface formations. For example, the preferential adsorption of  $\text{CO}_2$  compared to  $\text{CH}_4$  near the carbon-based pores used in the simulations of Firouzi and Wilcox (2012) was invoked to explain the different permeability observed for the two gases, either pure or in binary mixtures (see Fig. 18). The preferential adsorption of  $\text{CO}_2$  with respect to  $\text{CH}_4$  in coal beds is the basis of the enhanced coal bed methane recovery (White et al. 2005). Unfortunately, this process is also responsible for the differential swelling of the coal (i.e., coal swells more when  $\text{CO}_2$  is adsorbed than when  $\text{CH}_4$  is adsorbed), which causes a reduced permeability of methane as  $\text{CO}_2$  is injected. Brochard et al. (2012a) conducted a simulation study for the competitive adsorption of  $\text{CO}_2$  and  $\text{CH}_4$  in realistic models of carbon pores obtained with the reverse Monte Carlo method (Jain et al. 2006a,b; Nguyen et al. 2008). They considered temperatures and pressures representative for geological applications. They then applied a poromechanical model, developed independently by Brochard et al. (2012b), for predicting the material swelling as a function of the amount adsorbed. Representative results, shown in Figure 22, show that  $\text{CO}_2$  adsorption is highly selective compared to  $\text{CH}_4$  adsorption. Differential swelling is almost insensitive to the geological temperatures and pressures considered, while it appears to be proportional to the  $\text{CO}_2$  mole fraction in the pores. Although swelling of coal beds is certainly dependent on additional factors, including the stress imposed in the rock formation by the surroundings, these results could aid interpretation and prediction of experimental observables.

As another example to illustrate preferential distributions of different fluids at contact with a solid substrate, in Figure 23 we compare preliminary simulation snapshots obtained for pure ethanol (left) and for an ethanol-water mixture (right) on a free-standing (0001)  $\alpha\text{-Al}_2\text{O}_3$  substrate at 298 K and 0.1 MPa. When ethanol is the only fluid present, the results suggest the formation of a dense adsorbed layer on the substrate. When a small amount of water is added to the system, water molecules dislocate the adsorbed ethanol, they form a dense hydration layer, and the ethanol molecules are segregated further from the surface. Because those molecules (either ethanol or water) found in proximity to the substrate tend to show low mobility, should results similar to those presented in Figure 23 be observed also within narrow pores it is likely that pure ethanol will have low permeability within alumina-based rock formations, and that the addition of small amounts of water could potentially allow for an increased ethanol mobility. It is also possible that if the pores are extremely narrow, water molecules would fill the pores and block ethanol molecules from permeating the rock formation. Clearly, careful verification of such predictions needs to be conducted. This brief discussion points out the need of carefully analyzing the composition of the subsurface fluids, together with details concerning the pore network (e.g., pore size, shape, entrance, and chemical composition) for predicting the permeability of different fluid systems.

**Liquid-solid transitions under confinement.** Using macroscopic thermodynamic arguments (equating the free energies of confined solid and liquid phases, Warnock et al. 1986), or calculating the chemical potential as a function of temperature for confined liquid and solid phases (Evans and Marconi 1987), it is possible to derive the Gibbs-Thomson equation to relate the freezing temperature for a confined fluid to the pore size. The latter relation is invoked in the experimental technique of thermoporometry, used to characterize porous materials (Eyraud et al. 1988). Unfortunately, the Gibbs-Thomson relationship fails as the pore size becomes comparable to the molecular diameter. Alba-Simionesco et al. (2006) provided a clear and concise review on the subject. Recent results show that the freezing temperature of the confined fluid can increase or decrease compared to bulk values, depending on whether the fluid-wall interactions are weaker or stronger than fluid-fluid interactions, respectively. Sometimes exotic phases, not observable for bulk systems, can be observed under confinement (e.g., the hexatic phase) (Radhakrishnan et al. 2000, 2002).

Combining experiments and simulations leads to important observations regarding the fluid-solid transition for confined systems. For example, Coasne et al. (2009) investigated, using

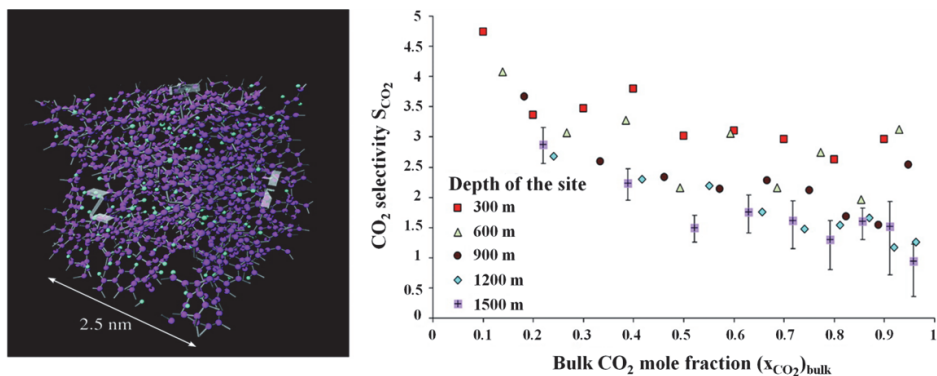


**Figure 22.** (left) Schematic representation of the model used to simulate a carbon adsorbent (i.e., coal bed). (right) Selectivity of  $\text{CO}_2$  with respect to  $\text{CH}_4$  adsorption as a function of bulk  $\text{CO}_2$  mole fraction. Different symbols represent data obtained at different geological conditions (depths of the coal bed). Note that in most cases the selectivity is well above 1. [Used by permission of the American Chemical Society © 2012, from Brochard et al. (2012a) *Langmuir*, Vol. 22, Fig. 1, p. 2661 and Fig. 6, p. 2664.]

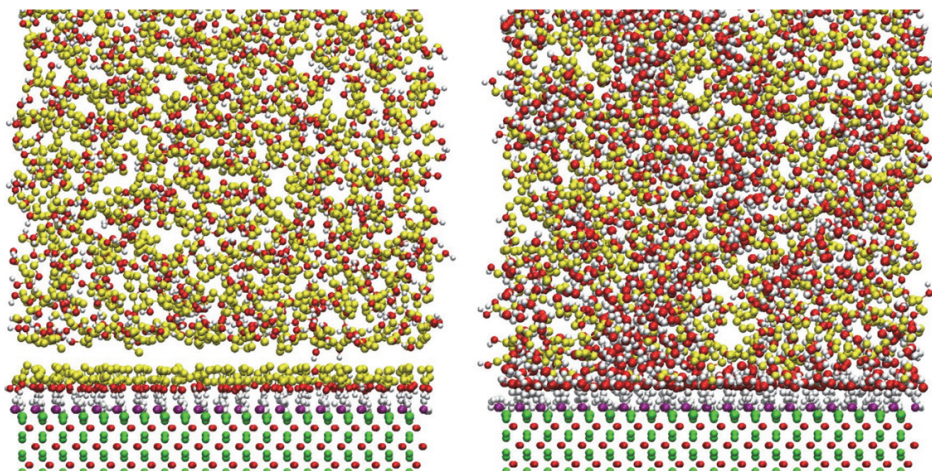


**Figure 23.** Preliminary simulation results for pure ethanol (left panel) and for a water-ethanol mixture containing 50% water molecules (right panel) at contact with a free-standing fully protonated (0001)  $\alpha$ - $\text{Al}_2\text{O}_3$  surface. Ethanol molecules are shown in yellow (red and white are for the OH groups). Simulations performed at 298 K and 0.1 MPa. Note that when ethanol is at contact with the substrate, a dense layer forms near the surface. As water molecules are added to the system, these replace ethanol and form one dense hydration layer near the substrate. Because those fluid molecules near the substrate tend to show lower mobility than those far from it, these preliminary simulation results suggest that adding some water could enhance the permeability of ethanol through alumina-based rock formations.

parallel tempering Monte Carlo techniques, the freezing of pure methane and argon, as well as of their mixtures in a slit-shaped graphitic pore. Because the pore is strongly attractive to both fluids, the freezing temperature for both confined substances, as well as for their mixtures, was found to be larger than that in the bulk. The phase diagram for the confined mixture showed an azeotrope, similarly to that observed for the bulk mixture. Regarding azeotropic mixtures, Czwartos et al. (2005) reported dielectric spectroscopy experiments for  $\text{CCl}_4/\text{C}_6\text{H}_{12}$  mixtures confined in carbon fibers and grand canonical Monte Carlo simulations for  $\text{Ar}/\text{CH}_4$  mixtures

confined in carbon-slit pores. The results are summarized in Figure 24. Both experiments and simulations show that qualitatively the phase diagram for either mixture does not change upon confinement (note the azeotrope). However, because all fluids considered are strongly attracted to the confining pores, the coexistence lines are shifted to higher temperatures upon confinement. The other important observation is that the composition of the azeotrope is enriched in the component that is most strongly attracted to the carbon pores ( $C_6H_{12}$  in the case of the  $CCl_4/C_6H_{12}$  mixture, Ar in the case of the Ar/ $CH_4$  mixture). A cautionary note should be made here, as the experiments could not assess the composition of the mixture under confinement. The authors speculate that the experimental mole fractions for the confined system under-estimate the mole fraction of  $C_6H_{12}$ , as this substance is more strongly attracted to the carbon surfaces.

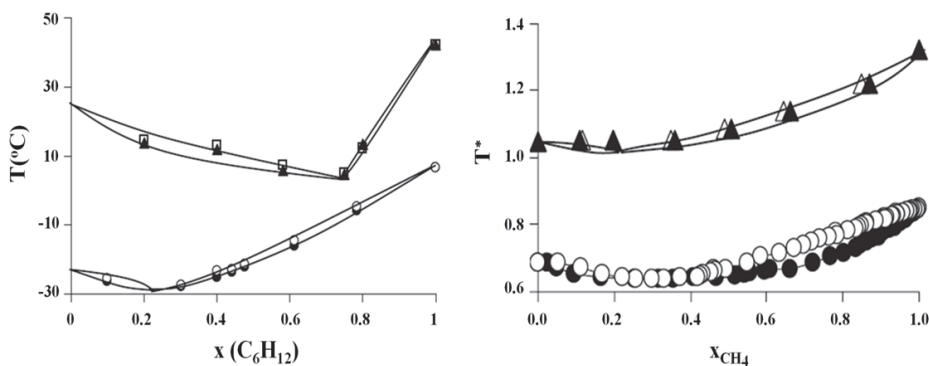


**Figure 24.** (left) Experimental phase diagram for  $CCl_4/C_6H_{12}$  mixtures (mole fraction) as measured by dielectric spectroscopy in activated carbon fibers. Circles are for the bulk mixtures, triangles and squares are for the mixtures at contact with the porous adsorbent. Because the experiments were conducted for fluid mixtures at contact with the porous material, the compositions reported are for the overall system. (right) Simulated phase diagram for Ar/ $CH_4$  mixtures in graphitic slit pores. Circles are for the bulk mixtures, triangles for the mixtures under confinement. In both panels open and closed symbols are liquid and solid coexistence data, respectively; lines are guides to the eye. [Used by permission of Taylor and Francis © 2005, from J. Czwartos et al. (2005) *Molecular Physics*, Vol. 103, Fig. 3, p. 3107 and Fig. 9, p. 3110.]

Given the interest in carbon-based pores for the possible combined application of  $CO_2$  sequestration and enhanced methane recovery, it is worth highlighting some results reported by Hung et al. (2005). These authors conducted Monte Carlo simulation studies for Lennard-Jones fluids confined within carbon nanotubes. The results showed that the tube diameter is very important in determining not only the solid-liquid transition for the confined fluid, but also the structure of the solid phase under confinement. In particular, when the tube diameter was  $\sim 9.6$  times the diameter of one fluid molecule the simulations did not show a solid structure similar to the one observed in the bulk. Further, while the molecules in contact with the confining walls showed an increase in the freezing temperature, those close to the nanotube center showed a depression in the freezing temperature. The simulation results appeared to be in reasonable agreement with dielectric spectroscopy experiments. There is no doubt that freezing will have a strong effect on the mobility of the confined fluids. It is possible that some fluid, maybe present in small amounts within the porous network, by freezing effectively blocks some pores and reduces the rock permeability. These effects could be facilitated by the strong expansions (from high to ambient pressures) typically observed when natural gas and/or other geological fluids are extracted from geological formations.

### Selected simulations of alkanes within alumina and silica-based pores

Simulations, in particular molecular dynamics (complemented by Monte Carlo and *ab initio* density functional theory, DFT), have become a routine tool to study the properties of bulk fluids, including those of water, alkanes, and their mixtures. Unfortunately, studying fluids at contact with a solid substrate is hindered by the uncertainties regarding the solid-fluid interaction potentials, and also by the fact that the relaxation time of the solid is typically much longer than that of the fluid. However, it is now recognized that simulation results can significantly improve the interpretation of experimental data, especially when direct observation is difficult, as in the case of confined fluids. Some examples have been given in the “*Properties of confined fluid*” section. More and more evidence suggests that semi-quantitative agreement can be obtained between simulation predictions (sometimes even obtained by implementing force fields not necessarily derived to reproduce experimental data for fluid-solid interfaces) and experimental observations. When some disagreement is observed, it could be used as a valid reason to improve the simulation models, but also to revisit the interpretation of the experimental data, which could lead to discoveries. We highlight below a few simulation studies for alkanes in contact with alumina and porous silica. Compared to the studies for simple fluids, which have been the basis for the general aspects discussed above, the studies for long alkanes are somewhat limited. As the importance of understanding fluid behavior and rock-fluid interactions in subsurface formations grows, so is the need to further the investigations summarized herein.

**Alkanes near alumina.** Alumina is frequently used as catalyst and catalyst support, and it also constitutes part of clay, a naturally occurring material. Understanding the behavior of fluids near to, or confined between, alumina surfaces is therefore of wide interest.

The Al-terminated  $\alpha$ -Al<sub>2</sub>O<sub>3</sub> surface shows significant relaxation of the solid atoms, as suggested by both theoretical (Konstadinidis et al. 1992; Manassidis and Gillan 1994; Streitz and Mintmire 1994) and experimental observations (Ahn and Rabalais 1997). It also readily reacts when exposed to water. The hydroxylated form of the  $\alpha$ -Al<sub>2</sub>O<sub>3</sub> surface shows limited relaxation (Wittbrodt et al. 1998). Whether or not the solid atoms near the interface relax compared to the positions they would occupy in the bulk of the material has important consequences in the structure predicted for interfacial fluids. For example, Li and Choi (2007) employed a number of techniques to study linear C-11 and C-200 alkanes on an alumina support. They first relaxed the Al-terminated alumina substrate using *ab initio* DFT, and then used molecular dynamics (MD) to study the structure of the liquid alkanes adsorbed onto the substrate, maintained rigidly. Representative results, shown in Figure 25, are interesting for a number of reasons: (1) the density profiles obtained for the short alkane are qualitatively, though not quantitatively, similar to those obtained for the long chains, which is consistent with surface force apparatus (SFA) experiments for alkanes of different lengths confined between mica surfaces; and (2) the relaxed alumina substrate promotes the formation of well-defined density layers formed by alkane segments (CH<sub>3</sub> groups) as the distance from the surface increases while the non-relaxed surface does not (these observations suggest that the relaxed alumina support is commensurate with the alkane molecules and promotes the formation of contact layers within which the alkane chains lay parallel to the solid surface).

Jin et al. (2000) obtained results to some extent analogous to those just discussed when they employed MD to study the structure of C-8, C-16, and C-32 alkanes confined between two parallel alumina surfaces. The alumina surfaces were hydroxylated, and the authors reported limited relaxation compared to bulk structures when DFT calculations were performed (Wittbrodt et al. 1998). Thus, a crystalline structure was assumed for the solid. The simulations were conducted at 300 K. Pronounced layering was observed in the atomic density profiles for up to 4-5 atomic layers (up to 2.0-2.5 nm) from each surface. The density profiles were qualitatively similar for all alkanes considered. This result (layering) appears to be consistent

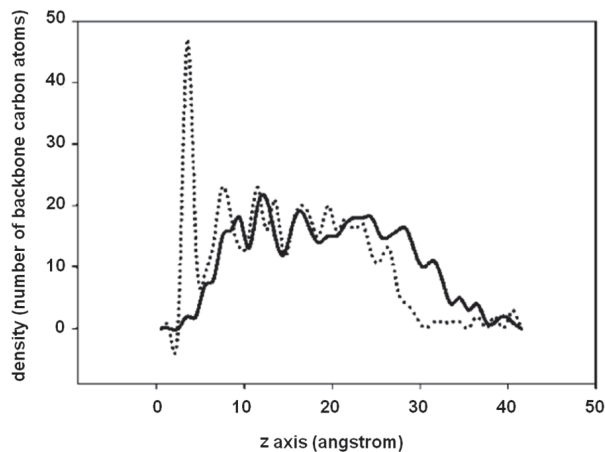


**Figure 25.** Density profiles for  $\text{CH}_2/\text{CH}_3$  groups as a function of the distance from a flat alumina substrate. Results are shown before the substrate was relaxed (black line) and after the relaxation (dotted line). Relaxing the surface yields pronounced layering in the film. [Used by permission of the American Chemical Society © 2007, from Li and Choi (2007) *J Phys Chem-C*, Vol. 111, Fig. 4, p. 1751.]

with a number of simulation results for liquid straight-chain alkanes confined between two parallel surfaces (Bitsanis and Hadziioannou 1990; Vacatello et al. 1990; Balasubramanian et al. 1995, 1996; Dijkstra 1997; Gao et al. 1997a,b; Wang and Fichthorn 1998), structured or unstructured (Magda et al. 1985). Compared to results obtained by Li and Choi (2007), the simulations reported by Jin et al. (2000) were conducted for fluid molecules confined within two parallel surfaces, which in general promotes longer-ranged ordering than does one free-standing surface. This difference might be the reason why Li and Choi did not report ordering for alkanes adsorbed on a non-relaxed surfaces, whereas Jin et al. found pronounced ordering for any type of confining surfaces.

In addition, by analyzing the layer-by-layer intra-molecular radial distribution functions Jin et al. (2000) showed that the alkane chains adsorbed onto the alumina substrate have a tendency to adopt a trans conformation, which has also been found for alkanes adsorbed on gold (Balasubramanian et al. 1995). Finally, the dynamics of the adsorbed alkane chains were found to be significantly delayed compared to that of bulk alkanes, and infrequent exchanges were observed between alkanes belonging to different layers (the simulations were only conducted for at most 1 ns; current computational capabilities would allow researchers to reach up to 50-100 ns). This latter observation suggests the existence of a correlation between spatial distribution and dynamic properties. Namely, the alkane chains that are located near the surfaces show less mobility than those found away from the surfaces, suggesting that when a technology is designed to “detach” the alkanes from the pore surfaces, enhanced permeability could be achieved.

Along these lines, de Sainte Claire et al. (1997) conducted MD simulations for a system composed of a free-standing Al-terminated alumina surface, a thin layer of pre-adsorbed alkanes (butane, octane, and dodecane), and a small cluster of 30 water molecules. They found that the water molecules penetrate the pre-adsorbed thin film of alkane chains because they are attracted to the alumina substrate via long-range electrostatic interactions. During the penetration process, a competition was found between the displacement of the hydrocarbon chains, and the densification of the adsorbed thin film. Both phenomena were caused by the penetrating water molecules. The process of penetration was found to become more difficult as the alkane chain length increased and as the temperature decreased. In Figure 26 we reproduce the simulation results for the evolution of the probability of finding water molecules at various distances from the alumina substrate when the 30 water molecules were placed near the bare alumina (left) or near the alumina substrate covered by 2.6 monolayers of octane. In the case

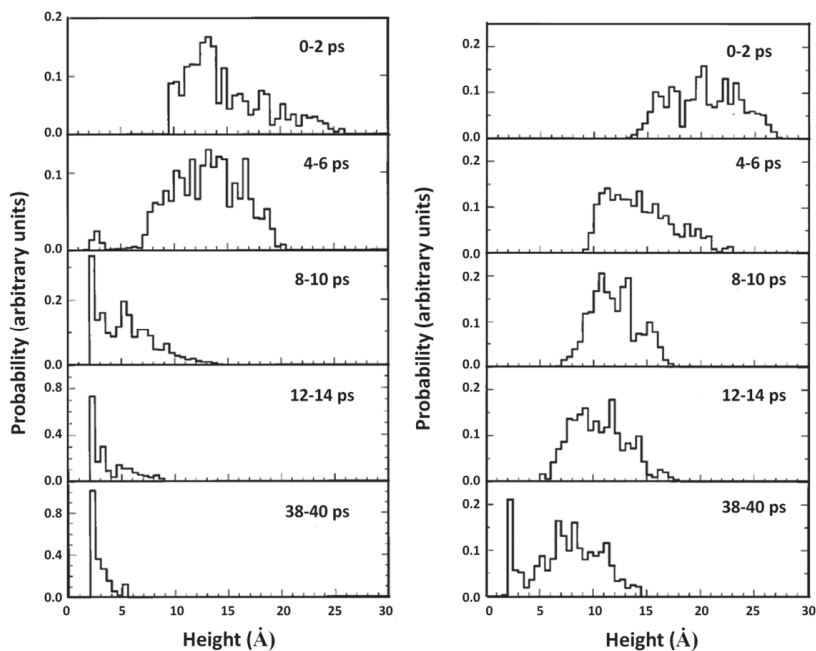


**Figure 26.** Time evolution of the density probability of observing water molecules at various vertical distances from the (0001) surface of  $\alpha$ - $\text{Al}_2\text{O}_3$ . In the left panel a cluster of 30 water molecules was placed initially at about 1.5 nm from the bare surface. On the right panel the cluster of 30 water molecules was placed on a surface on which 2.6 monolayers of octane were pre-adsorbed. The time intervals indicate the length of the MD simulations performed. Water molecules quickly adsorb and spread on the bare surface, yielding a monolayer (*left*). When the surface is covered by octane (*right*) water molecules manage to come in contact with the alumina substrate, although a perfect monolayer is not obtained within the 40 ps of the simulations presented. Simulations were performed at 300 K. [Used by permission of American Institute of Physics © 1997, from de Sainte Claire et al. (1997) *J Chem Phys*, Vol. 106, Fig. 6, p. 7339 and, Fig. 9, p. 7340.]

of water on bare alumina, water molecules readily form a monolayer on the substrate, which is in qualitative agreement with recent MD simulations (Argyris et al. 2011). When octane is present the water molecules still manage to come in contact with the substrate, although the process takes longer to complete and the distribution of water molecules after 40 ps spans the  $\sim 1.5$  nm near the substrate. Note that in recent years computational capabilities have become highly evolved, and it would now be possible to perform simulations such as those of Figure 26 for several hundreds of ns.

Studies such as the one just summarized are important for providing interpretation to detailed experimental studies of alkane-mineral interfaces, such as, for example, the broadband sum frequency generation studies recently reported by Buchbinder et al. (2010). Other simulation studies along similar lines have investigated the deposition of waxes on hematite (San-Miguel and Rodger 2003), sometimes in the presence of other compounds (San-Miguel and Rodger 2010).

Regarding confined mixtures, it should be pointed out that smectites, present in sediments and soil, have been found to host a variety of hydrated organic molecules in their interlayer (Kaiser and Guggenberger 2000; Kennedy et al. 2002; Kawahigashi et al. 2006), and that large amounts of methane appear to be stored in clay minerals present in marine sediments (Hinrichs et al. 2006; Ertel et al. 2010). These observations stimulated experimental (Cha et al. 1988;

Guggenheim and Koster van Groos 2003; Seo et al. 2009) and simulation (Sposito et al. 1999; Titiloye and Skipper 2000; Park and Sposito 2003; Cygan et al. 2004a; Zhang and Choi 2006; Zhou et al. 2011) studies for methane-water mixtures confined within various smectites. The simulation results suggest that under confinement one methane molecule is hydrated by ~12-13 water molecules and remains at contact with ~6 oxygen atoms on the clay surface. Because in bulk hydrates one methane molecule is hydrated by 21 waters (Koh et al. 2000), the simulations suggest that methane prefers to accumulate near the solid substrate when it is confined in smectites.

When MD simulations are conducted to study mixtures, one source of uncertainty is whether or not the system studied is at equilibrium. At equilibrium the chemical potential for each of the fluid molecules under confinement should be equal to that of the fluid molecules in a correspondent bulk mixture. Typically, grand canonical Monte Carlo simulations are conducted to ensure that the chemical potential of a fluid under confinement is equal to that of the fluid in the bulk (Nicholson and Parsonage 1982). Indeed, by implementing such algorithms it is possible to simulate adsorption isotherms for various fluids, pure or mixtures, into porous materials. However, for dense systems composed of long hydrocarbons, and maybe containing hydrogen-bonding fluids under confinement, the acceptance of addition/deletion Monte Carlo moves is likely to be very low, and advanced simulation schemes need to be implemented. To overcome this requirement, and taking advantage of the enormous computational resources that are becoming available, we have implemented MD procedures to attempt to investigate the equilibrium partition of different fluid molecules between bulk systems and nanometer-scale pores. In Figure 27 we show one simulation snapshot, obtained for a mixture of water and methane at contact with a narrow slit-shaped  $\text{Al}_2\text{O}_3$  pore of width ~1 nm. The alumina substrate is fully hydroxylated. Although the simulations are still preliminary, and proper assessment of their reliability has yet to be completed (e.g., we need to ensure that similar results are obtained when simulations are conducted from different initial configurations), the results clearly show that the bulk behavior of the water-methane mixture differs substantially compared to the behavior of the mixture under confinement. Water appears to be strongly attracted to the slit pore, while methane prefers to stay in the bulk region. A few water molecules escape the pore volume, but remain close to the pore entrance, where they can form energetically advantageous hydrogen bonds with other water molecules, and also interact favorably with the solid atoms. Although most methane molecules remain outside of the pore in the bulk, some methane molecules are found trapped within the pore. Contrary to what has been suggested in the case of smectites, the simulation snapshots of Figure 27 (see expanded view in the bottom panel) suggest that methane molecules prefer to accumulate near the pore center, where they are completely surrounded by water. Understanding how the structure of hydrated methane changes as the pore width and the pore chemistry change is important for a number of practical applications that include hydraulic fracturing. It appears that simulations, especially when synergistically coupled with experimental characterization, have the potential of helping this important quest.

**Alkanes in silica-based porous materials.** Many studies have focused on uncovering the properties of alkanes confined within silica-based pores. In particular, large attention has been given to zeolites, which are aluminosilicates. The composition of the zeolite has important consequences on its chemical physical properties. For example, when the aluminum content is high the zeolite is expected to become highly polar; as a consequence, preferential adsorption of polar molecules (e.g., water) is expected. Under such circumstances even small amounts of water present in the system can affect the adsorption of other gases (Brandani and Ruthven 2004; Galhotra et al. 2009; see, as a only partially related example, the simulation snapshot of Fig. 27). For example, the FAU type X zeolite, with a Si to Al ratio of 1-1.5, has been used in the form of membranes for the separation of methanol and water from systems containing hydrogen and carbon dioxide, respectively, in a large temperature interval (Sandstrom et al. 2010).

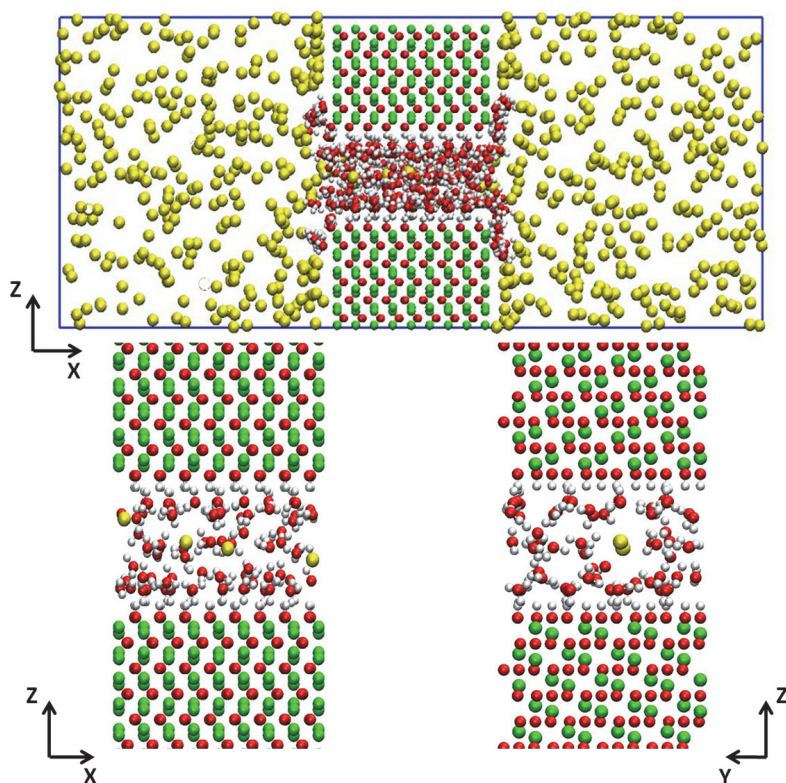


**Figure 27.** Preliminary simulation snapshot for a fluid system composed of methane (yellow spheres) and water molecules (red and white spheres represent oxygen and hydrogen atoms, respectively) partitioned between a bulk region (enriched in methane) and a slit-shaped pore of width  $\sim 1$  nm. The pore is obtained by two facing surfaces of hydroxylated  $\alpha$ - $\text{Al}_2\text{O}_3$ . The bottom panels are enlargements of the simulation snapshot in the top panel, showing how the methane molecules trapped within the pore are preferentially found near the pore center, surrounded by water molecules. Simulations were performed at 300 K and 8-10 MPa for a mixture containing 50% methane molecules.

Due to a number of practical applications not limited to extraction of hydrocarbons from subsurface formations (e.g., catalysis), the study of alkanes, as well as of their mixtures confined in zeolites is growing rapidly. In Figure 28 we reproduce high-resolution scanning transmission electron microscopy images for the HY zeolite recently reported by Lu et al. (2012). In this study iridium is deposited on the zeolite for catalytic purposes, which is beyond the scopes of this chapter. The figure is important for remembering the high degree of confinement expected for fluids confined within zeolites (see, for example, Fig. 17 for a discussion on this topic). Because of space limitations we concentrate primarily on pioneering recent contributions.

Smit pioneered the use of simulations, including Monte Carlo and MD, to understand the behavior of molecules confined within zeolites for explaining observations in catalysis. He studied simultaneously the effects of alkane adsorption within the zeolite pores, their diffusion, and their catalytic conversion. For example, Smit and Maesen (1995) employed grand canonical Monte Carlo simulations to study the adsorption of butane, hexane, and heptane in silicalite. They demonstrated that unexpected, and at the time still unexplained, features in experimental adsorption isotherms could be explained by a phase transition experienced by confined hexane and heptane molecules that lead to a collective freezing. The phase transition could only be

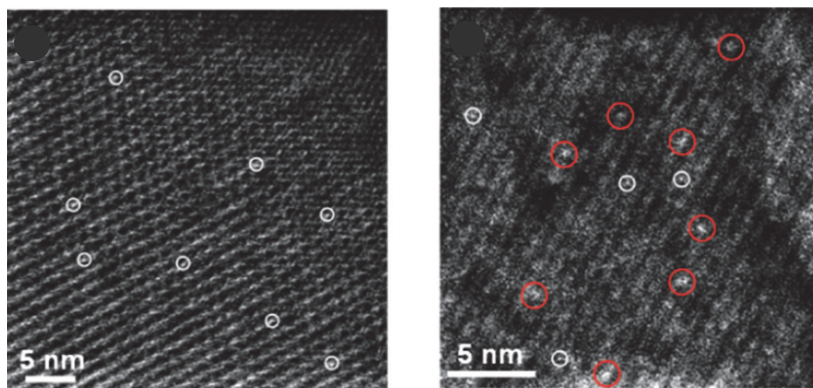


**Figure 28.** High resolution scanning transmission electron microscopy images of HY zeolite as prepared with  $\text{Ir}(\text{C}_2\text{H}_4)$ , (left), and after 1 h of flowing  $\text{H}_2$  at 300 K (right). The treatment causes individual Ir atoms (circled in white) to coalesce into clusters, circled in red. [Used by permission of the American Chemical Society © 2012, from Lu et al. (2012) *J Am Chem Soc*, Vol. 134, Fig. 1, p. 5022.]

observed for hexane and heptane because their length is commensurate with the porous structure of silicalite. For shorter and longer chains, similar phase transitions could not occur because of thermodynamic considerations, and typical type-I adsorption isotherms were obtained, both experimentally and by simulations. More recently adsorption isotherms have been calculated using Monte Carlo simulations by Ndjaka et al. (2004) for several short alkanes (methane, ethane, and propane) in a few different zeolites. The various zeolites selected are characterized by a relatively wide range of pore sizes, and the results, obtained implementing the Lennard-Jones parameters proposed by Vlugt et al. (1999), yield good comparison to experimental observations.

The diffusivity of methane, ethane, and propane was assessed via MD simulations within mordenite, zeolite EU-1, and silicalite (Nowak et al. 1991). The analysis of the simulation trajectories showed that the mobility of methane on the three substrates is not isotropic but is instead determined by the porous structure. As the adsorbate size increases, because of hindered diffusion, the diffusion coefficient decreases. Reasonable agreement was observed between the predicted diffusivities and experimental pulse field gradient NMR data (Briscoe et al. 1988). This contribution demonstrates the advantage of molecular simulations compared to experiments, as this computational approach allows researchers to identify the preferential trajectories for each adsorbed species, thus allowing a complete understanding of the properties of the confined fluids and how such properties depend on the morphology, chemical composition, etc., of the confining pores. Of course, satisfactory comparison to experiments is needed to ratify the reliability of the physical picture obtained.

As the computational capabilities evolved, it became possible to study the diffusion of linear and branched alkanes on various zeolites, and even to calculate the activation energies by producing Arrhenius-type plots (Webb et al. 1999). The models implemented to describe the zeolites have also become more and more realistic. Webb et al. (1999) showed that the geometry of the pores, the presence of protrusions, and that of void spaces along the channel walls strongly influence the diffusion coefficient, as well as the activation energy for diffusion of linear alkanes. The effects become even more pronounced when the alkane chains are branched (the branched alkanes simulated in this contribution contained one methyl group linked at various positions along the otherwise linear chain). The calculations were performed at low loadings and for up to 40 ns. Skoulidas and Sholl (2002) extended these types of calculations,

and investigated the effect of loading on the self-diffusion coefficient of small molecules (methane, helium, and argon) within silicalite. The results, in good experimental agreement, showed that the diffusion coefficient decreases as the loading increases. These authors also used the self-diffusion coefficients results to estimate transport diffusivities. The latter data have been instrumental for developing theoretical models to predict the permeability of zeolite membranes to various gases (Newsome and Sholl 2005).

Regarding studies on the effect of loading on permeability, it is worth remembering that Raghavan and Macelroy (1995) conducted equilibrium MD simulations for short alkanes adsorbed within models of silica gels at low loadings. They characterized the structure of the films adsorbed onto the solid substrate as a function of temperature. They found that the adsorbed hydrocarbon chains are characterized by a substantial broadening of the bond angle and dihedral angle distributions compared to the same molecules in the bulk. They also found that the diffusivity of the adsorbed chains increases as the loading increases because of screening of the fluid-pore interactions due to the pre-adsorbed molecules.

The simulation studies summarized here could be a starting point for addressing experimental observations of relevance for applications such as CO<sub>2</sub> sequestration. Key reactions and chemical mass transfer rates associated with progressive water-CO<sub>2</sub>-rock interactions can be assessed by batch experiments such as those conducted by Gysi and Stefansson (2012). These authors conducted batch experiments at 40 °C for up to 260 days for four mineral assemblages: A1 – mixtures of Ca-Mg-Fe carbonates and altered basaltic glasses; A2 – Fe hydroxides and/or oxyhydroxides; A3 – mixtures of Ca-Mg-Fe clays and altered basaltic glasses; and A4 – mixtures of Ca-Fe clays and altered basaltic glasses. They maintained these samples at contact with water containing different amounts of initial dissolved CO<sub>2</sub> (ranging from 24 to 305 mmol/Kg). Then they monitored the concentration of the various species in the aqueous phase as a function of time. The results, summarized in Figure 29, suggest that increased aqueous CO<sub>2</sub> concentrations modify considerably the natural water-basalt reaction pathways during CO<sub>2</sub> mineralization. Equilibrium studies for the preferential adsorption of various compounds on the rock surfaces, such as those briefly described here, coupled with appropriate *ab initio* DFT studies could be useful for better understanding such phenomena at conditions of geological importance.

### Simulation details

The interested reader is referred to specialized textbooks for a detailed discussion on simulation methods and algorithms (Nicholson and Parsonage 1982; Allen and Tildesley 1987; Frenkel and Smit 2002). This section is intended to summarize briefly some of the methods available to simulate systems of interest to subsurface applications, some of the models available to simulate alkanes, those that can be used to describe the solid substrate, and some of the experimental information that could validate the simulation results.

To study the properties of confined fluids from a theoretical/simulation perspective, a number of alternatives exist. The structure of confined fluids, as well as adsorption isotherms, can be calculated using classical density functional theory (Evans 1992) and integral equation theory (Henderson 1992) approaches. Both approaches require involved calculations for the minimization of the free energy, and often invoke approximations. An alternative, which is becoming widely accepted, is based on molecular simulations (Nicholson and Parsonage 1982). This latter approach is computationally expensive, and its reliability depends on the accuracy of the force fields implemented. It has the advantage of providing quantities that can be directly compared to experiments (e.g., self-diffusion coefficients, orientation of molecules near a substrate, radial distribution functions, vibrational frequencies, etc.). Very often molecular simulations are conducted within the MD formalism. However, it should be remembered that MD suffers from the difficulty of testing whether true equilibrium has been achieved. For example, the chromatography community has shown that MD simulations for confined systems

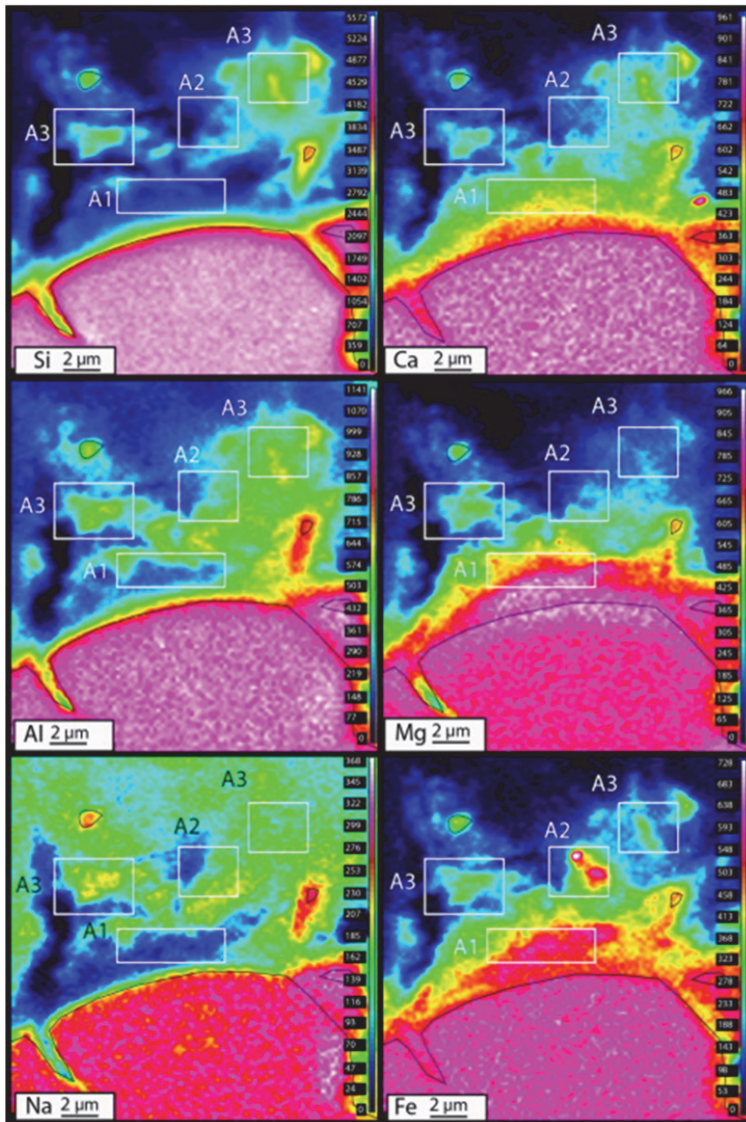


**Figure 29.** Elemental composition of mineral assemblages after a reaction time of 30 days. The samples were exposed to aqueous solutions with initial concentration of  $\text{CO}_2 < 50 \text{ mmol/Kg}$ , and maintained at  $40^\circ\text{C}$ . Compared to fresh basaltic glasses, A1 assemblages are depleted in Si, Al, and Na and enriched in Ca, Mg, and Fe; A2 assemblages are enriched in Fe and depleted of all other elements; A3 and A4 assemblages are enriched in Si, Al, Na, Ca, Mg, and Fe, although sometimes the amount of Na and Mg was found to be moderate. [Used by permission of Elsevier Pub © 2012, from Gysi and Stefansson (2012) *Geochim Cosmochim Acta*, Vol. 81, Fig. 9, p. 140.]

containing alkanes (in their case grafted to a silica substrate) and water are strongly influenced by the initial configurations (Klatte and Beck 1996; Schure 1998). Specifically, it was found that for water it is difficult to permeate hydrocarbon chains that have previously collapsed onto a silica substrate. Monte Carlo techniques provide more reliable results, independent of the initial configuration (Zhang et al. 2005).

An alternative approach to molecular simulations, which could be used to study the equilibrium properties of fluids confined within porous materials, is based on equations of state. These approaches are attractive because their analytical form provides quick estimates for phase equilibria and mixture composition, although they rely on rather strong simplifications for fluid-fluid and fluid-pore interactions and they cannot provide density distributions within the pores, nor dynamical properties for the confined species. However, they could be used to estimate the composition of the confined fluids, which is necessary to initiate more involved molecular dynamics simulations. The development of equations of states for confined fluids is due to numerous contributions. Zhu et al. (1999) considered fluids in cylindrical mesopores (e.g., MCM-41). Schoen and Diestler (1998) applied the perturbation theory to describe fluids in slit-shaped pores. Giaya and Thompson (2002) applied the latter methodology successfully to describe water in cylindrical pores. Zarragoicoechea and Kuz (2002) extended the van der Waals equation of state to fluids in square pores. Derouane (2007) further extended the approach and obtained agreement with experimental data for the reduction in the critical temperature compared to bulk values for the confined fluid (Derouane 2007). Travalloni et al. (2010) applied the van der Waals approach to model simple fluids and their mixtures confined in porous solids. The model manages to reproduce several adsorption isotherm types, successfully correlates to experimental data for pure hydrocarbons adsorbed in pores, and reasonably well predicts binary mixtures adsorption without the need of binary interaction parameters. The mixtures considered included toluene and 1-propanol in DAY-13 zeolites, and methane and ethane in MCM-41.

**Models for alkanes.** One model available to describe alkanes has been developed by Smith and coworkers both at the explicit and at the united-atom levels (Smith and Yoon 1994). With subtle modifications, this model has been used to study, for example, interactions between polymer nanofibers (Buell et al. 2010), and it reliably reproduces structural and dynamical properties of bulk alkanes. Alternative force fields for alkanes include the widely applied united-atom version of the transferable potentials for phase equilibria (TraPPE-UA; Martin and Siepmann 1998, 1999; Chen et al. 2001; Stubbs et al. 2004). Bolton et al. (1999) employed *ab initio* DFT to parameterize the interactions between the alkane model of Smith and coworkers and Al-terminated alumina substrates. They then compared the results obtained when either the explicit or the united-atom models were used to simulate octane at contact with alumina. The results suggest that when the structure of interfacial octane is considered, united-atom and explicit models yield comparable results. However, rotational and translational dynamics are not satisfactory when the united atom model is employed, suggesting the need of including an explicit description of the hydrogen atoms within the hydrocarbon chain.

Significant work has also been done in predicting the stability of clathrates in the water-methane system. Considering the selection of appropriate force fields, the contribution from Alavi et al. (2007) should be highlighted. These authors employed MD simulations and implemented careful free-energy calculation techniques to establish the occupancy of methane in H clathrate hydrates at 300 K and 2 GPa. They compared the OPLS united atom Lennard-Jones potential, the Tse-Klein-McDonald five-site force field, and the Murad-Gubbins five-site potential to describe methane. The results show that the force field implemented strongly influences the predicted occupancy. The OPLS and the Tse-Klein-McDonald models yield occupancy of 5 methane molecules per cage, while the Murad-Gubbins model yields smaller occupancy. The differences in the results are due to the less attractive methane-methane potentials implemented by the Murad-Gubbins model.

**Models for the solid substrates.** Solid mineral substrates can be simulated implementing the popular CLAYFF force field (Cygan et al. 2004b). However, it is suggested to validate the force field by reproducing known experimental observations for the system of interest. When interested in studying carbon-based materials, the interested reader could take advantage of the vast literature developed to study adsorption in realistic models of activated carbons (Petersen et al. 2003; Palmer et al. 2010). However, a rational effort to investigate the effect of confinement on the properties of alkanes and of their mixtures requires, in our opinion, the employment of simplified models (e.g., the slit-shaped pore), especially when mixtures are considered. One microscopic model that is simple enough to allow researchers to obtain meaningful insights, yet complex enough to reproduce important experimental observations, has been recently proposed by Kowalczyk et al. (2010). This model has proven successful in simulating the adsorption of small hydrocarbons, as well as that of mixtures containing hydrocarbons and hydrogen. The results are satisfactory when compared to experimental data obtained in carbon molecular sieves. Additionally, the anomalous transport of small molecules (hydrogen vs. methane) in carbon molecular sieves can be explained by using this model. It was found that the size of the nanopore constrictions determines the anomalous diffusion, while the size of the cages does not influence the transport properties of the confined fluids.

**Validation of simulation predictions.** When possible, simulation data should be compared to desorption energies estimated from temperature-programmed desorption experiments (Slayton et al. 1995), chromatographic results, and batch techniques (Partyka and Douillard 1995; Askin and Inel 2001; Dabrowski et al. 2003; Diaz et al. 2004). Electron energy loss spectroscopy (Machida et al. 2002) and attenuated total reflection Fourier transform infrared spectroscopy (ATR-FTIR) (Dubowski et al. 2004; Almeida et al. 2008) can be used to study surface species on flat surfaces. Raman (Resini et al. 2005; Kim and Stair 2009) and transmission IR (Mawhinney and Yates 2001; Yeom et al. 2004) spectroscopies could provide information for hydrocarbons adsorbed on high-surface-area powders. One technique that is becoming very popular for studying structural details of molecules with any orientation with respect to an interface is the vibrational sum-frequency generation (SFG), which has been used previously to study molecules on oxide surfaces (Nanjundiah and Dhinojwala 2005; Hayes et al. 2009; Stokes et al. 2009). For instance, Sefer et al. (1995) studied liquid hexadecane at the silica interface, and found a preferential orientation parallel to the interface. Buchbinder et al. (2010) studied linear and cyclic alkanes and alkenes at the liquid-alumina interface. The results show that liquid alkanes, both linear and cyclic, prefer to lay parallel to the solid substrate. On the contrary, unsaturated olefins did not show consistent trends. As noted above, the diffusion constant of gases in pores can be measured experimentally by conducting macroscopic uptake rate measurements and microscopic ones by conducting pulsed field gradient nuclear magnetic resonance (PFG NMR) and quasi-elastic neutron scattering (Kärger and Ruthven 1991; June et al. 1992; Maginn et al. 1996; Reyes et al. 1997; Runnebaum and Maginn 1997). In our opinion microscopic observations (e.g., NMR and/or neutron scattering) are preferable to macroscopic ones, because they provide a direct comparison to the results predicted by simulations.

## SUMMARY AND RECOMMENDATIONS

An atomistic to molecular-level understanding of how C-O-H fluids (e.g., water, CO<sub>2</sub>, CH<sub>4</sub>, higher hydrocarbons, etc.) interact with and participate in reactions with other solid Earth materials is central to the development of predictive models that aim to quantify a wide array of geochemical processes. The importance of the adsorption, microstructure and dynamics of important hydrocarbon and related fluids has been highlighted as well as the sensitivity of C-O-H fluid species to perturbations by a change in physical conditions or proximity to solute molecules and interfaces. Despite the large body of work that documents the nature of these processes and associated interactions with its local surroundings, it is premature to assume that

we have a complete understanding of the mechanisms that give rise to the particular properties exhibited by hydrocarbon fluids. Understanding is more limited as one goes both above and below ambient conditions. For example, there is continuing discussion on the metastability of hydrocarbon species as a system experiences more extreme elevated temperature and pressure relevant to deep Earth environments. This is of particular interest, since we have seen that nanoporous confinement of C-O-H fluids at ambient conditions leads to structural and dynamical features that deviate markedly from bulk system behavior. In the context of natural systems, interrogation of fluids and fluid-solid interactions at elevated temperatures and pressures is an area requiring much more work, particularly for complex solutions containing geochemically relevant aqueous species interacting with relevant C-O-H fluids within the interfacial regime. We have tried to describe a series of prototypical interfacial and surface problems using a number of examples to stimulate the thinking of Earth scientists interested applying some of these outcomes to confined systems of mineralogical importance.

Our ability to predict the molecular-level properties of fluids and fluid-solid interactions relies heavily on the synergism between novel experiments, such as neutron scattering or nuclear magnetic resonance and molecular-based simulations. Tremendous progress has been made in closing the gap between experimental observations and predicted behavior based on simulations, owing to improvements in the experimental methodologies and instrumentation on the one hand, and the development of new potential models for C-O-H fluid species on the other. There has been an emergence of studies taking advantage of advanced computing power that can accommodate the demands of *ab initio* molecular dynamics. On the neutron instrumentation side, while much of the quasi-elastic work described above has been performed using instrumentation located at reactor based sources, the advent of second-generation spallation neutron sources like ISIS, new generation sources like the SNS at the Oak Ridge National Laboratory, and the low repetition rate second-target station at ISIS now offer significant opportunities for the study of interfacial and entrained liquids. Development of unique sample cells that allow interrogation of higher temperature-pressure conditions relevant to crust and mantle settings are needed that can allow interrogation of complex fluid-solid interactions. An improvement of the counting statistics by one to two orders of magnitude on many instruments, such as vibrational and time-of-flight spectrometers at SNS, will allow parametric studies of many hydrocarbon-based systems that otherwise would be prohibitively time consuming. The extended- $Q$  SANS diffractometer and liquids reflectometer at SNS will offer very high intensity and unparalleled  $Q$ -range to extend the accessible length scale in real space, from 0.05 nm to 150 nm. The backscattering spectrometer will provide very high intensity and excellent energy resolution through unprecedented range of energy transfers, thereby allowing simultaneous studies of translational and rotational diffusion components in various systems. The vibrational spectrometer, with two orders of magnitude improvement in performance and the capability to perform simultaneous structural measurements, should present exciting opportunities as well, and support a new population of users interested in quantifying behavior of hydrocarbons and other fluid species relevant to Deep Earth.

## ACKNOWLEDGMENTS

The authors are grateful to Robert Hazen and Dimitri Sverjensky for their thorough reviews and insightful comments. Support comes from the Sloan Foundation, Deep Carbon Observatory administered by the Geophysical Laboratory of the Carnegie Institution of Washington; and the Department of Energy, Office of Basic Energy Sciences, Geosciences Program. The authors wish to also thank David Tomasko at Ohio State, Gernot Rother, Mirek Gruszkiewicz, and Eugene Mamontov at Oak Ridge National Laboratory, and Karl Mueller at Pacific Northwest National Laboratory for their continued support of our experimental efforts.

## REFERENCES

- Abragam A (1961) *The Principles of Nuclear Magnetism*, Clarendon Press, Oxford
- Aeberhardt K, Bui QD, Normand V (2007) Using low-field NMR to infer the physical properties of glassy oligosaccharide/water mixtures. *Biomacromolecules* 8:1038-1046
- Ahn J, Rabalais JW (1997) Composition and structure of the  $\text{Al}_2\text{O}_3$  {0001}-(1 $\times$ 1) surface. *Surf Sci* 388:121-131
- Alavi S, Ripmeester JA, Klug DD (2007) Molecular dynamics study of the stability of methane structure H clathrate hydrates. *J Chem Phys* 126:124708-1 - 124708-6
- Alba-Simionesco C, Coasne B, Dosseh G, Dudziak G, Gubbins KE, Radhakrishnan R, Sliwiska-Bartkowiak M (2006) Effects of confinement on freezing and melting. *J Phys Condens Matter* 18:R15-R68
- Alcantar N, Israelachvili J, Boles J (2003) Forces and ionic transport between mica surfaces: Implications for pressure solution. *Geochim Cosmochim Acta* 67:1289-1304
- Allen MP, Tildesley D (1987) *Computer Simulations of Liquids*. Oxford University Press: New York
- Almeida AR, Moulijn JA, Mul G (2008) *In situ* ATR-FTIR study on the selective photo-oxidation of cyclohexane over anatase  $\text{TiO}_2$ . *J Phys Chem C* 112:1552-1561
- Anzalone A, Boles J, Greene G, Young K, Israelachvili J, Alcantar N (2006) Confined fluids and their role in pressure solution. *Chem Geol* 230:220-231
- Aranovich G, Donohue M (1998) Analysis of adsorption isotherms: lattice theory predictions, classification of isotherms for gas-solid equilibria, and similarities in gas and liquid Adsorption behavior. *J Colloid Interface Sci* 200:273-290
- Argyris D, Cole DR, Striolo A (2009) Dynamic behavior of interfacial water at the silica surface. *J Phys Chem C* 113:19591-19600
- Argyris D, Ho TA, Cole DR, Striolo A (2011) Molecular dynamics studies of interfacial water at the alumina surface. *J Phys Chem C* 115:2038-2046
- Askin A, Inel O (2001) Evaluation of the heat of adsorption of some *n*-alkanes on alumina and zeolite by inverse gas chromatography. *Sep Sci Technol* 36:381-397
- Baerlocher C, McCusker LB, Olson DH (2007) *Atlas of Zeolites Framework Types*. Elsevier: Amsterdam
- Balasubramanian S, Klein ML, Siepmann JI (1995) Monte-Carlo investigations of hexadecane films on a metal-substrate. *J Chem Phys* 103:3184-3195
- Balasubramanian S, Klein ML, Siepmann JI (1996) Simulation studies of ultrathin films of linear and branched alkanes on a metal substrate. *J Phys Chem* 100:11960-11963
- Bee M (2003) Localized and long-range diffusion in condensed matter: state of the art of QENS studies and future prospects. *Chem Phys* 292:121-141
- Belonoshko AB (1989) The Thermodynamics of the aqueous carbon-dioxide fluid within thin pores. *Geochim Cosmochim Acta* 53:2581-2590
- Benes NE, Jobic H, Verweij H (2001) Quasi-elastic neutron scattering study of the mobility of methane in microporous silica. *Microporous Mesoporous Mater* 43:147-152
- Bhatia SK, Chen HB, Sholl DS (2005) Comparisons of diffusive and viscous contributions to transport coefficients of light gases in single-walled carbon nanotubes. *Mol Simulation* 31:643-649
- Bhatia SK, Nicholson D (2006) Transport of simple fluids in nanopores: Theory and simulation. *Aiche J* 52:29-38
- Bhatia SK, Nicholson D (2007) Anomalous transport in molecularly confined spaces. *J Chem Phys* 127:124701, doi: 10.1063/1.2768969
- Bitsanis I, Hadziioannou G (1990) Molecular-dynamics simulations of the structure and dynamics of confined polymer melts. *J Chem Phys* 92:3827-3847
- Blümich B, Casanova F, Appelt S (2009) NMR at low magnetic fields. *Chem Phys Lett* 477:231-240
- Bolton K, Bosio SBM, Hase WL, Schneider WF, Hass KC (1999) Comparison of explicit and united atom models for alkane chains physisorbed on alpha- $\text{Al}_2\text{O}_3$  (0001). *J Phys Chem B* 103:3885-3895
- Brandani F, Ruthven DM (2004) The effect of water on the adsorption of  $\text{CO}_2$  and  $\text{C}_3\text{H}_8$  on type X zeolites. *Ind Eng Chem Res* 43:8339-8344
- Briscoe NA, Johnson DW, Shannon MD, Kokotailo GT, Mccusker LB (1988) The framework topology of zeolite Eu-1. *Zeolites* 8:74-76
- Brochard L, Vandamme M, Pellenq RJM, Fen-Chong T (2012a) Adsorption-induced deformation of microporous materials: coal swelling induced by  $\text{CO}_2$ - $\text{CH}_4$  competitive adsorption. *Langmuir* 28:2659-2670
- Brochard L, Vandamme M, Pellenq RJM (2012b) Poromechanics of microporous media. *J Mech Phys Solids* 60:606-622
- Brovchenko I, Geiger A, Oleinikova A (2004) Water in nanopores: II. The liquid-vapour phase transition near hydrophobic surfaces. *J Phys Condens Matter* 16:S5345-S5370
- Brovchenko I, Geiger A, Oleinikova A (2005) Surface critical behavior of fluids: Lennard-Jones fluid near a weakly attractive substrate. *Eur Phys J B* 44:345-358
- Brovchenko I, Oleinikova A (2008) Complexity versus universality - fluid in the nearly solid surface. *Chem Unserer Zeit* 42:152-159

- Buchbinder AM, Weitz E, Geiger FM (2010) Pentane, hexane, cyclopentane, cyclohexane, 1-hexene, 1-pentene, cis-2-pentene, cyclohexene, and cyclopentene at vapor/alpha-alumina and liquid/alpha-alumina interfaces studied by broadband sum frequency generation. *J Phys Chem C* 114:554-566
- Buell S, Rutledge GC, Van Vliet KJ (2010) Predicting polymer nanofiber interactions via molecular simulations. *ACS Appl Mater Inter* 2:1164-1172
- Buntkowsky G, Breitzke H, Adamczyk A, Roelofs F, Emmler T, Gedat E, Grünberg B, Xu Y, Limbach HH, Shenderovich I, Vyalikh A, Findenegg G (2007) Structural and dynamical properties of guest molecules confined in mesoporous silica materials revealed by NMR. *Phys Chem Chem Phys* 9:4843-4853
- Busch A, Gensterblum Y, Krooss BM, Litke R (2004) Methane and carbon dioxide adsorption-diffusion experiments on coal: upscaling and modeling. *Int J Coal Geol* 60:151-168
- Cai Q, Buts A, Seaton NA, Biggs MJ (2008) A pore network model for diffusion in nanoporous carbons: Validation by molecular dynamics simulation. *Chem Eng Sci* 63:3319-3327
- Cavenati S, Grande CA, Rodrigues AE (2004) Adsorption equilibrium of methane, carbon dioxide, and nitrogen on zeolite  $13X$  at high pressures. *J Chem Eng Data* 49:1095-1101
- Cha SB, Ouar H, Wildeman TR, Sloan ED (1988) A 3rd-surface effect on hydrate formation. *J Phys Chem* 92:6492-6494
- Chathoth SM, Mamontov E, Melnichenko YB, Zamponi M (2010) Diffusion and adsorption of methane confined in nano-porous carbon aerogel: A combined quasi-elastic and small-angle neutron scattering study. *Microporous Mesoporous Mater* 132:148-153
- Chen B, Potoff JJ, Siepmann JI (2001) Monte Carlo calculations for alcohols and their mixtures with alkanes. Transferable potentials for phase equilibria. 5. United-atom description of primary, secondary, and tertiary alcohols. *J Phys Chem B* 105:3093-3104
- Cheng AL, Huang WL (2004) Selective adsorption of hydrocarbon gases on clays and organic matter. *Org Geochem* 35:413-423
- Clarkson CR, Bustin RM (1996) Application of adsorption potential theory to coal/methane adsorption isotherms at elevated temperature and pressure; implications for reservoir characterization. Abstracts with Programs Geol Soc Am 28:42
- Coasne B, Czwartos J, Sliwiska-Bartkowiak M, Gubbins KE (2009) Effect of pressure on the freezing of pure fluids and mixtures confined in nanopores. *J Phys Chem B* 113:13874-13881
- Coasne B, Hung FR, Pellenq RJM, Siperstein FR, Gubbins KE (2006) Adsorption of simple gases in MCM-41 materials: The role of surface roughness. *Langmuir* 22:194-202
- Cole DR, Chialvo AA, Rother G, Vlcek L, Cummings PT (2010) Supercritical fluid behavior at nanoscale interfaces: Implications for CO<sub>2</sub> sequestration in geologic formations. *Philos Mag* 90:2339-2363
- Cole DR, Gruszkiewicz MS, Simonson JM, Chialvo AA, Melnichenko YB (2004) Influence of nanoscale porosity on fluid behavior. *In: Water-Rock Interaction. Vol 1.* Wanty R, Seal R (eds) p 735-739
- Cole DR, Herwig K, Mamontov E, Laese LZ (2006) Neutron scattering and diffraction studies of fluids and fluid-solid interactions. *Rev Mineral Geochem* 63:313-362
- Cole DR, Mamontov E, Rother G (2009) Structure and dynamics of fluids in microporous and mesoporous Earth and engineered materials. *In: Neutron Applications in Earth, Energy, and Environmental Sciences.* Liang L, Rinaldi R, Schober H (eds) Springer, p 547-570
- Combariza AF, Sastre G, Corma A (2011) Molecular dynamics simulations of the diffusion of small chain hydrocarbons in 8-ring zeolites. *J Phys Chem C* 115:875-884
- Cracknell RF, Nicholson D, Quirke N (1995) Direct molecular-dynamics simulation of flow down a chemical-potential gradient in a slit-shaped micropore. *Phys Rev Lett* 74:2463-2466
- Cygan RT, Guggenheim S, Koster van Groos AF (2004a) Molecular models for the intercalation of methane hydrate complexes in montmorillonite clay. *J Phys Chem B* 108:15141-15149
- Cygan RT, Liang JJ, Kalinichev AG (2004b) Molecular models of hydroxide, oxyhydroxide, and clay phases and the development of a general force field. *J Phys Chem B* 108:1255-1266
- Czwartos J, Coasne B, Gubbins KE, Hung FR, Sliwiska-Bartkowiak M (2005) Freezing and melting of azeotropic mixtures confined in nanopores: experiment and molecular simulation. *Molec Phys* 103:3103-3113
- Dabrowski A, Podkościelny P, Bulow M (2003) Comparison of energy-distribution functions calculated for gas-solid and liquid-solid adsorption data. *Colloid Surface A* 212:109-114
- Davis HT (1992) Kinetic theory of strongly inhomogeneous fluids. *In: Fundamentals of Inhomogeneous Fluids.* Henderson D (ed) Dekker: New York, p 551-592
- Dawson R, Khoury F, Kobayash R (1970) Self-diffusion measurements in methane by pulsed nuclear magnetic resonance. *AIChE J* 16:725-729
- Denayer JFA, Devriese LI, Couck S, Martens J, Singh R, Webley PA, Baron GV (2008) Cage and window effects in the adsorption of *n*-alkanes on chabazite and SAPO-34. *J Phys Chem C* 112:16593-16599
- Derouane EG (2007) On the physical state of molecules in microporous solids. *Microporous Mesoporous Mater* 104:46-51

- de Sainte Claire P, Hass KC, Schneider WF, Hase WL (1997) Simulations of hydrocarbon adsorption and subsequent water penetration on an aluminum oxide surface. *J Chem Phys* 106:7331-7342
- Diaz E, Ordóñez S, Vega A, Coca J (2004) Adsorption characterisation of different volatile organic compounds over alumina, zeolites and activated carbon using inverse gas chromatography. *J Chromatogr A* 1049:139-146
- Dijkstra M (1997) Confined thin films of linear and branched alkanes. *J Chem Phys* 107:3277-3288
- Donohue MD, Aranovich GL (1999) A new classification of isotherms for Gibbs adsorption of gases on solids. *Fluid Phase Equilib* 158:557-563
- Dubowski Y, Viecei J, Tobias DJ, Gomez A, Lin A, Nizkorodov SA, McIntire TM, Finlayson-Pitts BJ (2004) Interaction of gas-phase ozone at 296 K with unsaturated self-assembled monolayers: A new look at an old system. *J Phys Chem A* 108:10473-10485
- Dvovashkin M, Valiullin R, Kärger J, Einicke W-D, Glaser R (2007) Direct assessment of transport properties of supercritical fluids confined to nanopores. *J Am Chem Soc* 129:10344-10345
- Ernst RR, Bodenhausen G, Wokaun A (1987) Principles of Nuclear Magnetic Resonance in One and Two Dimensions, Clarendon Press, Oxford
- Ertel TF, Heuer VB, Prieto-Mollar X, Vogt C, Sylva SP, Seewald J, Hinrichs KU (2010) The biogeochemistry of sorbed methane in marine sediments. *Geochim Cosmochim Acta* 74:6033-6048
- Evans R (1992) Density functionals in the theory of nonuniform fluids. *In: Fundamentals of Inhomogeneous Fluids*. Henderson D (ed) Dekker, New York, p 85-176
- Evans R, Marconi UMB (1987) Phase-equilibria and solvation forces for fluids confined between parallel walls. *J Chem Phys* 86:7138-7148
- Eyraud C, Quinson JF, Brun M (1988) The role of thermoporometry in the study of porous solids. *In: Characterization of Porous Solids I. Vol 39*. Unger KK, Rouquerol J, Sing KSW, Kral H (eds) Studies in Surface Science and Catalysis, Elsevier, Amsterdam p 295-305
- Fernandez M, Pampel A, Takahashi R, Sato S, Freude D, Kärger J (2008) Revealing complex formation in acetone-*n*-alkanes mixtures by MAS PFG NMR diffusion measurement in nanoporous hosts. *Phys Chem Chem Phys* 10:4165-4171
- Firouzi M, Wilcox J (2012) Molecular modeling of carbon dioxide transport and storage in porous carbon-based materials. *Microporous Mesoporous Mater* 158:195-203
- Floquet N, Coulomb JP, Bellat JP, Simon JM, Weber G, Andre G (2007) Heptane adsorption in silicalite-1: Neutron scattering investigation. *J Phys Chem C* 111:18182-18188
- Floquet N, Coulomb JP, Weber G, Bertrand O, Bellat JP (2003) Structural signatures of type IV isotherm steps: Sorption of trichloroethene, tetrachloroethene, and benzene in silicalite-I. *J Phys Chem B* 107:685-693
- Ford DM, Glandt ED (1995) Molecular simulation study of the surface-barrier effect - dilute gas limit. *J Phys Chem* 99:11543-11549
- Frenkel D, Smit B (2002) Understanding Molecular Simulations- From Algorithms to Applications. Academic Press: San Diego, CA
- Fry RA, Kwon KD, Komarneni S, Kubicki JD, Mueller KT (2006) Solid-state NMR and computational chemistry study of mononucleotides adsorbed to alumina. *Langmuir* 22:9281-9286
- Fry RA, Tsomaia N, Pantano CG, Mueller KT (2003) F-19 MAS NMR quantification of accessible hydroxyl sites on fiberglass surfaces. *J Am Chem Soc* 125:2378-2379
- Gaede HC, Gawrisch K (2004) Multi-dimensional pulsed field gradient magic angle spinning NMR experiments on membranes. *Magn Reson Chem* 42:115-122
- Galhotra P, Navea JG, Larsen SC, Grassian VH (2009) Carbon dioxide (C<sup>16</sup>O<sub>2</sub> and C<sup>18</sup>O<sub>2</sub>) adsorption in zeolite Y materials: effect of cation, adsorbed water and particle size. *Energy Environ Sci* 2:401-409
- Gao JP, Luedtke WD, Landman U (1997a) Origins of solvation forces in confined films. *J Phys Chem B* 101:4013-4023
- Gao JP, Luedtke WD, Landman U (1997b) Structure and solvation forces in confined films: Linear and branched alkanes. *J Chem Phys* 106:4309-4318
- Geier O, Vasenkov S, Kärger J (2002) PFG NMR study of long-range diffusion in beds of NaX zeolite: evidence for different apparent tortuosity factors in the Knudsen and bulk regimes. *J Chem Phys* 117:1935-1938
- Gelb LD, Gubbins KE, Radhakrishnan R, Sliwinski-Bartkowiak M (1999) Phase separation in confined systems. *Rep Prog Phys* 62:1573-1659
- Giaya A, Thompson RW (2002) Water confined in cylindrical micropores. *J Chem Phys* 117:3464-3475
- Greene GW, Kristiansen K, Meyer EE, Boles J, Israelachvili J (2009) Role of electrochemical reactions in pressure solution. *Geochim Cosmochim Acta* 73:2862-2874
- Gruskiewicz MS, Rother G, Wesolowski DJ, Cole DR, Wallacher D (2012) Direct measurements of pore fluid density by vibrating tube densimetry. *Langmuir* 28:5070-5078
- Guggenheim S, Koster van Groos AF (2003) New gas-hydrate phase: Synthesis and stability of clay-methane hydrate intercalate. *Geology* 31:653-656
- Guichet X, Fleury M, Kohler E (2008) Effect of clay aggregation on water diffusivity using low field NMR. *J Colloid Interface Sci* 327:84-93

- Guo ZL, Zhao TS, Shi Y (2005) Simple kinetic model for fluid flows in the nanometer scale. *Phys Rev E* 71:035301-035304
- Guo ZL, Zhao TS, Xu C, Shi Y (2006) Simulation of fluid flows in the nanometer: kinetic approach and molecular dynamic simulation. *Int J Comput Fluid D* 20:361-367
- Gysi AP, Stefansson A (2012) CO<sub>2</sub>-water-basalt interaction. Low temperature experiments and implications for CO<sub>2</sub> sequestration into basalts. *Geochim Cosmochim Acta* 81:129-152
- Hayes PL, Chen EH, Achtyl JL, Geiger FM (2009) An optical voltmeter for studying cetyltrimethylammonium interacting with fused silica/aqueous interfaces at high ionic strength. *J Phys Chem A* 113:4269-4280
- Heffelfinger GS, Vanswol F (1994) Diffusion in Lennard-Jones fluids using dual control-volume grand-canonical molecular-dynamics simulation (Dev-Gcmd). *J Chem Phys* 100:7548-7552
- Heitjans P, Kärger J (eds) (2005) *Diffusion in Condensed Matter: Methods, Materials, Models*. Springer, Berlin
- Helbaek M, Hafskjold B, Dysthe DK, Sorland GH (1996) Self-diffusion coefficients of methane or ethane mixtures with hydrocarbons at high pressure by NMR. *J Chem Eng Data* 41:598-603
- Henderson D (1992) Integral equation theories for inhomogeneous fluids. *In: Fundamentals of Inhomogeneous Fluids*. Henderson D (ed), Dekker: New York p 177-200
- Hinrichs KU, Hayes JM, Bach W, Spivack AJ, Hmelo LR, Holm NG, Johnson CG, Sylva SP (2006) Biological formation of ethane and propane in the deep marine subsurface. *Proc Natl Acad Sci USA* 103:14684-14689
- Ho TA, Argyris D, Cole DR, Striolo A (2012) Aqueous NaCl and CsCl solutions confined in crystalline slit-shaped silica nanopores of varying degree of protonation. *Langmuir* 28:1256-1266
- Hoyt DW, Turcu RVF, Sears JA, Rosso KM, Burton SD, Felmy AR, Hu JZ (2011) High-pressure magic angle spinning nuclear magnetic resonance. *J Magn Reson* 212:378-385
- Hu HX, Li XC, Fang ZM, Wei N, Li QS (2010) Small-molecule gas sorption and diffusion in coal: Molecular simulation. *Energy* 35:2939-2944
- Hung FR, Gubbins KE, Radhakrishnan R, Szostak K, Beguin F, Dudziak G, Sliwinska-Bartkowiak M (2005) Freezing/melting of Lennard-Jones fluids in carbon nanotubes. *Appl Phys Lett* 86: 103110-1 - 103110-3
- Huo H, Peng L, Grey CP (2009) Low temperature <sup>1</sup>H MAS NMR spectroscopy studies of proton motion in zeolite HZSM-5. *J Phys Chem C* 113:8211-8219
- Indrawati L, Strohshine RL, Narsimhan G (2007) Low-field NMR: A tool for studying protein aggregation. *J Sci Food Agric* 87:2207-2216
- Jain SK, Gubbins KE, Pellenq RJM, Pikunic JP (2006a) Molecular modeling and adsorption properties of porous carbons. *Carbon* 44:2445-2451
- Jain SK, Pellenq RJM, Pikunic JP, Gubbins KE (2006b) Molecular modeling of porous carbons using the hybrid reverse Monte Carlo method. *Langmuir* 22:9942-9948
- Jepps OG, Bhatia SK, Searles DJ (2003) Wall mediated transport in confined spaces: Exact theory for low density. *Phys Rev Lett* 91:1260102-1 - 1260102-4
- Jiang JW, Sandler SI, Schenk M, Smit B (2005) Adsorption and separation of linear and branched alkanes on carbon nanotube bundles from configurational-bias Monte Carlo simulation. *Phys Rev B* 72:045447-045457
- Jin RY, Song KY, Hase WL (2000) Molecular dynamics simulations of the structures of alkane/hydroxylated alpha-Al<sub>2</sub>O<sub>3</sub>(0001) interfaces. *J Phys Chem B* 104:2692-2701
- Jobic H (2000a) Diffusion of linear and branched alkanes in ZSM-5. A quasi-elastic neutron scattering study. *J Mol Catal A Chem* 158:135-142
- Jobic H (2000b) Inelastic scattering of organic molecules in zeolites. *Physica B* 276:222-225
- Jobic H, Bee M, Kärger J, Vartapetian RS, Balzer C, Julbe A (1995) Mobility of cyclohexane in a microporous silica sample - a quasi-elastic neutron-scattering and NMR pulsed-field gradient technique study. *J Membr Sci* 108:71-78
- Jobic H, Rosenbach N, Ghoufi A, Kolokolov DI, Yot PG, Devic T, Serre C, Férey G, Maurin G (2010) Unusual chain-length dependence of the diffusion of *n*-alkanes in the metal-organic framework MIL-47(V): The blowgun effect. *Chem Eur J* 16:10337-10341
- Jobic H, Theodorou DN (2007) Quasi-elastic neutron scattering and molecular dynamics simulation as complementary techniques for studying diffusion in zeolites. *Microporous Mesoporous Mater* 102:21-50
- Johnston JC, Iuliucci RJ, Facelli JC, Fitzgerald G, Mueller KT (2009) Intermolecular shielding contributions studied by modeling the C-13 chemical-shift tensors of organic single crystals with plane waves. *J Chem Phys* 131:144503-1 - 144503-11
- June RL, Bell AT, Theodorou DN (1992) Molecular-dynamics studies of butane and hexane in silicalite. *J Phys Chem* 96:1051-1060
- Kainourgiakis M, Steriotis T, Charalambopoulou G, Strobl M, Stubos A (2010) Determination of the spatial distribution of multiple fluid phases in porous media by ultra-small-angle neutron scattering. *Appl Surf Sci* 256:5329-5333
- Kaiser K, Guggenberger G (2000) The role of DOM sorption to mineral surfaces in the preservation of organic matter in soils. *Org Geochem* 31:711-725

- Kantzas A, Bryan JL, Mai A, Hum FM (2005) Applications of low field NMR techniques in the characterization of oil sand mining, extraction and upgrading processes. *Can J Chem Eng* 83:145-150
- Kärger J, Caro J, Cool P, Coppens MO, Jones D, Kapteijn F, Rodriguez-Reinoso F, Stocker M, Theodorou D, Vansant EF, Weitkamp J (2009) Benefit of microscopic diffusion measurement for the characterization of nanoporous materials. *Chem Eng Technol* 32:1494-1511
- Kärger J, Ruthven D (1991) Diffusion in Zeolites and Other Microporous Solids. Wiley, New York
- Kärger J, Ruthven DM, Theodorou DN (2012) Diffusion in Nanoporous Materials. John Wiley & Sons, New York
- Kärger J, Stallmach F, Vasenkov S (2003) Structure-mobility relations of molecular diffusion in nanoporous materials. *Magn Reson Imaging* 21:185-191
- Kärger J (2008) Diffusion measurement by NMR techniques. In: Adsorption and Diffusion. Karge HG, Weitkamp J (ed) Springer, Berlin, p 85-133
- Kawahigashi M, Kaiser K, Rodionov A, Guggenberger G (2006) Sorption of dissolved organic matter by mineral soils of the Siberian forest tundra. *Global Change Biol* 12:1868-1877
- Kennedy MJ, Pevear DR, Hill RJ (2002) Mineral surface control of organic carbon in black shale. *Science* 295:657-660
- Kim HS, Stair PC (2009) Resonance Raman spectroscopic study of alumina-supported vanadium oxide catalysts with 220 and 287 nm excitation. *J Phys Chem A* 113:4346-4355
- Kim TS, Dauskardt RH (2010) Molecular mobility under nanometer scale confinement. *Nano Lett* 10:1955-1959
- Klatte SJ, Beck TL (1996) Microscopic simulation of solute transfer in reversed phase liquid chromatography. *J Phys Chem* 100:5931-5934
- Knudsen M (1909) The laws of the molecular current and the internal friction current of gases by channels. *Ann Phys Berlin* 29:75-130
- Koh CA, Wisbey RP, Wu XP, Westacott RE, Soper AK (2000) Water ordering around methane during hydrate formation. *J Chem Phys* 113:6390-6397
- Konstadinidis K, Thakkar B, Chakraborty A, Potts LW, Tannenbaum R, Tirrell M, Evans JF (1992) Segment level chemistry and chain conformation in the reactive adsorption of poly(methyl methacrylate) on aluminum-oxide surfaces. *Langmuir* 8:1307-1317
- Kowalczyk P, Gauden PA, Terzyk AP, Furmaniak S (2010) Microscopic model of carbonaceous nanoporous molecular sieves-anomalous transport in molecularly confined spaces. *Phys Chem Chem Phys* 12:11351-11361
- Krishna R, van Baten JM (2011) A molecular dynamics investigation of the unusual concentration dependencies of Fick diffusivities in silica mesopores. *Microporous Mesoporous Mater* 138:228-234
- Krutyeva M, Yang X, Vasenkov S, Kärger J (2007) Exploring the surface permeability of nanoporous particles by pulsed field gradient NMR. *J Magn Reson* 185:300-307
- Lemmon EW, Huber ML, McLinden MO (2010) NIST Standard Reference Database 23: Reference Fluid Thermodynamic and Transport Properties-REFPROP, Version 9.0. National Institute of Standards and Technology, Standard Reference Data Program, Gaithersburg
- Levitt MH (2001) Spin Dynamics Basics of Nuclear Magnetic Resonance. John Wiley and Sons, New York
- Li CL, Choi P (2007) Molecular dynamics study of the adsorption behavior of normal alkanes on a relaxed  $\alpha$ -Al<sub>2</sub>O<sub>3</sub> (0001) surface. *J Phys Chem C* 111:1747-1753
- Li WZ, Liu ZY, Che YL, Zhang D (2007) Molecular simulation of adsorption and separation of mixtures of short linear alkanes in pillared layered materials at ambient temperature. *J Colloid Interface Sci* 312:179-185
- Liebscher A, Heinrich CA (eds) (2007) Fluid-Fluid Interactions. Reviews in Mineralogy and Geochemistry Vol. 65. Mineralogical Society of America, Chantilly VA
- Lim YI, Bhatia SK (2011) Simulation of methane permeability in carbon slit pores. *J Membrane Sci* 369:319-328
- Lim YI, Bhatia SK, Nguyen TX, Nicholson D (2010) Prediction of carbon dioxide permeability in carbon slit pores. *J Membrane Sci* 355:186-199
- Lithoxoos GP, Labropoulos A, Peristeras LD, Kanellopoulos N, Samios J, Economou IG (2010) Adsorption of N<sub>2</sub>, CH<sub>4</sub>, CO and CO<sub>2</sub> gases in single walled carbon nanotubes: A combined experimental and Monte Carlo molecular simulation study. *J Supercrit Fluid* 55:510-523
- Lu J, Aydin C, Browning ND, Gates BC (2012) Hydrogen activation and metal hydride formation trigger cluster formation from supported iridium complexes. *J Am Chem Soc* 134:5022-5025
- Machida S, Hamaguchi K, Nagao M, Yasui F, Mukai K, Yamashita Y, Yoshinobu J, Kato HS, Okuyama H, Kawai M (2002) Electronic and vibrational states of cyclopentene on Si(100)(2×1). *J Phys Chem B* 106:1691-1696
- Maciolek A, Ciach A, Evans R (1998) Critical depletion of fluids in pores: Competing bulk and surface fields. *J Chem Phys* 108:9765-9774

- Maciolek A, Evans R, Wilding NB (1999) Effects of confinement on critical adsorption: Absence of critical depletion for fluids in slit pores. *Phys Rev E* 60:7105-7119
- Magda JJ, Tirrell M, Davis HT (1985) Molecular-dynamics of narrow, liquid-filled pores. *J Chem Phys* 83:1888-1901
- Maginn EJ, Bell AT, Theodorou DN (1996) Dynamics of long *n*-alkanes in silicalite: A hierarchical simulation approach. *J Phys Chem* 100:7155-7173
- Magusin PCMM, Schuring D, van Oers EM, de Haan JW, van Santen RA (1999) *n*-Pentane hopping in zeolite ZK-5 studied with C-13 NMR. *Magn Reson Chem* 37:S108-S117
- Malbrunot P, Vidal D, Vermesse J, Chahine R, Bose TK (1992) Adsorption measurements of argon, neon, krypton, nitrogen, and methane on activated carbon up to 650 MPa. *Langmuir* 8:577-580
- Mamontov E, Kumzerov YA, Vakhrushev, SB (2005) Diffusion of benzene confined in oriented nanochannels of chrysotile asbestos fibers. *Phys Rev E* 72:051502-1 - 0515072-7
- Manassis I, Gillan MJ (1994) Structure and energetics of alumina surfaces calculated from first principles. *J Am Ceram Soc* 77:335-338
- Martin MG, Siepmann JI (1998) Transferable potentials for phase equilibria. 1. United-atom description of *n*-alkanes. *J Phys Chem B* 102:2569-2577
- Martin MG, Siepmann JI (1999) Novel configurational-bias Monte Carlo method for branched molecules. Transferable potentials for phase equilibria. 2. United-atom description of branched alkanes. *J Phys Chem B* 103:4508-4517
- Mason EA, Malinaus AP, Evans RB (1967) Flow and diffusion of gases in porous media. *J Chem Phys* 46:3199-3216
- Mawhinney DB, Yates JT (2001) FTIR study of the oxidation of amorphous carbon by ozone at 300 K - direct COOH formation. *Carbon* 39:1167-1173
- McCollom TM (2013) Laboratory simulations of abiotic hydrocarbon formation in Earth's deep subsurface. *Rev Mineral Geochem* 75:467-494
- Menon VC, Komarneni S (1998) Porous adsorbents for vehicular natural gas storage: A review. *J Porous Mat* 5:43-58
- Mentzen BF (2007) Crystallographic determination of the positions of the monovalent H, Li, Na, K, Rb, and Tl cations in fully dehydrated MFI type zeolites. *J Phys Chem C* 111:18932-18941
- Meresi G, Wang YZ, Cardoza J, Wen WY, Jones AA, Gosselin J, Azar D, Inglefield PT (2001) Pulse field gradient NMR study of diffusion of pentane in amorphous glassy perfluorodioxole. *Macromolecules* 34:4852-4856
- Metais A, Mariette F (2003) Determination of water self-diffusion coefficient in complex food products by low field <sup>1</sup>H PFG NMR: comparison between the standard spin-echo sequence and the T<sub>1</sub>-weighted spin-echo sequence. *J Magn Reson* 165:265-275
- Millot B, Methivier A, Jobic H (1998) Adsorption of *n*-alkanes on silicalite crystals. a temperature-programmed desorption study. *J Phys Chem B* 102:3210-3215
- Mitra S, Mukhopadhyay R (2003) Molecular dynamics using quasielastic neutron scattering. *Current Sci* 84:653-662
- Mitra S, Mukhopadhyay R (2004) Quasi-elastic neutron scattering study of dynamics in condensed matter. *Pramana J Phys* 63:81-89
- Mueller R, Kanungo R, Kiyono-Shimobe M, Koros WJ, Vasenkov S (2012) Diffusion of methane and carbon dioxide in carbon molecular sieve membranes by multinuclear Pulsed Field Gradient NMR. *Langmuir* 28:10296-10303
- Myers AL, Monson PA (2002) Adsorption in porous materials at high pressure: Theory and experiment. *Langmuir* 18:10261-10273
- Nanjundiah K, Dhinojwala A (2005) Confinement-induced ordering of alkanes between an elastomer and a solid surface. *Phys Rev Lett* 95: 154301-1 - 154301-4
- Ndjaka JMB, Zwaneburg G, Smit B, Schenk M (2004) Molecular simulations of adsorption isotherms of small alkanes in FER-, TON-, MTW- and DON-type zeolites. *Microporous Mesoporous Mater* 68:37-43
- Neumann DA (2006) Neutron scattering and hydrogenous materials. *Mater Today* 9:34-41
- Newsome DA, Sholl DS (2005) Predictive assessment of surface resistances in zeolite membranes using atomically detailed models. *J Phys Chem B* 109:7237-7244
- Nguyen TX, Bhatia SK, Jain SK, Gubbins KE (2006) Structure of saccharose-based carbon and transport of confined fluids: hybrid reverse Monte Carlo reconstruction and simulation studies. *Molec Simulation* 32:567-577
- Nguyen TX, Cohaut N, Bae JS, Bhatia SK (2008) New method for atomistic modeling of the microstructure of activated carbons using hybrid reverse Monte Carlo simulation. *Langmuir* 24:7912-7922
- Nicholson D, Parsonage NG (1982) Computer Simulation and the Statistical Mechanics of Adsorption. Academic Press, London
- Nivarthi SSS, McCormick AV, Davis HT (1994) Diffusion anisotropy in molecular sieves: A Fourier transform PFG NMR study of methane in A1PO4-5. *Chem Phys Lett* 229:297-301

- Nowak AK, Denouden CJJ, Pickett SD, Smit B, Cheetham AK, Post MFM, Thomas JM (1991) Mobility of adsorbed species in zeolites - methane, ethane, and propane diffusivities. *J Phys Chem* 95:848-854
- Oleinikova A, Brovchenko I, Geiger A (2006) Behavior of a wetting phase near a solid boundary: vapor near a weakly attractive surface. *Eur Phys J B* 52:507-519
- Packer KJ (2003) Magnetic resonance in porous media: forty years on. *Magn Reson Imaging* 21:163-168
- Palmer JC, Lobet A, Yeon SH, Fischer JE, Shi Y, Gogotsi Y, Gubbins KE (2010) Modeling the structural evolution of carbide-derived carbons using quenched molecular dynamics. *Carbon* 48:1116-1123
- Pampel A, Fernandez M, Freude D, Kärger J (2005) New options for measuring molecular diffusion in zeolites by MAS PFG NMR. *Chem Phys Lett* 407:53-57
- Pampel A, Kärger J, Michel D. (2003) Lateral diffusion of a transmembrane peptide in lipid bilayers studied by pulsed field gradient NMR in combination with magic angle sample spinning. *Chem Phys Lett* 379:555-561
- Pantano CG, Fry RA, Mueller KT (2003) Effect of boron-oxide on surface hydroxyl coverage of aluminoborosilicate glass fibers: a  $^{19}\text{F}$  solid-state NMR Study. *Phys Chem Glass* 44:64-68
- Paoli H, Methivier A, Jobic H, Krause C, Pfeifer H, Stallmach F, Kärger J (2002) Comparative QENS and PFG NMR diffusion studies of water in zeolite NaCaA. *Microporous Mesoporous Mater* 55:147-158
- Parcher JF, Strubinger JR (1989) High-pressure adsorption of carbon-dioxide on super-critical-fluid chromatography adsorbents. *J Chromatogr* 479:251-259
- Park SH, Sposito G (2003) Do montmorillonite surfaces promote methane hydrate formation? Monte Carlo and molecular dynamics simulations. *J Phys Chem B* 107:2281-2290
- Partyka S, Douillard JM (1995) Nature of interactions between organic pure liquids and model rocks - a calorimetric investigation. *J Petrol Sci Eng* 13:95-102
- Petersen T, Yarovsky I, Snook I, McCulloch DG, Opletal G (2003) Structural analysis of carbonaceous solids using an adapted reverse Monte Carlo algorithm. *Carbon* 41:2403-2411
- Pires J, Bestilleiro M, Pinto M, Gil A (2008) Selective adsorption of carbon dioxide, methane and ethane by porous clays heterostructures. *Sep Purif Technol* 61:161-167
- Pitteloud C, Powell DH, Gonzalez MA, Cuello GJ (2003) Neutron diffraction studies of ion coordination and interlayer water structure in smectite clays: lanthanide(III)-exchanged Wyoming montmorillonite. *Colloid Surf A* 217:129-136
- Pollard WG, Present RD (1948) On gaseous self-diffusion in long capillary tubes. *Phys Rev* 73:762-774
- Potter J, Konnerup-Madsen J (2003) A review of the occurrence and origin of abiogenic hydrocarbons in igneous rocks. *Geol Soc Spec Pubs* 214:151-173
- Pynn R (2009) Neutron scattering – a non-destructive microscope for seeing inside matter. *In: Neutron Applications in Earth, Energy, and Environmental Sciences*. Liang L, Rinaldi R, Schober H (eds) Springer, Berlin, p 15-36
- Radhakrishnan R, Gubbins KE, Sliwinska-Bartkowiak M (2000) Effect of the fluid-wall interaction on freezing of confined fluids: Toward the development of a global phase diagram. *J Chem Phys* 112:11048-11057
- Radhakrishnan R, Gubbins KE, Sliwinska-Bartkowiak M (2002) Global phase diagrams for freezing in porous media. *J Chem Phys* 116:1147-1155
- Radlinski AP (2006) Small-angle neutron scattering and the microstructure of rocks. *Rev Mineral Geochem* 63:363-397
- Raghavan K, Macelroy JMD (1995) Molecular-dynamics simulations of adsorbed alkanes in silica micropores at low-to-moderate loadings. *Molec Simulation* 15:1-33
- Rajendran A, Hocker T, Di Giovanni O, Mazzotti M (2002) Experimental observation of critical depletion: Nitrous oxide adsorption on silica gel. *Langmuir* 18:9726-9734
- Resini C, Montanari T, Busca G, Jehng JM, Wachs IE (2005) Comparison of alcohol and alkane oxidative dehydrogenation reactions over supported vanadium oxide catalysts: *in situ* infrared, Raman and UV-vis spectroscopic studies of surface alkoxide intermediates and of their surface chemistry. *Catal Today* 99:105-114
- Reyes SC, Sinfelt JH, DeMartin GJ, Ernst RH, Iglesia E (1997) Frequency modulation methods for diffusion and adsorption measurements in porous solids. *J Phys Chem B* 101:614-622
- Riehl JW, Koch K (1972) NMR relaxation of adsorbed gases - methane on graphite. *J Chem Phys* 57:2199-2208
- Rodriguez MA, Rubio J, Rubio F, Liso MJ, Oteo JL (1997) Application of inverse gas chromatography to the study of the surface properties of slates. *Clay Clay Miner* 45:670-680
- Roman-Perez G, Moaied M, Soler JM, Yndurain F (2010) Stability, adsorption, and diffusion of  $\text{CH}_4$ ,  $\text{CO}_2$ , and  $\text{H}_2$  in clathrate hydrates. *Phys Rev Lett* 105:145901-145904
- Rother G, Krukowski E, Wallacher D, Grimm N, Bodnar R, Cole DR (2012) Pore size effects on the sorption of supercritical carbon dioxide in mesoporous CPG-10 silica. *J Phys Chem C* 116(1):917-922
- Rother G, Melnichenko YB, Cole DR, Frielinghaus H, Wignall GD (2007) Microstructural characterization of adsorption and depletion regimes of supercritical fluids in nanopores. *J Phys Chem C* 111:15736-15742
- Rouquerol F, Rouquerol J, Sing K (1999) Adsorption by Powders and Porous Solids. Principles, Methodology and Applications. Academic Press, San Diego, CA

- Runnebaum RC, Maginn EJ (1997) Molecular dynamics simulations of alkanes in the zeolite silicalite: Evidence for resonant diffusion effects. *J Phys Chem B* 101:6394-6408
- Saalwachter K (2003) Detection of heterogeneities in dry and swollen polymer networks by proton low-field NMR spectroscopy. *J Am Chem Soc* 125:14684-14685
- Saengsawang O, Schuring A, Remsungnen T, Hannongbua S, Newsome DA, Dammers AJ, Coppens MO, Fritzsche S (2010) Diffusion of *n*-pentane in the zeolite ZK5 studied by high-temperature configuration-space exploration. *Chem Phys* 368:121-125
- Sandstrom L, Palomino M, Hedlund J (2010) High flux zeolite X membranes. *J Membrane Sci* 354:171-177
- San-Miguel MA, Rodger PM (2003) Wax deposition onto Fe<sub>2</sub>O<sub>3</sub> surfaces. *Phys Chem Chem Phys* 5:575-581
- San-Miguel MA, Rodger PM (2010) Templates for wax deposition? *Phys Chem Chem Phys* 12:3887-3894
- Schloemer S, Krooss BM (2004) Molecular transport of methane, ethane and nitrogen and the influence of diffusion on the chemical and isotopic composition of natural gas accumulations. *Geofluids* 4:81-108
- Schoen M, Diestler DJ (1998) Analytical treatment of a simple fluid adsorbed in a slit-pore. *J Chem Phys* 109:5596-5606
- Schreiber A, Bock H, Schoen M, Findenegg GH (2002) Effect of surface modification on the pore condensation of fluids: experimental results and density functional theory. *Molec Phys* 100:2097-2107
- Schure MR (1998) Particle simulation methods in separation science. *In: Advances in Chromatography*. Vol 39. Brown PR (ed) Marcel Dekker, New York, p 435-441
- Schuring A, Auerbach SM, Fritzsche S (2007) A simple method for sampling partition function ratios. *Chem Phys Lett* 450:164-169
- Seferl GA, Du Q, Miranda PB, Shen YR (1995) Surface crystallization of liquid *n*-alkanes and alcohol monolayers studied by surface vibrational spectroscopy. *Chem Phys Lett* 235:347-354
- Sel O, Brandt A, Wallacher D, Thommes M, Smarsly B (2007) Pore hierarchy in mesoporous silicas evidenced by *in situ* SANS during nitrogen physisorption. *Langmuir* 23:4724-4727
- Seland JG, Ottaviani M, Hafskjold B (2001) A PFG-NMR study of restricted diffusion in heterogeneous polymer particles. *J Colloid Interface Sci* 239:168-177
- Seo YJ, Seol J, Yeon SH, Koh DY, Cha MJ, Kang SP, Seo YT, Bahk JJ, Lee J, Lee H (2009) Structural, mineralogical, and rheological properties of methane hydrates in smectite clays. *J Chem Eng Data* 54:1284-1291
- Septon MA, Hazen RM (2013) On the origins of deep hydrocarbons. *Rev Mineral Geochem* 75:449-465
- Sherwood Lollar B, Lacrampe-Couloume G, Slater GF, Ward J, Moser DP, Gihring TM, Lin LH, Onstott TC (2006) Unravelling abiogenic and biogenic sources of methane in the Earth's deep subsurface. *Chem Geol* 226:328-339
- Singh SK, Sinha A, Deo G, Singh JK (2009) Vapor-liquid phase coexistence, critical properties, and surface tension of confined alkanes. *J Phys Chem C* 113:7170-7180
- Sircar S (1999) Gibbsian surface excess for gas adsorption - revisited. *Ind Eng Chem Res* 38:3670-3682
- Skipper NT, Lock PA, Titiloye JO, Swenson J, Mirza ZA, Howells WS, Fernandez-Alonso F (2006) The structure and dynamics of 2-dimensional fluids in swelling clays. *Chem Geol* 230:182-196
- Skipper NT, Smalley MV, Williams GD, Soper AK, Thompson CH (1995) Direct measurement of the electric double-layer structure in hydrated lithium vermiculite clays by neutron-diffraction. *J Phys Chem* 99:14201-14204
- Skoulidas AI, Ackerman DM, Johnson JK, Sholl DS (2002) Rapid transport of gases in carbon nanotubes. *Phys Rev Lett* 89:185901-1 - 185901-4
- Skoulidas AI, Sholl DS (2002) Transport diffusivities of CH<sub>4</sub>, CF<sub>4</sub>, He, Ne, Ar, Xe, and SF<sub>6</sub> in silicalite from atomistic simulations. *J Phys Chem B* 106:5058-5067
- Slayton RM, Aubuchon CM, Camis TL, Noble AR, Tro NJ (1995) Desorption-kinetics and adlayer sticking model of *n*-butane, *n*-hexane, and *n*-octane on Al<sub>2</sub>O<sub>3</sub>(0001). *J Phys Chem* 99:2151-2154
- Sleep NH, Meibom A, Fridriksson T, Coleman RG, Bird DK (2004) H<sub>2</sub>-rich fluids from serpentinization: Geochemical and biotic implications. *Proc Natl Acad Sci USA* 101:12818-12823
- Smit B, Maesen TLM (1995) Commensurate freezing of alkanes in the channels of a zeolite. *Nature* 374:42-44
- Smith GD, Yoon DY (1994) Equilibrium and dynamic properties of polymethylene melts from molecular-dynamics simulations. 1. *n*-tridecane. *J Chem Phys* 100:649-658
- Sokhan VP, Nicholson D, Quirke N (2002) Fluid flow in nanopores: Accurate boundary conditions for carbon nanotubes. *J Chem Phys* 117:8531-8539
- Span R, Wagner W (1996) A new equation of state for carbon dioxide covering the fluid region from the triple-point temperature to 1100 K at pressures up to 800 MPa. *J Phys Chem Ref Data* 25:1509-1596
- Sposito G, Skipper NT, Sutton R, Park SH, Soper AK, Greathouse JA (1999) Surface geochemistry of the clay minerals. *Proc Natl Acad Sci USA* 96:3358-3364
- Stallmach F, Graser A, Kärger J, Krause C, Jeschke M, Oberhagemann U, Spange S (2001) Pulsed field gradient NMR studies of diffusion in MCM-41 mesoporous solids. *Microporous Mesoporous Mater* 44:745-753
- Stallmach F, Kärger J, Krause C, Jeschke M, Oberhagemann U (2000) Evidence of anisotropic self-diffusion of guest molecules in nanoporous materials of MCM-41 Type. *J Am Chem Soc* 122:9237-9242

- Stepanov AG, Shegai TO, Luzgin MV, Jobic H (2003) Comparison of the dynamics of *n*-hexane in ZSM-5 and 5A zeolite structures. *Eur Phys J E* 12:57-61
- Stoessel RK, Byrne PA (1982) Methane solubilities in clay slurries. *Clay Clay Miner* 30:67-72
- Stokes GY, Chen EH, Walter SR, Geiger FM (2009) Two reactivity modes in the heterogeneous cyclohexene ozonolysis under tropospherically relevant ozone-rich and ozone-limited conditions. *J Phys Chem A* 113:8985-8993
- Straadt IK, Thybo AK, Bertram HC (2008) NaCl-induced changes in structure and water mobility in potato tissue as determined by CLSM and LF-NMR. *LWT-Food Sci Tech* 41:1493-1500
- Streitz FH, Mintmire JW (1994) Electrostatic-diffused model for alumina surfaces. *Thin Solid Films* 253:179-184
- Striolo A (2006) The mechanism of water diffusion in narrow carbon nanotubes. *Nano Lett* 6:633-639
- Striolo A, Gubbins KE, Gruskiewicz MS, Cole DR, Simonson JM, Chialvo AA (2005) Effect of temperature on the adsorption of water in porous carbons. *Langmuir* 21:9457-9467
- Strubinger JR, Parcher JF (1989) Surface Excess (Gibbs) Adsorption-isotherms of supercritical carbon-dioxide on octadecyl-bonded silica stationary phases. *Anal Chem* 61:951-955
- Stubbs JM, Potoff JJ, Siepmann JI (2004) Transferable potentials for phase equilibria. 6. United-atom description for ethers, glycols, ketones, and aldehydes. *J Phys Chem B* 108:17596-17605
- Thommes M, Findenegg GH, Schoen M (1995) Critical depletion of a pure fluid in controlled-pore glass - experimental results and grand-canonical ensemble Monte-Carlo simulation. *Langmuir* 11:2137-2142
- Titiloye JO, Skipper NT (2000) Computer simulation of the structure and dynamics of methane in hydrated Na-smectite clay. *Chem Phys Lett* 329:23-28
- Travalloni L, Castier M, Tavares FW, Sandler SI (2010) Thermodynamic modeling of confined fluids using an extension of the generalized van der Waals theory. *Chem Eng Sci* 65:3088-3099
- Triolo R, Agamalian M (2009) Chapter 20: The combined ultra-small and small-angle neutron scattering (USANS/SANS) technique for Earth sciences. *In: Neutron Applications in Earth, Energy, and Environmental Sciences*. Liang L, Rinaldi R, Schober H (eds) Springer, Berlin p 571-594
- Tsomaia N, Brantley SL, Hamilton JP, Pantano CG, Mueller KT (2003) NMR evidence for formation of octahedral and tetrahedral Al and repolymerization of the Si network during dissolution of aluminosilicate glass and crystal. *Am Mineral* 88:54-67
- Vacatello M, Yoon DY, Laskowski BC (1990) Molecular arrangements and conformations of liquid normal-tridecane chains confined between 2 hard walls. *J Chem Phys* 93:779-786
- Villalobos M, Leckie JO (2000) Carbonate adsorption on goethite under closed and open CO<sub>2</sub> conditions. *Geochim Cosmoch Acta* 64:3787-3802
- Vlugt TJH, Krishna R, Smit B (1999) Molecular simulations of adsorption isotherms for linear and branched alkanes and their mixtures in silicalite. *J Phys Chem B* 103:1102-1118
- Vogel M (2010) NMR studies on simple liquids in confinement. *Eur Phys J* 189:47-64
- von Smoluchowski M (1910) Regarding the kinetic theory of transpiration and diffusion hyperdiffuse gases. *Ann Phys Berlin* 33:1559-1570
- Wang JC, Fichthorn KA (1998) Effects of chain branching on the structure of interfacial films of decane isomers. *J Chem Phys* 108:1653-1663
- Wang JW, Kalinichev AG, Kirkpatrick RJ (2004) Molecular modeling of water structure in nano-pores between brucite (001) surfaces. *Geochim Cosmochim Acta* 68:3351-3365
- Wang JW, Kalinichev AG, Kirkpatrick RJ (2006) Effects of substrate structure and composition on the structure, dynamics, and energetics of water at mineral surfaces: A molecular dynamics modeling study. *Geochim Cosmochim Acta* 70:562-582
- Wang JW, Kalinichev AG, Kirkpatrick RJ, Cygan RT (2005) Structure, energetics, and dynamics of water adsorbed on the muscovite (001) surface: A molecular dynamics simulation. *J Phys Chem B* 109:15893-15905
- Wang YF, Bryan C, Xu HF, Gao HZ (2003) Nanogeochemistry: geochemical reactions and mass transfers in nanoparticles. *Geology* 31:387-390
- Wang YF, Bryan C, Xu HF, Pohl P, Yang Y, Brinker CJ (2002) Interface chemistry of nanostructured materials: Ion adsorption on mesoporous alumina. *J Colloid Interface Sci* 254:23-30
- Warnock J, Awschalom DD, Shafer MW (1986) Geometrical supercooling of liquids in porous-glass. *Phys Rev Lett* 57:1753-1756
- Webb EB, Grest GS, Mondello M (1999) Intracrystalline diffusion of linear and branched alkanes in the zeolites TON, EUO, and MFI. *J Phys Chem B* 103:4949-4959
- Webber JBW (2010) Studies of nano-structured liquids in confined geometries and at surfaces. *Prog Nucl Magn Reson Spectrosc* 56:78-93
- White CM, Smith DH, Jones KL, Goodman AL, Jikich SA, LaCount RB, DuBose SB, Ozdemir E, Morsi BI, Schroeder KT (2005) Sequestration of carbon dioxide in coal with enhanced coalbed methane recovery - A review. *Energy Fuel* 19:659-724
- Wittbrodt JM, Hase WL, Schlegel HB (1998) *Ab initio* study of the interaction of water with cluster models of the aluminum terminated (0001) alpha-aluminum oxide surface. *J Phys Chem B* 102:6539-6548

- Wu H, Zhou W, Yildirim T (2009) Methane sorption in nanoporous metal-organic frameworks and first-order phase transition of confined methane. *J Phys Chem C* 113:3029-3035
- Wu JG, Li SB, Li GQ, Li C, Xin Q (1994) FT-IR investigation of methane absorption on silica. *Appl Surf Sci* 81:37-41
- Wu W (1982) Small-angle X-Ray study of particulate reinforced composites. *Polymer* 23:1907-1912
- Xu M, Harris KDM, Thomas JM, Vaughan DEW. (2007) Probing the evolution of adsorption on nanoporous solids by *in situ* solid-state NMR spectroscopy. *Chem Phys Chem* 8:1311-1313
- Yeom YH, Wen B, Sachtler WMH, Weitz E (2004) NO<sub>x</sub> reduction from diesel emissions over a nontransition metal zeolite catalyst: A mechanistic study using FTIR spectroscopy. *J Phys Chem B* 108:5386-5404
- Yong Z, Mata V, Rodrigues AE (2002) Adsorption of carbon dioxide at high temperature - a review. *Sep Purif Technol* 26:195-205
- Zarragoicoechea GJ, Kuz VA (2002) van der Waals equation of state for a fluid in a nanopore. *Phys Rev E* 65:021110-1 - 021110-4
- Zhang JF, Choi SK (2006) Molecular dynamics simulation of methane in potassium montmorillonite clay hydrates. *J Phys B At Mol Opt Phys* 39:3839-3848
- Zhang L, Sun L, Siepmann JI, Schure MR (2005) Molecular simulation study of the bonded-phase structure in reversed-phase liquid chromatography with neat aqueous solvent. *J Chromatogr A* 1079:127-135
- Zhang SY, Talu O, Hayhurst DT (1991) High-pressure adsorption of methane in Nax, Mgx, Cax, Srx, and Bax. *J Phys Chem* 95:1722-1726
- Zhou Q, Lu XC, Liu XD, Zhang LH, He HP, Zhu JX, Yuan P (2011) Hydration of methane intercalated in Na-smectites with distinct layer charge: Insights from molecular simulations. *J Colloid Interface Sci* 355:237-242
- Zhu HY, Ni LA, Lu GQ (1999) A pore-size-dependent equation of state for multilayer adsorption in cylindrical mesopores. *Langmuir* 15:3632-3641
- Zorine VE, Magusin PCM, van Santen RA (2004) Rotational motion of alkanes on zeolite ZK-5 studied from <sup>1</sup>H-<sup>13</sup>C NMR cross-relaxation. *J Phys Chem B* 108:5600-5608

